Kinetics of a surface reaction studied with microcalorimetry

KINETICS OF A SURFACE REACTION STUDIED WITH MICROCALORIMETRY

J. J. G. M. VAN BOKHOVEN

KINETICS OF A SURFACE REACTION STUDIED WITH MICROCALORIMETRY

KINETICS OF A SURFACE REACTION STUDIED WITH MICROCALORIMETRY

PROEFSCHRIFT

TER VERKRIJGING VAN DE GRAAD VAN DOCTOR IN DE TECHNISCHE WETENSCHAPPEN AAN DE TECHNISCHE HOGESCHOOL EINDHOVEN, OP GEZAG VAN DE RECTOR MAGNIFICUS, PROF. DR. IR. G. VOSSERS, VOOR EEN COMMISSIE AANGEWEZEN DOOR HET COLLEGE VAN DEKANEN IN HET OPENBAAR TE VERDEDIGEN OP DINSDAG 21 MEI 1974 TE 16.00 UUR.

DOOR

JACOBUS JOHANNES GERARDUS MARIA VAN BOKHOVEN

GEBOREN TE EINDHOVEN IN 1943

1974
BRONDER-OFFSET B.V. – ROTTERDAM

DIT PROEFSCHRIFT IS GOEDGEKEURD DOOR

DE PROMOTOR PROF. G.C.A. SCHUIT

EN

DE COPROMOTOR PROF. A.L. STUYTS

In herinnering aan mijn moeder
Aan mijn vader
Aan Thea

De onderzoekingen die ten grondslag liggen aan dit proefschrift werden verricht in het Chemisch Laboratorium van de Rijksverdedigingsorganisatie TNO te Rijswijk (Z-H).

Het Bestuur van de Rijksverdedigingsorganisatie is dank verschuldigd vanwege de toestemming om de resultaten van het onderzoek in de vorm van een proefschrift te publiceren.

Aan de Directie van het Chemisch Laboratorium betuig ik mijn dank voor de interesse en de medewerking die ik tijdens de voorbereiding van dit proefschrift heb ondervonden.

Medewerkers van het Chemisch Laboratorium hebben onontbeerlijke bijdragen geleverd in elk stadium van het onderzoek: zowel aan de constructie van de apparatuur en de uitvoering van de experimenten, als aan de interpretatie en presentatie van de meetresultaten. Voor deze directe hulp, maar ook voor de inspiratie die ik van hen heb ondervonden, ben ik oprecht dankbaar.

CONTENTS

CHAPTER I

INTRODUCTION

I.1 BACKGROUND

The Chemical Laboratory of the National Defence Research Organisation in the Netherlands is occupied in the research and development of means and methods to protect human beings in a toxic environment (1, 2). Part of the research is directed towards the purification of air which is contaminated with noxious compounds that are potential chemical warfare agents.

The organophosphorus compounds capable of enzyme inhibition, constitute the most threatening group of warfare agents. The pharmacological activity of these "nerve gases" is described in detail in literature (3). In man and animals these gases are operative through inactivation of the enzyme cholinesterase. This enzyme effectuates the fission of acetylcholine, which is the chemical transmitter of a stimulus between nerve cells (4). If the acethylcholine is not decomposed, it accumulates and the receiving cell remains stimulated. This disturbance of the neural transmission finally leads to the death of the victim.

The charcoal filters, widely used in gasmasks and large filtre installations to purify contaminated air, adsorb nerve gases physically. The adsorption is strong but reversible. If desorption occurs the noxious vapour is harmful as yet. Therefore it is desirable to decompose the vapour during its residence on the adsorbent.

A study of the feasibility of such decomposition was started. Fundamental investigations of the kinetic parameters will be treated in this thesis.

In close connection to these investigations a spectroscopic study was performed simultaneously by Kuiper. This study aimed at a qualitative understanding of decomposition reactions of adsorbed species. Between the two studies there has been a frequent interaction. Often reference will be made to the work of Kuiper described in his thesis (5).

I.2 PRINCIPLES FOR PURIFICATION OF DECONTAMINATED AIR

Purification of air from respiratory toxic vapours is mainly performed by physical adsorption and sometimes by chemisorption. Both these processes have been applied since chemical warfare was started during World War I (6). Physical adsorption has the advantage to be aspecific towards the nature of the vapour. Active charcoal is always used as adsorbent material because of its high specific surface area and because its adsorption capacity is relatively little affected by the uptake of atmospheric water.

For some agents, among which hydrogen cyanide and cyanogen chloride, physical interaction is too weak to provide sufficient protection. During World War II an impregnation of the charcoal adsorbent was developed (7) that was capable to chemisorb and hydrolyse these agents. The impregnation material is a mixture of copper, chromium and silver salts. Smišek and Černý (8) mention a number of chemical effects of anorganic impregnations upon warfare agents. Most of these chemical interactions between adsorbent and vapour do concern a surface reaction, consuming the impregnation material. Few others are catalytic, decomposing the toxic agent into less noxious volatile compounds. A catalytic process is generally to be preferred because a limited amount of catalytic material is essentially capable to convert large quantities of toxic vapour. The realisation of a catalyst in the proper sense, however, is certainly not possible presently. The unsettled probles concern not only the activity, but also the poisoning of the catalyst.

It seems to be easier attainable to realise a decontaminating adsorbent. Such adsorbent has two functions that are also characteristic for a catalyst: (a) it adsorbs the agent, (b) it decomposes the agent. It differs from a catalyst in that the reaction products remain, at least partly, adsorbed, thus destroying the activity as regards decontamination.

Since a broad variety of agents has to be covered, a general type of decomposition reaction has to be chosen. Two possibilities present themselves: hydrolysis and oxidation. For both types of reaction the additional

required reactant, water or oxygen, is profusely present in the atmospheric air. Generally hydrolysis proceeds faster than oxidation at ambient temperatures. Therefore hydrolysis seems to be the more promising type of reaction to be used for decontaminating adsorbents.

I.3 OUTLINE OF THE INVESTIGATIONS

The primary intention of the present study is to obtain insight into the basis of adsorbent activity towards hydrolysis of adsorbed organophosphorus compounds. The problem of loss of activity during the decontamination reaction is left out of consideration.

Attention is directed towards one definite adsorbent-adsorbate system. Isopropyl methylphosphonofluoridate (sarin) is chosen as a representative organophosphorus warfare agent. Active alumina is taken as an adsorbent, because its chemical and physical surface properties have been studied extensively.

Organophosphorus compounds are known to hydrolyse in aqueous solution. Dependent on the pH of the solution, acid or base hydrolysis occurs. The reactions for sarin are illustrated in the scheme below:

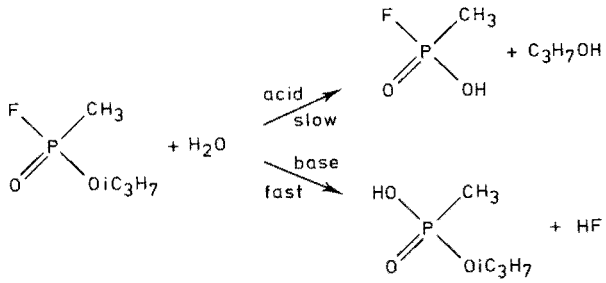

The measurement of the reaction kinetics presents a difficult problem. Preliminary measurements were performed with an extraction procedure, in which the remaining concentration of sarin gave a measure for the decomposition rate. The results of this procedure were not accurate enough to establish the kinetics of the decomposition of adsorbed sarin. After being improved by Kuiper (5) the method was capable to yield valuable additional information on the particular kinetics. For several reasons it seems favourable to use a calorimetric technique for the kinetic measurements. The heat

development ($\dot{Q}$) of a reaction is directly related to the reaction rate ($-\frac{dc}{dt}$):

$$\dot{Q} = -\frac{dc}{dt}(-\Delta H_r)$$

where ΔH_r is the reaction enthalpy. The greatest advantages of the technique for the present problem are:

- the reaction rate can be followed *in situ.*
- the technique is not dependent upon the nature of the system adsorbent-adsorbate.

The required equipment, however, was not available and had to be constructed. For this reason a separate general study was made on calorimetric technique, which led to a choice of the most reliable design. This is described in Chapter II, which presents also a new classification of types of calorimeters. This classification differs from existing ones in that it explicitly departs from the essentially measured quantities. The development of the appropriate technique was considered sufficiently important for the present study to devote two separate chapters to it.

Calorimetry as a tool in kinetic studies often suffers from thermal inertia, which tends to blur the signal. In the reaction system presently in discussion, this problem is particularly serious, because always two heat effects occur: adsorption and reaction. The heat of adsorption, which is developed first, is large. Its thermal signal overshadows the heat of reaction for some time. Chapter III deals with a method to correct for thermal inertia. The procedure is essentially sound for the measuring system, even considering its imperfections; this is proved by a number of special thermal experiments. Although the attainable correction for the adsorbent-adsorbate system is not perfect, more and particularly relevant information on the kinetics of the system can be obtained. The correction procedure was developed during the period in which the kinetic investigations were performed. Therefore relatively few decomposition experiments could be actually corrected.

The interpretation of the kinetic data on sarin decomposition required information on the mobility of adsorbed sarin. Chapter IV describes a method to estimate the mobility of sarin on several adsorbents. It utilizes sarin which is labeled with the radioactive ^{32}P.

In Chapters V and VI the kinetic results and their interpretation are treated. Necessary qualitative information on the nature of the decomposi-

tion process is available from the simultaneously performed investigations by Kuiper. Under the choosen conditions defluoridation of sarin appears to be the more important reaction. The kinetics of the defluoridation reaction show a resemblance with those of many chemisorption processes. This originates from a common feature: in both cases the differently active sites of nonuniform surfaces are subsequently consumed in the process.

The extent and the basis of the nonuniformity are studied by adapting methods, known from literature, to the present reaction system. The difference in activity of the surface sites appears to be connected to the activation enthalpy of the reaction. The distribution function of the activation enthalpy is established from temperature variation.

Finally two remaining questions are answered tentatively. The first concerns the experimentally determined frequency factor; this differs by a factor 10^{10} from the one predicted by the theory of absolute reaction rate. The other question is related to the origin of the distribution in activation enthalpies.

REFERENCES

1. "Protection against toxic compounds", Chemical Laboratory TNO, Rijswijk, The Netherlands (1973).
2. H. Kienhuis a.o., Chem. Weekbl. 66 (1970) 21.
3. Handbuch der Experimentellen Pharmakologie, Cholinesterases and Anticholinesterase Agents, Band XV, (Ed. G.B. Koelle), Springer-Verlag, Berlin (1963).
4. E.D. Adrian, W. Feldberg, B.A. Kilby, Brit. J. Pharmacol. 2 (1947) 56.
5. A.E.T. Kuiper, Thesis, Eindhoven (1974).
6. The problem of chemical and biological warfare, Vol. 1, "The rise of CB weapons", Edited by SIPRI, Almqvist & Wiksell, Stockholm (1971), Chapter I.
7. W.A. Noyes, Jr., "Science in World War II, Chemistry", Boston (1948), p. 296.
8. M. Šmisek, S. Černý, "Active Carbon", Elsevier Publ. Comp, Amsterdam (1970), p. 188.

CHAPTER II

CALORIMETRIC TECHNIQUE

Once calorimetry was chosen as the technique for the kinetic measurement of decomposition of adsorbed vapours (see Chapter I), it seemed useful to make some general investigations into the field of calorimetry in order to get insight in instrumental possibilities. This could be helpful in making a suitable choice of type of calorimeter to be used. This study has resulted into the choice of a heat flow meter. Moreover, it led to a classification for calorimeters that is exclusively based upon the measured quantity.

II.1 GENERAL APPLICABILITY OF CALORIMETRY

Calorimetry is a tool generally applicable to detect or measure processes, whether they are physical, chemical or biochemical. All of these processes are accompanied by development or consumption of heat. Information on such processes may hence be obtained from heat measurements. Parameters that are related to heat development become quantitatively recognisable through calorimetric methods.

This wide applicability may be considered as an advantage but it has its dark side. In calorimetric measurements just one aspecific quantity is detected. The method is thus purely quantitative and lacks any indication as to the character of the process developing the energy. So calorimetry must necessarily be sustained by qualitative methods that define the nature of the heat source.

Calorimetric experiments on systems in which more than one process

occur simultaneously (whatever the nature of the process) yield information on a composed quantity. This quantity can only be split up into the component parts belonging to the separate processes if other experimental information is available, or if theoretical assumptions can be made on the relative contributions of the processes. Obviously this limitation is closely connected to the aspecificity of calorimetry.

II.2 CLASSIFICATIONS OF CALORIMETERS

There is no generally accepted notation to characterise the many different types of calorimeters. Traditional names as "isothermal", "ice" and "transformation" calorimeter are not or not always based upon a rational system having some general validity.

A broad distinction can be made between calorimeters working at constant or nearly constant temperature ("static") and calorimeters working at varying temperature ("dynamic"). This distinction however, has nothing to do with the essence of the heat measurement. The choice of an increasing temperature *e.g.* , is connected with the creation of favourable circumstances for the process to occur.

It is more desirable to apply a criterion that is directly related to the quantities involved in the measurement. Existing rational systems are based more upon secondary features than upon the nature of the measurement. In these systems calorimeters are being thought to comprise a calorimeter proper and a jacket, as shown schematically in the figure below:

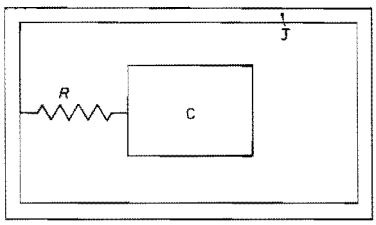

C calorimeter proper, consisting of vessel plus sample, characterized by one temperature

J jacket

$\mathscr{R}$ thermal resistance between calorimeter and jacket

Kubaschewski and Hultgren, being interested in metallurgical thermochemistry (1), proposed a classification that is based upon criteria defined earlier by Wittig (2). The determining quantities are the temperature of the calorimeter (T_c), the temperature of the jacket or surroundings (T_s) and the heat production in the sample (L).

- if $T_c = T_s$ = constant and L is the only variable, the calorimeter is truly isothermal. The condition $T_c = T_s$ for every L is equivalent to the requirement of a very fast heat exchange between the calorimeter and its surroundings.
- if $T_c = T_s$ the calorimeter is adiabatic. In this case heat interchange is prevented because the equality in temperature is a consequence of controlled adaptation of T_s to T_c.
- if $T_s - T_c$ is constant, there is a constant flow between the parts, and the instrument is called a heat flow calorimeter.
- if T_c varies under the influence of L and T_s is constant, the calorimeter is proposed to be named an isoperibol calorimeter; this definition has been widely accepted in literature.

This enumeration does not cover all the posibilities as Kubaschewski and Hultgren note themselves. Other types that have been developed since, can be fitted into the system. *E.g.* the condition that T_c increases linearly with temperature, T_s is constant and L is variable, holds for a differential scanning calorimeter.

The criteria of Wittig enable to define unambiguously many types of calorimeters static as well as dynamic. An important drawback is the impossibility to derive the measuring principle directly from the criteria. This drawback is found to a smaller extent in a classification given by Gravelle (3). His classification is governed by one criterion: the thermal interaction between the two parts. Gravelle's classification is:

- in an isothermal calorimeter jacket and measurement part are held at equal temperatures by a perfect mutual heat exchange. The temperature of the jacket is controlled at a constant level; the heat necessary for this is the measure for the unknown quantity.
- in an adiabatic calorimeter heat exchange is precluded. The change of temperature is measured; it is directly related to the heat to be gauged. In practice two methods are used to prevent or limit heat exchange: a high heat resistance between the parts is applied, or the temperature difference between the parts is maintained at zero by a continuous adjustment of the jacket temperature.
- in a conduction calorimeter heat exchange occurs via a well defined heat resistance; the temperature drop over this resistance is measured and is a direct gauge for the amount of heat flowing to or from the calorimeter.

A differential scanning calorimeter cannot be fit into Gravelle's classification. Essential for the operation of a differential scanning calorimeter is the use of a reference vessel; this renders the instrument too complex to be fit into the system.

Comparing the two classifications one sees that the definitions of isothermal and adiabatic calorimeters are equivalent. The name heat flow calorimeter, however, covers quite differently defined instruments. The definition of heat flow meter used by Gravelle seems to be the more generally accepted one and will be applied further on here.

Alternative criteria for classification

The classifications of Kubaschewski and Hultgren and that of Gravelle are based primarily upon the thermal relation between the internal and external parts and not upon the nature of the measured quantity. Essentially two measuring principles are met in calorimetry:

1. Measurement of energy.
2. Measurement of a temperature difference.

These measuring principles are rather easily distinguished in the classes of Gravelle: in the class of isothermal calorimeters the generated or required energy is registrated, whereas in both other classes temperature differences are indicative. The classification of Kubaschewski and Hultgren offers hardly any hold as to the measured quantity.

Ad 1. Measurements of energy may be performed in a number of ways, which, however, have one feature in common. The temperature of the system to be measured is forced to follow a prescribed time dependent program. If no heat producing or consuming processes occur a definite known amount of heat is then required. If, however, such processes do proceed, they threaten to disturb the temperature course. The additional (counteracting) energy required to prevent the disturbance is the measure for the quantity to be known. This principle has different manifestations; two examples will be given:

- static: in an isothermal calorimeter the temperature program is very simple: the temperature has to be constant. This may be achieved in different ways. In a "phase change" calorimeter *e.g.*, a phase transformation of a surrounding material provides the compensating energy. In most

cases electrical compensation is applied. The Peltier effect offers the possibility for both positive and negative compensation (4).

- dynamic: in so called differential scanning calorimetry the temperature is linearly increased. The additional amount (positive or negative) of energy that is necessary to balance heat effects of the system is measured. In practice a reference vessel is indispensable for this method.

Ad 2. The principle of temperature difference measurement is encountered in two manifestations corresponding to the adiabatic and heat flow or conduction instruments in Gravelle's classification.

The operation of "ΔT" calorimeters will now be formulated. Also the extent of the equivalence or distinction between adiabatic and conduction instruments will be defined quantitatively.

To this end the heat flow circuit of the measuring part is presented in its electrical analogon (see Fig. II.1) in which the symbols of electric resistance and capacity stand for the thermal resistances and capacities (see section 6 of this Chapter). The thermogenesis W is split up into two parts:

$$W = \frac{\Delta T}{\mathscr{R}_{tp}} + \frac{d(\Delta T)}{dt}\,(\mathscr{C}_s + \mathscr{C}_v) \qquad [1]$$

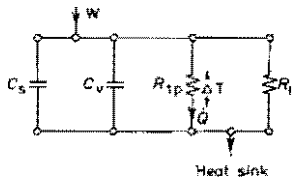

Fig. II.1

The electrical analogon of the measuring part of a power measuring calorimeter.

$\mathscr{C}_s$, $\mathscr{C}_v$	thermal capacity of sample resp. vessel
$\mathscr{R}_{tp}$	thermal resistance of thermopile
$\mathscr{R}_l$	thermal resistance of leakages
W	thermogenesis
$\dot{Q}$	measured flux

The first term is the measured heat flux $\dot{Q}$, the second term is the adiabatic component and represents the "loading" of the sample capacity.

In fact $\dot{Q}$ is to be considered as a distorted representation of W. This distortion sometimes complicates the interpretation of the thermograms considerably as will be seen in the next chapter.

In adiabatic measurements $\mathscr{R}$ is made as large as possible; so $\dot{Q}$ approaches zero and the second term predominates.

In conduction calorimetry both terms may be important, dependent upon the way in which the heat originates (see Chapter III). It is seen that the loading term is more important when the time constant of the circuit (product of $\mathscr{R}$ and $\mathscr{C}_s + \mathscr{C}_v$) is greater. The proportion between the two terms in [1] determines to what extent a calorimeter is adiabatic.

Both static and dynamic use of ΔT instruments is possible, although dynamic instruments are more liable to disturbances of the temperature equilibrium.

Conclusion

Existing classifications do not account explicitly for the principle of the heat measurement and put too much stress upon secondary instrumental features. A classification based upon the two measuring principles that are always encountered, *viz.* energy and ΔT, is a more logic one. For ΔT instruments a distinction may be made between conduction and adiabatic calorimeters, although a sharp division of these types is not possible. In both classes a static and dynamic operation is possible.

II.3 CRITERIA FOR INSTRUMENT CHOICE

The choice or the design of a reaction calorimeter has to be decided on account of the specific nature of the reaction system to be studied and by the kind of information that is desired. Information on thermodynamic parameters requires other conditions to be fulfilled than information on kinetic parameters.

The specific nature of the reaction system comprises the description of the reactants and the definition of the experimental conditions. Explicit factors influencing the choice of a calorimeter design are (5):

1. Number and nature of phases taking part in the reaction.

2. Amount of reactant.
3. Reaction rate and duration of the reaction.
4. Pressure in the reaction vessel.
5. Accuracy of the measurements.

Ad 1. The first factor determines the method to contact the reagents. In the present case a solid and a vapour phase are involved. Because study of reaction kinetics requires a sharply defined starting point, a method for rapidly contacting the vapour and the adsorbent must be applied. If the solid phase is considered to be "immobile", two possibilities present themselves: (a) the vapour may be carried from the dosing vessel to the adsorbent in an indifferent carrier gas; in this way the transport takes place by convection; (b) a vacuum may be applied to allow the vapours to flow from the dosing vessel to the adsorbent. Saturated sarin vapour pressure at room temperature is about 2.5 Torr.
The mean free path ($\bar{L}$), calculated with

$$\bar{L} = 10^{-5} \frac{T}{273} \frac{760}{P} \text{ cm}$$

where p is expressed in Torr and T in ^{o}K, is about 300000 Å for saturated sarin vapour. The mean free path at a pressure of 1 atmosphere is 50000 Å. Pores that contribute importantly to the surface area have radii smaller than roughly 10000 Å. Whether one works with a vacuum or with a carrier gas, it is seen that the transport in the pores is determined by Knudsen diffusion.

Both these methods may have further pros and cons with respect to the conduction of the heat developed. The presence of an indifferent gas around the adsorbent enhances the heat transfer to the walls of the vessel but also increases the loss of heat from the vessel. A continuous carrier gas stream may cause thermal instabilities, whereas a permanently evacuated reaction vessel inevitably contains leakages which may give rise to disturbing heat effects. The influence of these effects is hardly to be predicted quantitatively.

Ad 2 and 3. The second and third factors determine the level of stability and sensitivity. A small reaction rate necessarily implies a long duration of the experiment and a low heat production per unit of time. A long dura-

tion compels the use of a stable instrument. Also it must be sensitive enough to measure the accompanying low heat evolutions. A great sensitivity (or low detection limit), however, is only then significant, if the stability lies in the order of magnitude of the detection limit.

Ad 4. The pressure in the reaction vessel follows not only from the reagent concentration required, but is also determined by other considerations (see *ad* 1.).

Ad 5. The demands set to accuracy are determined by the purposes for which the results are acquired. Often calorimetric measurements have to be highly accurate. *E.g.* if ΔH is measured for the calculation of an equilibrium constant, the accuracy in ΔH has to be in the order of 0.01% for K to be calculated with an accuracy in the order of 10% (6). To establish the kinetic order of a reaction an accuracy of a few percents is often sufficient.

II.4 SELECTION

The purpose of the calorimetric measurements on the system presently in discussion is the determination of kinetic properties. So an accuracy of a few percents probably will be satisfactory.

The quantification of the factors sensitivity and stability depends on requirements set by reaction rate and enthalpy. Because such quantities were unknown behorehand, estimations had to be made.

Firstly the volume of the reaction vessel was chosen to be 10 cm^3. Specific surface and density of the adsorbed were taken to have average values of 100 m^2/g and 1 g/cm^3. The surface coverage was set equal to one. The following estimates were made:

- a reaction enthalpy of 10 kcal/mole
- a half lifetime of the adsorbed vapour of 10 hours.

Under these rather pessimistic estimates, heat fluxes in the order of 100 microwatt per gram adsorbent must be expected. To measure these with an accuracy of several percents the detection limit has to be in the order of a few microwatts. At the time of the start of the investigations hardly any microcalorimeter with the required sensitivity was available commercially; reaction vessels and supply lines were not apt to the reaction system under study nor were they easily adaptable.

Therefore, it was decided to construct a microcalorimeter designed for the reaction system under study.

There is little doubt that the properties of sensitivity and stability are best acquired in conduction calorimeters (3, 5). The best instruments reach a detection limit of about 1 μW and a long range stability of the same order (2).

It was possible to attain these specifications using a particular type of heat sensor. These sensors (manufactured by TPD-TH/TNO*) are essentially thermopiles of silver-constantan thermocouples in a very high number per unit of sensing surface (about 300/cm^2). The sensitivity of these meters amounts to 10,5 W/V.

Stability of calorimeters is primarily acquired by a constant temperature environment. The influence of temperature fluctuations which always remain may be mitigated by thermal or electrical compensation circuits. As has been seen, the stability of the microcalorimeter must be in the order of magnitude of microwatts. To attain this level it was necessary to apply thermal and electrical compensation simultaneously.

II.5 DESCRIPTION OF DESIGN

The microcalorimetric instrument built for the reaction system adsorbent-adsorbed vapour is shown in Fig. II.2.

The microcalorimeter is of the heat flow type (Gravelle's annotation) and is directly derived from the "heat generation meter" of Van Geel (7). The features distinguishing it from Van Geel's calorimeter are twofold:

- A vacuum is applied as heat insulation between the environment and measuring part.
- The possibility to dose vapours to the reaction vessels has been created.

In the newly proposed classification the instrument is of the "ΔT measurement" type.

Two concentric cylinders constitute the structure of the microcalorimeter (see Fig. II.2). The outer one (F) is made out of brass and has a height of 20 and a diameter of 22 cm. The inner one (D) is made out of aluminium and its diameter and height are respectively 13 and 17 cm. The rooms in between the cylinders and within the inner cylinder can be evacu-

* Technisch Physische Dienst TH/TNO, Delft, The Netherlands.

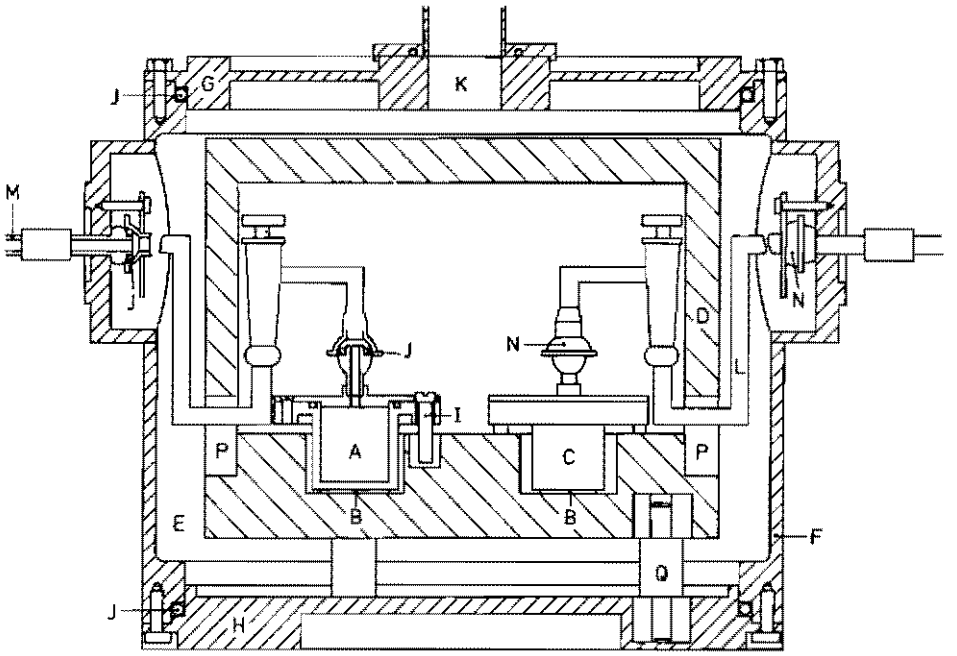

Fig. II.2

Design of calorimeter constructed for measurements on adsorbed vapours.

A, C	sample vessels	J	rubber "O"-rings
B	heat flow meters	K	vacuum tube for isolation room
D	aluminium cover	L	glass tubes
E	isolation room	M	vacuum stainless steel tubing
F	brass outer cylinder	N	ball joints
G, H	brass covers	P	saving in aluminium cover
I	PVC bolts	Q	PVC support

ated simultaneously to a pressure better than 5.10^{-5} Torr via tube K. A thermal contact between inner and outer cylinder can be established magnetically; copper discs with an iron core can be positioned in such a way that they contact both the outer and inner cylinder. This "heat valve" makes a faster equilibration possible. The cover (G) and bottom (H) of the outer cylinder are dismountable and fit by means of vacuum tight O-rings (J).

The inner cylinder (D) consists of a thick bottom block and a pot shaped cover. A couple of heat flow meters (B) are glued onto the bottom of two cylindrical excavations. The heat flow meters as shown in Fig. II.2 are silicon rubber discs with a thickness of 2 mm and a diameter of 23 mm. A more detailed description is given below. There are two sample vessels (A and C) standing on the heat flow meters; their positions are rendered reproducible and secured by three PVC bolts (I). These vessels are made out of copper and gold plated to prevent corrosion. The stainless steel covers fit onto the vessels with a rubber "O" ring, tightened by means of bolts.

A glass tube with cock (N) connects each vessel with the transit through the outer wall. Both ends of the tube fit by means of ball joints. The glass tubes are led through savings in the aluminium cover (P). These savings directly connect the inner chamber with the isolation vacuum. The electrical leads from the heat flow meters are conducted to the outer wall through a hole in the centre of the aluminium block (not drawn in the figure). They pass the outer (vacuum) wall through openings which are filled up with lute. The vacuum for both the isolation room and the sample vessels is provided by a mercury diffusion pump backed by a rotary pump; the pumping speed is 6 l/sec. The vacuum lines both to the isolation vacuum and the vessels are provided with flexible bellies that can be disconnected easily. The microcalorimeter is placed in a thermostat that is controlled within $\pm$ 0.003^{o}C. It can be lifted above the water level pneumatically.

The thermopiles are electrically connected in opposite direction; this connection offers an electric compensation for identical temperature differences over the thermopiles.

The construction of the flat round heat flow meters is described in detail by De Jong and Marquenie (8) and by Van Ooijen (9). Fig. II.3 shows the structure of the sensors. A constantan wire is wound around a teflon tape; the wire is electro silvered at one side of the tape. The tape is spiralised to form a disc and is further filled up to a solid body with silicon rubber. In this way many silver-constantan thermocouples are electrically arranged in series, while all hot junctions find themselves together at the upper surface and the cold junctions at the lower surface. A temperature difference between the two surfaces causes a thermo-emf over each subsequent pair of thermocouples; the resulting effect of a temperature difference is measured by the cumulative emf's of about a thousand ther-

mocouple pairs. The relation between temperature difference and heat flow through the disc is proportional. A calibration procedure is necessary to determine the proportionality constant.

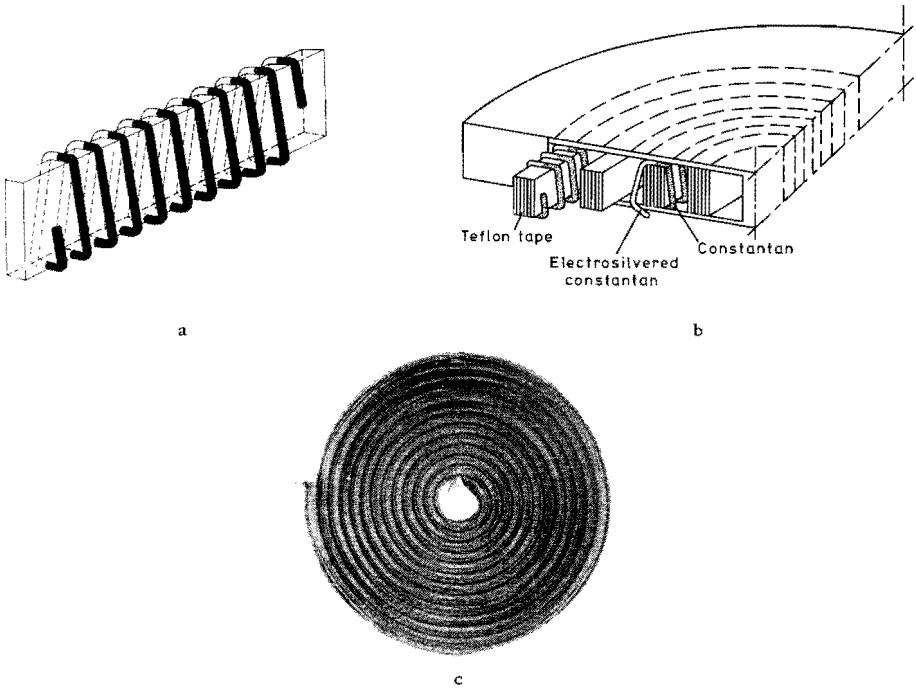

Fig. II.3

Heat flow meter of flat disc type; (a) teflon tape with thermocouple wire, (b) schematic cross section, (c) view of the disc before filling with rubber.

The sensitivity of these sensors as such is 10.5 W/V. Integrating them in a measuring system may affect this number on account of heat losses. Calibration of the calorimetric system as a whole makes it possible to eliminate the influence of the heat losses.

During the investigations another type of heat flow meters was mounted, which was better adapted to the demands of rapid responses. This cylindrical type of heat flow meter and the position after it had been built in is shown in Fig. II.4. The construction of the heat flow meters is shown in the Figures II.5a and b. A spiralised wire, similar to the one shown in Fig. II.3a, but without teflon tape, is wound around an anodised aluminium cylinder with a wall thickness of 0.3 mm. The hot junctions contact this cylinder, whereas the cold junctions are very close to the heat sink. About

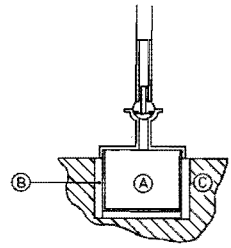

Fig. II. 4

The cylindrically shaped heat flow meters built into the aluminium block.

A reaction vessel, B heat flow meter, C aluminium block.

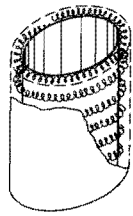

Fig. II. 5a

Schematic picture of the structure of a cylindrical heat flow meter.

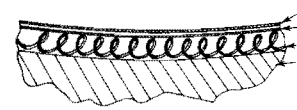

Fig. II. 5b

Part of a cross section through vessel, heat flow meter and heat sink;

A reaction vessel, B aluminium cylinder, C thermopile, D heat sink.

250 thermocouple pairs constitute one loop around the aluminium cylinder. There are 21 loops, so the thermopile contains 5250 pairs. For the sake of mechanical strength the room in between aluminium cylinder and heat sink was filled up with lute.

Appropriate reaction vessels were made smoothly fitting in the inner surface of the cylindrical sensor. Silver was chosen as material for these vessels because its thermal properties are better than those of copper. The heat conductivities (λ) and the capacities per volume (ρc_p) are compared below;

the desive factor is the quotient of conductivity and capacity:

	λ (w/m ^{o}C)	ρC_p (KJ/m^3 ^{o}C)	$\lambda/\rho C_p$ (cm^2/sec)
copper	395	3420	1.15
silver	410	2460	1.67

It might be noted here that the sensitivity of a heat flow meter is not proportional to the number of thermocouples. If the number of thermocouples of a heat flow meter with thermal resistance $\mathscr{R}$ is enlarged from n_1 to n_2, the corresponding heat resistance of the thermopile decreases roughly proportionally, from $\mathscr{R}$ to $\frac{n_1}{n_2}.\mathscr{R}$. For n_1 couples the temperature difference over the thermopile in a stationary heat flow $\dot{Q}$ is given by $\Delta T_1 = \dot{Q}\mathscr{R}$. The corresponding thermo-emf U, follows from:

$$U_1 = n_1 \epsilon \Delta T_1 = n_1 \epsilon \dot{Q} \mathscr{R}$$

where ϵ is the thermo-electric coefficient. The same heat flow in a thermopile with n_2 couples causes a temperature difference of

$$\Delta T_2 = \dot{Q} \frac{n_1}{n_2} \mathscr{R}$$

Now the thermo-emf is given by:

$$U_2 = n_2 \epsilon Q \frac{n_1}{n_2} \mathscr{R}$$

or

$$U_2 = n_1 \epsilon \dot{Q} \mathscr{R}$$

which is the same as in the case of n_1 couples. This conclusion is valid under the condition that the loss of heat is negligible in both cases or that it is proportional to the number of couples. The importance of a large number of thermocouples must not be found primarily in sensitivity. The prime advantage is the fast response resulting from the low thermal resistance. Another great advantage is that the phenomenon under study proceeds more isothermally.

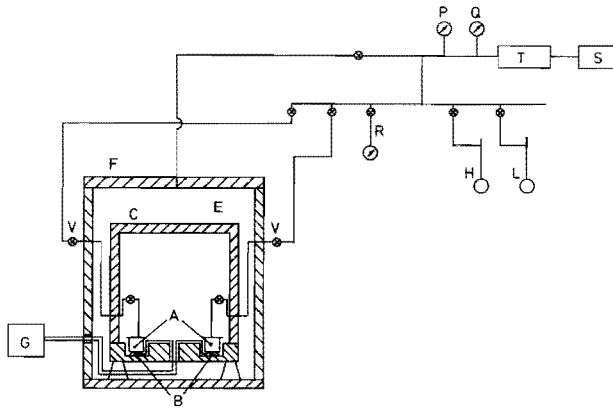

Fig. II. 6

The vapour dosing system and a schematic picture of the calorimeter.

A	reaction and reference vessel	L	water dosing vessel
B	heat flow meter	P	Penning pressure meter
C	aluminium inner cylinder	Q	Pirani pressure meter
E	isolation room	R	vapour pressure meter
F	brass outer cylinder	S	oil rotary pump
G	recorder	T	mercury diffusion pump
H	adsorbate dosing vessel		

The gas dosing system (see Fig. II.6) has been made out of glass. The transition to the stainless steel tubing which leads to the outer calorimeter wall was made by attaching the two materials with an appropriate lute. Vapours of agents or water may be led to the adsorbent from vessels H and L, which contain the liquids. Lower relative pressures may be established with a cooling device containing a built-in Peltier-element. Penning and Pirani gauges provide the possibility to read the pressure in the vacuum system within the range of $3\text{-}10^{-6}$ Torr. With a separate Pirani pressure meter (R) the vapour pressure of the adsorbates could be measured.

II.6 DISCUSSION OF THE DESIGN

The basic intentions in designing the microcalorimeter have been the achievement of:

- a sensitivity in the order of magnitude of 10 W/V; a recorder with a range of 20 μV full scale is then proper to detect heat flows of about 1 μW.
- a long range stability of the zero-line within a few microwatts.

During the experiments it appeared that a third property could be highly important; the response time of the calorimeter has an essential effect upon the amount of information that could be obtained from thermokinetic curves of the reaction systems in question; if the response is too slow, the heat flow is represented in a distorted way.

Two aspects will be discussed in this chapter: sensitivity and stability. The response time will be treated in the next chapter. The phenomenon named zero-signal will be lightly touched on.

II.6.1 Sensitivity and detectivity

The required sensitivity is primarily accomplished by the use of the heat flow meters described in the foregoing section. The sensitivity of these sensors is lowered when they are functioning in the calorimetric measuring system. A number of sources for heat loss are responsible for this:

- heat disappears along the gas dosing pipes. To minimize this flow a glass tube was interconnected between the sample vessels and the transit through the wall. The heat conductivity coefficient of glass is about 20 times smaller than that of stainless steel. Although a thicker tube wall is needed, the net result in thermal resistance is positive.
- heat is transferred from the reaction vessels to the aluminium block and cover by radiation. In the case of cylindrical heat flow meters the loss through the vessel walls is considerably lower.
- the reaction vessels used with the disc heat flow meters lose heat through the three bolts that are necessary to position the vessels reproducibly and tightly.

The sensitivity value given by the manufacturer as 10.5 W/V for the disc heat flow meters dropped to 11.3 W/V after attachment on the aluminium block.

The heat conductivity of the three PVC bolts and the glass connec-

tion pipes could be calculated to be respectively a factor 10^4 and 10^5 smaller than that of the flat heat flow disc. So the decrease in sensitivity must be ascribed to loss of heat by radiation.

It might be interesting to know what factors are determining the theoretical detection limit and the actual one. A comparison of these quantities is an indication to what extent noise originating from other sources than thermal fluctuations has been introduced.

Smith, Jones and Chasmar (10) conceived a method to quantify the detectivity (ultimate detection limit) of radiation detectors. Chavet (11), following this method, described the detectivity of microcalorimeters. The ultimate detection limit of microcalorimeters is determined by thermal fluctuations. These are random temperature variations which occur as a result of statistical energy exchange. The heat flow caused by these fluctuations appears as an intrinsic noise in the signal of the calorimeter. The power that is equivalent to this noise (W_o) may be written as:

$$W_o^2 = 4\,k\,T^2\,\mathscr{G}\,\Delta\nu$$

in which W_o = noise equivalent power
k = constant of Boltzmann (1.38×10^{-23} J/°K)
T = temperature (°K)
$\mathscr{G}$ = heat conductance between sample and heat sink (W/°C)
$\Delta\nu$ = band width of the measuring system (sec^{-1}).

$\mathscr{G}$ can be replaced by $\mathscr{C}/\tau$; τ is time constant of the reaction vessel and $\mathscr{C}$ is heat capacity of sample plus container. If the electric system is correctly damped, $\Delta\nu$ may be replaced by $\pi/4\theta$, in which θ is the period of the recorder. For W_o it follows then

$$W_o^2 = \frac{\pi k\,T^2\mathscr{C}}{\tau\theta}$$

When the appropriate values of the calorimeter equipped with the disc heat flow meters are substituted ($\mathscr{C}$ = 63 J/°C, τ = 1200 sec, θ = 1.5 sec) W_o becomes 3.7×10^{-10} Watt. The experimental noise is about 0.4 microwatt. The "figure of merit" (M) defined by Chavet as the quotient of intrinsic and experimental noise equals 9×10^{-4}. This number is an indication to what extent the signal noise of the calorimeter is to be ascribed to thermal fluc-

tuations. Table II.1 shows the figures of merit of a few isothermal power measuring calorimeters. It may be concluded from these data that the limit set by thermal fluctuations is far from being approached by any instrument and that other sources are responsible for the actual noise. In our case the main source must be found in Johnson noise in the electrical circuit of thermopiles and recorder.

Table II.1

Figure of merit of some isothermal power measuring calorimeters according to Boyd (9)

Reference	W_m (W)	C (J/°C)	τ (sec)	W_o (pW)	$10^6 M$	operating temp. (°C)
Kelen (19)	15	14	480	20	1	35-450
Gordon (20)	5	3.8	450	13	3	150-220
Mann (21)	0.1	1.3	90	25	300	25
Chavet (11)	0.09	10	180	35	400	35
Calvet and Pratt (22)	0.07	63	480	33	500	10- 40
Blet-Talbot (23)	0.03	0.01	15	16	500	25
present work	0.4	80	1000	370	900	0- 60

Johnson noise is a variable emf that is spontaneously generated in resistors (12). Its magnitude is given by

$$\overline{E_f^2} = 4\ kT\ \Delta f\ R$$

in which $\overline{E_f^2}$ = the mean square value of the fluctuations with frequency f
Δf = a small frequency interval around f
R = electrical resistance.

The consequence of Johnson noise is best clarified when the course of heat flows in the measuring part of the calorimeter is represented by a "thermal network". Thermal flows are governed by relations that are completely similar to the laws that are valid for electrical currents (13). The analogous quantities are:

temperature difference T - voltage difference V
heat flow W - current i

thermal capacity	$\mathscr{C}$	-	electrical capacity C
thermal resistance	$\mathscr{R}$	-	electrical resistance R
thermal admittance	$\mathscr{A}$	-	electrical admittance A

The thermal network is shown in Fig. II.7; it is an idealised model that differs from reality, because the represented functions (capacities, resistances) are not quite unambiguous. The capacities of sample plus vessel do have some internal resistance and the thermal resistances possess heat capacities. Between sample and vessel a heat resistance exists, as well as between thermopile and vessel. These omissions, however, are not essential here.

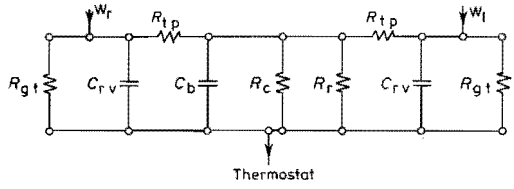

Fig. II.7

Idealised thermal network of the calorimeter.

$\mathscr{C}_{rv}$, $\mathscr{C}_{lv}$, $\mathscr{C}_{b}$	heat capacities of resp. right vessel, left vessel, aluminium block	$\mathscr{R}_{c}$	resistance of PVC supports
		$\mathscr{R}_{r}$	resistance of vacuum room
		$\mathscr{R}_{tp}$	resistance of thermopile
$\mathscr{R}_{gt}$	resistance of glass tube	W_l, W_r	heat fluxes to be measured

It may be seen from a detail of this network (Fig. II.1) that a constant power (W) can be written as:

$$W = \Delta T_{tp} \, (\mathscr{G}_l + \mathscr{G}_{tp}) \qquad [2]$$

where $\mathscr{G}_l$ and $\mathscr{G}_{tp}$ are the conductivities of the heat leakages and the thermopile. If e is the temperature dependence of the thermo-emf of one thermocouple and n the number of thermocouples, the total emf over one thermopile equals:

$$E = ne \, \Delta T_{tp} \qquad [3]$$

By combination of [2] and [3] one obtains:

$$W = \frac{E(\mathscr{S}_{tp} + \mathscr{S}_l)}{ne}$$

Experimentally the factor $(\mathscr{S}_{tp} + \mathscr{S}_l)/ne$ appeared to be 11.6 W/V. The minimum detectable power is determined by Johnson noise of the particular system (now called E_j) which occurs in the combined thermopile-recorder circuit:

$$\overline{E_j^2} = 4\ kT\ \Delta f\ (R_{tp} + R_{rec})$$

in which R_{rec} is the input resistance of the recorder and R_{tp} the resistance of the two thermopiles. R_{tp} appears to be negligible compared to R_{rec}. Δf has to be taken as $\pi/2$ according to the manufacturer. The lowest detectable power W_j is given by

$$W_j = \frac{\mathscr{S}_{tp} + \mathscr{S}_l}{ne} = 0.5\ \mu W.$$

This value compares well with the experimentally registered noise of 0.4 microwatt. Improvement of the noise level has to be found in the emf measuring system.

II.6.2 Stability

Measurement of heat fluxes with an absolute accuracy that is in the order of the detection limit, is only significant if the temperature instabilities around the thermopiles do not generate spurious heat fluxes that equal this detection limit. Thus temperature fluctuations should be of a lower order than the temperature differences that cause heat flows of about one microwatt. Knowing that one heat flow disc contains about one thousand pairs of thermocouples and that the emf is about 40 $\mu V/^{o}C$, one can easily calculate that a power of one microwatt needs a driving force of about $10^{-6}\ ^{o}C$. So the amplitude of random fluctuations of the inner block should not exceed this number.

Obviously the primary caution must be the stabilisation of the environmental remperature; this is accomplished by positioning the calorimeter

entirely in a water bath thermostat, controlled within about $\pm$ 0.003°C. The remaining variations are further attenuated by some structural properties of the calorimeter. As a whole the calorimeter constitutes a thermal damping circuit; its network may be read from Fig. II.7. Temperature fluctuations of the thermostat approach both sides of the thermopiles; heat may be transferred to the hot junctions via the glass tubes. Conduction through the PVC feet and radiation through the vacuum space transfer heat to the aluminium block and further to the cold junctions.

It is possible to calculate the time constants of the different $\mathscr{RC}$-circuits that determine the temperature behaviour around the thermopiles. Considering the left thermopile *e.g.* the two $\mathscr{RC}$-circuits, characterized by ($\mathscr{R}_{gt}$ $\mathscr{C}_{rv}$) at the one hand and ($\mathscr{C}_B$ $\frac{\mathscr{R}_c \mathscr{R}_r}{\mathscr{R}_c + \mathscr{R}_r}$) at the other hand, constitute the temperature difference over this thermopile primarily. Assuming that all resistances have no capacity and all capacities have no resistance, the time constants may be calculated straightforward. $\mathscr{R}_c$ (the resistance of the PVC feet) is directly calculated from the known dimensions and conductivity (d = 2 cm, S = 1.8 cm^2, λ_{PVC} = 0.232 $\frac{W}{m\,^oC}$)

$$\mathscr{R}_c = \frac{d}{3S\lambda} = 140\,^oC/W$$

The thermal resistance originating from conduction of the room in between the inner and outer wall of atmospheric pressure can be calculated to be 25°C/W (λ_{alr} = 0.024 kcal/mhr°C, exchanging surface 0.25 m^2, distance 2.10^{-2} m). This resistance is reduced greatly if the pressure falls below the value at which the mean free path of the gasmolecules is of the same order of magnitude as the distance between the exchanging surfaces (Smoluchovski effect). At a pressure of 5.10^{-3} Torr the mean free path is about 2 cm. A pressure of 5.10^{-5} Torr appeared to be readily attainable in the isolation room. Heat transfer by conduction becomes negligible compared to transfer by radiation. $\mathscr{R}_r$ is the thermal resistance that is offered to the radiation transfer between inner and outer cylinder. Heat transfer by radiation is governed by the law of Stefan-Boltzmann:

$$W = \sigma T^4$$

If W is expressed in W/m^2 and T in °K, than σ equals 5.78×10^{-8} $W/m^2\,{}^oC^4$.

For optically not-black surfaces an emissivity factor has to be added: $W = \epsilon \sigma T^4$. Quantitatively the emissivity is equal to the absorbancy which is the fraction of energy that is absorbed from an incident beam. To calculate the heat transfer through the vacuum room the inner and outer cylinder are considered to be two opposite surfaces of equal area (S); each ray leaving one surface is assumed to reach the other. If the temperature of the outer chromium-plated cylinder is called T_c and of the inner cylinder T_A, the quantities of heat radiated from the surfaces are respectively $W_c = \epsilon_c \sigma T_c^4$ and $W_A = \epsilon_A \sigma T_A^4$. Every beam of light rays is reflected many times between the two surfaces; each time its energy diminishes with a factor $(1-\epsilon_A)$ or $(1-\epsilon_c)$. From the amount of energy radiated by the outer surfaces (W_c) only a fraction is finally absorbed by the inner cylinder:

$$\dot{Q}_{c \to A} = \sigma \epsilon_c T_c^4 S \left\{ \epsilon_A + \epsilon_A (1-\epsilon_A)(1-\epsilon_c) + \epsilon_A (1-\epsilon_A)^2 (1-\epsilon_c)^2 + .. \right\}$$

$$\dot{Q}_{c \to A} = \sigma \epsilon_c \epsilon_A T_c^4 \frac{S}{1-(1-\epsilon_A)(1-\epsilon_c)}$$

A similar expression holds for the heat transfer in the opposite direction. The net result for the heat transfer from outer to inner cylinder amounts:

$$\dot{Q} = \frac{\epsilon_c \epsilon_A}{\epsilon_c + \epsilon_A - \epsilon_c \epsilon_A} \sigma S (T_c^4 - T_A^4)$$

If in a situation of thermal equilibrium ($T_c = T_A = T_1$) the temperature of the outer cylinder is abruptly changed to T_2, a balance can be set up from which the temperature change of the inner cylinder can be calculated.

A sudden change, illustrated in the scheme below,

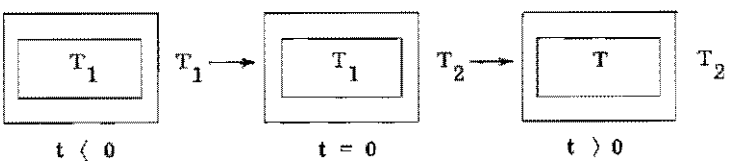

causes a radiation heat flow; the heat balance is given by:

$$(V \rho C_p)_{block} \frac{dT}{dt} = \frac{\epsilon_c \epsilon_A \sigma S}{\epsilon_c + \epsilon_A - \epsilon_c \epsilon_A} (T_2^4 - T^4)$$

The solution of this differential equation, with the starting condition $T = T_1$ for $t = 0$, is given by:

$$\frac{1}{T_2^3}\left\{\frac{1}{4}\ln\left(\frac{T - T_2}{T + T_2}\cdot\frac{T_1 + T_2}{T_1 - T_2}\right) - \arctan\frac{T}{T_2} + \arctan\frac{T_1}{T_2}\right\} =$$

$$= -\frac{\sigma\,\varepsilon_c\,\varepsilon_A\,S}{\varepsilon_c + \varepsilon_A - \varepsilon_c\,\varepsilon_A}\,t$$

Because only small temperature variations are considered, some approximations may be made: $\frac{T_1 + T_2}{T + T_2}$ is set equal to one and arctan (T_1/T_2) - arctan (T/T_2) is neglected towards the logarithmic term. It remains:

$$\ln\frac{T - T_2}{T_1 - T_2} = 4T_2^3\,B\,t \qquad [4]$$

if for the sake of simplicity $\frac{\sigma\,\varepsilon_c\,\varepsilon_A\,S}{(\varepsilon_c + \varepsilon_A - \varepsilon_c\,\varepsilon_A)\,V\,\rho\,C_p}$ is set equal to B.

Equation [4] may also be written as:

$$\frac{T - T_2}{T_1 - T_2} = e^{-4T_2^3\,B\,t} \qquad [5]$$

From [5] a thermal resistance for radiation may be defined; if $\frac{1}{4T_2^3\,B}$ is considered to be a time constant the thermal resistance for radiation equals:

$$\mathscr{R}_r = \frac{1}{4T_2^3}\,\frac{\varepsilon_c + \varepsilon_A - \varepsilon_c\,\varepsilon_A}{\varepsilon_c\,\varepsilon_A\,S}$$

This resistance is defined within a small temperature interval. It appears to be strongly dependent upon temperature. Quantification of $\mathscr{R}_r$ requires an estimation of the emissivity coefficients. Emissivity coefficients are strongly influenced by the surface state.

It seems acceptable to assume both for the aluminium inner cylinder and the chromium plated outer cylinder a value of $\varepsilon = 0.1$ (15).

If S is taken as the average value of inner and outer surface area,

it is possible to calculate $\mathscr{R}_r$, *viz.* 160°C/W . The influence of T upon R_r can be seen from Fig. II.8 in which the radiation resistance is plotted as a function of the temperature for different values of ε.

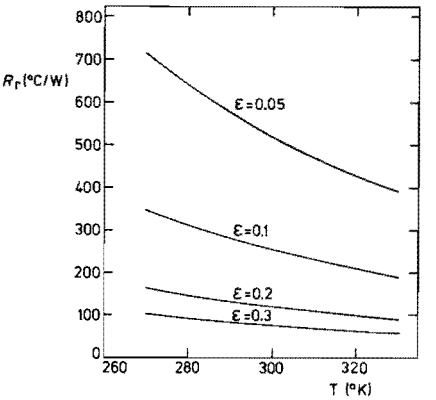

Fig. II.8

The influence of temperature upon the heat resistance of the vacuum room between inner and outer cylinder for several emissivity coefficients.

Comparing the value of $\mathscr{R}_r$ with that of $\mathscr{R}_c$ one may see that the two resistances are nearly equal. So improvement of the thermal isolation has to be found in both resistances. The transfer by radiation can be limited by applying one or more radiation shields. One shield, having the same emissivity coefficient as the opposing surfaces reduces the heat transfer to half the original value, whereas the use of shields with lower emissivities are more than proportionally effective. $\mathscr{R}_c$ might be enhanced by the use of supports of lower cross section or of a lower conductivity; *e.g.* teflon has a λ of 0.04 W/m°C. The attainment of a considerably lower heat transfer and consequently a higher time constant than the current calorimeter design seems possible with relatively simple measures.

The resulting thermal resistance amounts to

$$\mathscr{R}_t = \frac{\mathscr{R}_c \; \mathscr{R}_r}{\mathscr{R}_c + \mathscr{R}_r} .$$

The corresponding time constant is the product of this resistance and the heat capacity of the aluminium block (3900 J/°C); the magnitude is 3.74 x

10^5 sec at 300° K.

Temperature fluctuations caused by the temperature control of the thermostat have an amplitude of 0.003°C and a frequency of about 0.0085 sec^{-1} (one cycle in two minutes). The attenuation of these fluctuations is given by (16):

$$\frac{T_{surr}}{T_{int}} = \frac{1}{\sqrt{1 + \omega^2 \tau^2}} = 5.10^{-5}$$

So the fluctuations originating from control mechanism are attenuated to a level of 10^{-7} °C.

The third thermal connection between surrounding cylinder and calorimeter is established by the glass tubes. This connection differs from the other two in that it contacts the outer cylinder through glass tube and reaction vessel to the hot junctions of the thermopile. It opposes the influence of temperature fluctuations *via* $\mathscr{R}_t$. The magnitude of this resistance $\mathscr{R}_{gt}$ may be calculated from the dimensions of the glass tube (S = 14 mm^2; l = 14 cm) and the heat conductivity coefficient of glass (1.5 W/m°C): $\mathscr{R}_{gt} = 3.5 \times 10^4$ °C/W. The heat capacity of a copper vessel with cover is 63 J/°C. The time constant of the circuit ($\mathscr{R}_{gt}$ $\mathscr{C}_{s+v}$) amounts to 2.2×10^6 sec. This is about a factor 6 greater than the time constant of the circuit ($\mathscr{R}_t$ $\mathscr{C}_b$). In the case of silver vessels τ is about 10^5 sec ($\mathscr{C}$ = 8 J/°C and $\mathscr{R} = 1.2 \times 10^4$ °C/W); this is approximately a factor 4 smaller than the matching time constant. In this respect the use of the silver vessels is not an improvement. Apparently the optimal situation of equal time constants has not been reached. A difference in the long range stability after the replacement of the vessels was not noticed.

It might be repeated here that this thermal compensation for temperature fluctuations works for each vessel separately; it limits the temperature difference over each thermopile. Because of the non-ideality of this compensation, temperature differences between the hot and cold junctions remain. Symmetric temperature differences in both piles are compensated for electrically. However, this is only true in so far the sensitivities of the thermopiles are equal.

Electric compensation appeared to be meaningful; both for the copper and the silver vessels fluctuations in the zero line were about 40 times greater if no electric compensation was applied.

The two compensation mechanisms, thermal and electrical, do not reinforce each other necessarily. In particular cases they may even counteract. If e.g. the thermal compensation for one of the two vessels is perfect, then the ideal zero of this vessel may be spoiled because the incomplete thermal compensation of the other vessel generates an emf that adds an interfering signal.

Zero signal

A phenomenon reported by various authors (11, 17, 18) is an apparent heat effect that is seen in absence of any heat producing process. In our case this signal has a magnitude of about 1 to 2 μV and always has the same sign. It varied slightly between the different experiments but was nearly constant during an experiment. None of the authors explain the zero-signal fully. Wadsö and Monk (17) studied the influence of liquid flow velocities upon the magnitude of the effect in their flow microcalorimeter but did not explain the origin of the phenomenon.

A possible explanation may be found in an inhomogeneous temperature distribution in the thermostat. Temperature differences of at most $0.005^{\circ}C$ have been registrated. A temperature gradient in some direction over the calorimeter would cause a constant heat transfer through the thermopiles; in the very probable case of lack of symmetry a resulting emf remains visible. However, the replacement of the flat thermopiles by the cylindrically shaped ones did not diminish the signal, whereas in the cylindrical geometry, apart from the reference effect, much more internal compensation in one thermopile is to be expected. Therefore, the explanation of a heat flow across the calorimeter in some direction by a temperature gradient seems unlikely.

Another interpretation, also based upon temperature inhomogeneity, was investigated. A constant temperature difference between the entrance locations of the vapour dosing tubes gives rise to a remarkable heat flow circuit: entrance-glass tube-vessel-block-vessel-glass tube-entrance. A fall in temperature over this circuit causes a heat flow that is doubly "seen". It passes both thermopiles in such direction that the emf signals are added. The order of magnitude of the temperature difference required for the experimental zero-signal can be estimated. If the heat resistances of the aluminium block and the reaction vessels and thermopiles are neglected

compared to those of the glass tubes, ΔT becomes $0.3^{o}C$. This number is unrealistically high if it is compared with the measured number of $0.005^{o}C$. On account of a similar quantitative consideration a spurious heat flow through the circuit thermostat - $\mathscr{R}_c$ - $\mathscr{R}_{tp}$ - $\mathscr{R}_{gt}$ -thermostat must be precluded as an origin of the zero-signal.

REFERENCES

1. O. Kubaschewski, R. Hultgren, in "Experimental Thermochemistry", Vol. 2. Ed. H. Skinner, Wiley (Interscience), New York (1962) p. 343.
2. F. Wittig, N.P.L. Symposium No. 9 (1958), Met. Chem., H.M.S.O. (1959) p. 1A.
3. P.C. Gravelle, Adv. Catal. 22 (1972) 191.
4. J.L. Macqueron, MMe A. Gérie, M. Laurent, G. Sinicki, C.R. Acad. Sc., Paris, t 266 Serie B (1968) p. 1297.
5. H.A. Skinner, J.M. Sturtevant, S. Sunner, in "Experimental Thermochemistry", Vol. 2. Ed. H. Skinner, Wiley (Interscience), New York (1962) p. 157.
6. R.C. Wilhoit, J. Chem. Ed. 44, A 685 (1967).
7. J.L.C. van Geel, Thesis, Delft (1969).
8. J. de Jong, L. Marquenie, Instr. Practice 16 (1962) 45.
9. H. van Ooijen, Klei en Keramiek 17 (1967) 113.
10. R.A. Smith, F.E. Jones, R.P. Chasmar, "The detection and measurement of infrared-radiation", Oxford, Clarendon Press (1957) p. 204.
11. I. Chavet, J. Sc. Instr. 40 (1963) 391.
12. Ref. 10, p. 17.
13. Ref. 10, p. 49.
14. J.D. Boyd, J. of Physics E; Sc. Instr. 3 (1970) 432.
15. E. Schmidt, E. Eckert, Forsch. Ing.-Wes. 6 (1935) 175.
16. P. Harriot, "Process Control", McGraw-Hill, London (1964) p. 26.
17. P. Monk, S. Wadsö, Acta Chem. Scand. 22 (1968) 1842.
18. E. Calvet, H. Prat, "Recent Progress in microcalorimetry", (transl. by H. Skinner), Pergamon Press London, (1963).
19. A. Kelen, Appl. Sci. Res. B4 (1955) 309.
20. P. Gordon, Rev. Sci. Instrum. 25 (1954) 1173.
21. W.B. Mann, J. Res. Nat. Bur. Stand. 53 (1954) 277.
22. E. Calvet, H. Prat, "Microcalorimétrie, Applications Physicochimiques et Biologiques", Masson, Paris (1956).
23. D. Blet-Talbot, J. Phys. Radium 19, suppl. 7 (1958) 102 A.

CHAPTER III

CORRECTION OF THERMOGRAMS

III.1 INTRODUCTION

A serious problem in the interpretation of experimental thermograms has been indicated in the preceeding Chapter: a recorded thermogram is not a true representation of the thermogenesis. The thermal inertia of sample and vessel causes the signal to lag partly behind the origin of heat. The line shape of the heat flows becomes blurred. No direct information on the kinetics of the system in question can therefore be obtained.

In this respect the phenomenon is comparable to the broadening of spectroscopic absorption and of X-ray diffraction lines for that part which originates from instrumental characteristics. In both examples a finite interval of the quantity to be scanned, respectively wave length and diffraction angle, is needed to measure the wave intensity. As a consequence the intensities at different values of the scanned quantity are mixed up and the original intrinsic line shapes in the spectrum or diffraction pattern are deformed.

In thermokinetic experiments time may be considered as the scanning parameter. A heat flow measured at one definite time derives from contributions originating from many time intervals. As a result the information on the real heat flow is mixed up with regard to time.

In the system presently in discussion, this phenomenon appeared to predominate in the first phase of the experiments. The problem is related to the occurrence of two partly simultaneous phenomena; an adsorption process and a chemical reaction. The adsorption produces a relatively large

amount of heat in a short time. This heat needs a long time (100 to 200 min, dependent upon the type of heat flux meter) to flow to the heat sink. The actual reaction heat is measured not before the end of adsorption heat registration. However, as soon as it was measured as such, its distortion appeared to be small (see section 2 of this Chapter).

Although valuable information was obtained from the unaffected parts of the recorded thermograms, a full explanation of the kinetics pertinent to the reaction system was impossible. A better insight required information from the period in which the adsorption heat obscured the heat of reaction. For this reason it was tried to reconstruct the thermogenesis of the reaction in its beginning phase.

III.2 QUANTITATIVE FORMULATION OF THE PROBLEM OF DISTORTION

Stating the problem of distortion is equivalent to finding the answer to how to reconstruct the thermogenesis from the thermogram.

Provided that the calorimetric measuring system is a linear system, which will be shown to be true in section III.4, several methods are available to calculate the thermogenesis (f) from the thermogram (h). Characteristic for a linear system are its proportionality between output and input signal and the additivity of different input signals (1). For a linear system the relation between f and h may be derived, if the response curve (g) is known. The response curve is defined as the pattern of the thermogram that originates from an infinitely short heat flux pulse (2). A narrow block pulse may be considered as a reasonable and practicable approximation to a Dirac function (see Fig. III.1).

Any arbitrary real heat flux function can be considered to be composed of a number of subsequent approximate Dirac functions, each of different height (see Fig. III.2). Each separate pulse gives a contribution to the final thermogram, this contribution being of the shape of g. All contirbutions can be added, if linearity of the system is assumed.

Quantitatively the relation between f and h may be derived as follows. If the time is split up into intervals of width Δx, the total heat flow appearing in the thermogram at time $n\,\Delta x$ is given by the summation of the respective contributions of all preceeding intervals. The contribution from the pulse at time $i\,\Delta x$ to the function h at time $n\,\Delta x$ is given by:

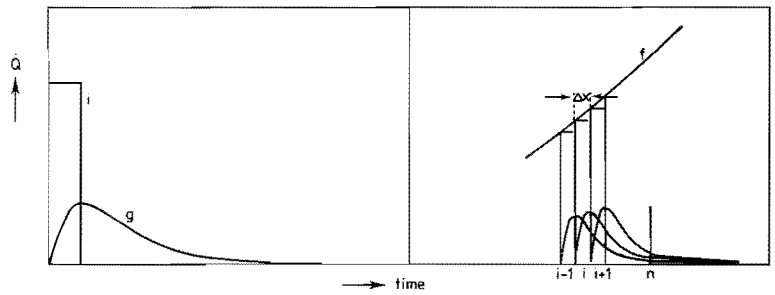

Fig. III. 1
Measurement of the response curve: the block signal (i) is an approximation of a Dirac pulse; g is the response curve.

Fig. III. 2
A heat flux curve (f) may be separated into approximate Dirac pulses, each of which gives rise to a contribution of shape g in the thermogram.

$$h(n\ \Delta x)_i = f(i\ \Delta x)\ g\{(n-i)\Delta x\}$$

The total measured flux is found by summation over all pulses prior to n:

$$h(n\ \Delta x) = \sum_{i=1}^{n} f(i\ \Delta x)\ g\{(n-i)\Delta x\}\ \Delta x$$

or

$$h(n) = \sum_{i=1}^{n} f(i)\ g(n-i) \quad \text{if } \Delta x \text{ is taken as unit of time.}$$

For infinitely short time intervals this summation may be written as an integral:

$$h(x) = \int_{o}^{x} f(y)\, g(x-y)\, dy \qquad [1]$$

Usually h(x) is called the convolution product of f and g and may be formulated more compactly as:

$$h(x) = f(x) * g(x) \qquad [2]$$

Apparently the thermogenesis f is connected to the experimental thermogram h through the response curve. The response curve is characteristic for a calorimeter plus sample. Its shape is determined by the total thermal path

between the place of thermogenesis and the heat sink. Its experimental determination is always a delicate problem in chemical kinetics. This will be discussed in section 5 of this chapter.

III.3 METHODS FOR CORRECTION

Several methods may be applied to find f, if h and g are known. In his review (3) Gravelle mentions three methods:

a. Manual correction
b. Analog correction
c. Off-line procedures.

Ad a. In this method the response curve is considered to be a series composed of exponentials. This view emanates from a general theory on heat flow calorimetry developed by Laville (4), who represents a heat flow calorimeter by a simplified thermal model in order to give a quantitative treatment of its behaviour. The model describes the heat flow calorimeter (see Fig. III.3) as a heat conducting body receiving a heat flow through a definite fraction of its surface (S_1) and losing heat through another fraction (S_2).

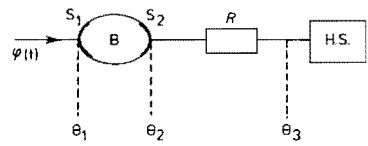

Fig. III.3

The thermal model of Laville (4) for a heat flow calorimeter.

φ (t)	heat flow to be measured	$\mathscr{R}$	measuring thermopile
B	vessel plus contents	HS	heat sink
S_1	heat receiving surface area	θ	temperature
S_2	heat losing surface area		

The lost heat flows through a thermal resistance, the measuring thermopile, to the heat sink; the driving force is the temperature difference over the thermopile. From the fundamental equation for heat conduction

$$\frac{\delta\theta}{\delta t} = \frac{\lambda}{\rho c_p}(\nabla^2\theta + w)$$

and the boundary conditions

$$K \frac{d\theta_1}{dn_1} = \varphi(t) \quad \text{and} \quad K \frac{d\theta_2}{dn_2} + P(\theta_2 - \theta_3) = 0$$

the temperature dynamics of this system may be described. The expression found for the response curve is:

$$g(t) = \sum_{i=1}^{\infty} a_i \, e^{-t/\tau_i}$$

The assumption that the sample receives its heat on a definite part of its surface is subject to objections. It is realistic only if the response curve is measured by feeding heat into the sample locally, which is certainly not an ideal method. Although the procedure is frequently used, it is too rough an approximation for investigations on adsorbents and catalysts. The model of Laville does not account for a homogeneously distributed thermogenesis in a solid or liquid sample.

Notwithstanding this inherent imperfection it appears to be possible in practice to describe response curves satisfactorily by a limited number of exponentials, usually not more than four (5).

The time constants of the exponentials (τ_i), and the pre-exponential factors (a_i) of the separate terms may be found in different ways from the g-curve. In simple cases the time constants may be read from a graphical

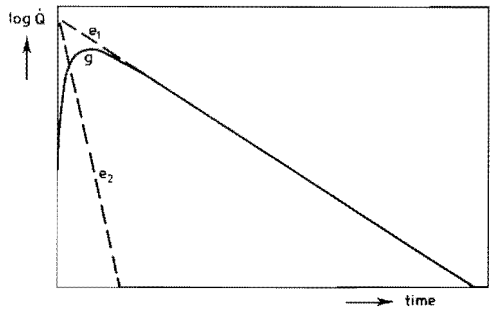

Fig. III.4

The analysis of a response curve composed of two exponentials: $g = e_1 + e_2$. The straight part of log g, extrapolated to $t=0$, represents e_1. The difference between g and e_1 represents e_2.

plot; this is shown in figure III.4. Valeur and Moirez (6) mention a number of other useful methods to separate a function in its component exponentials; the method of modulating functions is described in detail. Direct search methods are sometimes useful in solving the problem (7). Generally the methods operate the better, the more the time constants differ in value mutually.

The manual correction method, conceived by Calvet and Camia (8) is fully described by Garrigues a.o. (9). It comprises successive corrections for each of the time constants, which have to be known with great precision. The method presumes that each time constant delivers a contribution to the total distortion of the thermogenesis. The relation between the distorted thermogram and the thermogenesis is reflected in the following equations (10):

$$h_1(t) = h(t) + \tau_1 \frac{dh(t)}{dt}$$

$$h_2(t) = h_1(t) + \tau_2 \frac{dh_1(t)}{dt}$$

$$\vdots$$

$$h_n(t) = h_{n-1}(t) + \tau_n \frac{dh_n(t)}{dt}$$

The h_i's represent observables that have been corrected for distortions corresponding to time-constants 1 through i. The thermogenesis is given by:

$$f(t) = \lim_{n \to \infty} h_n(t)$$

By construction of the tangent to a definite h-curve for a number of points the correct correction terms may be found. The resulting curve is subjected to the same procedure.

The method is quite laborious; only two successive corrections are practicable (3).

The largest time-constant (τ_1) is evidently responsible for the largest correction in h. In most experiments the response curves of adsorbent samples have a τ_1 of about 7 minutes. In case of sarin decomposition experiments the heat development at 100 minutes is in good approximation given

by $h = \frac{A}{t}$ (A is constant). It follows that $\tau_1 \frac{dh}{dt} = -\frac{\tau_1 A}{t^2}$. The relative amount of the correction at 100 minutes is about 7% and diminishes rapidly thereafter.

Ad b. The analog or on-line method also requires an analysis of the response curve in a number of exponentials. In fact it is an automation of the manual correction method. The procedure is an immediate compensation in the electrical output for each time constant (5). This is realised by the operation of a series of electrical RC-circuits upon the calorimeter output signal. The number and time-constants of these circuits correspond quantitatively to the time constants of the response curve. The electrical scheme is shown in figure III. 5. From this it can be derived that an input h_i is transformed to an output h_{i+1} through the equation

$$h_{i+1} = \frac{R_2}{R_1} (h_i + R_1 C_i \frac{dh_i}{dt})$$

under the condition that $R_2 \ll R_1$. This requirement necessarily reduces the magnitude of the signal and forces to strong intermediate amplifications.

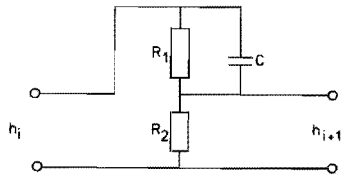

Fig. III. 5

One stage of an electrical compensation circuit; the number of stages is equal to the number of exponentials in the response curve; for symbols and further explanation see text.

The great advantage over other methods is the instantaneous character of the correction. However, the required amplifications between the successive steps introduce an electrical noise level that is unacceptable for high demands of sensitivity.

Ad c. Two off-line calculation procedures were developped by Brie, Guivarch and Petit (11). The convolution product of equation [1] may be rewritten as a summation:

$$h(n) = \sum_{i=0}^{n} f(i)\, g(n-i) \qquad n = 0, 1, 2, \ldots$$

This summation comprises n+1 equations and n+1 unknowns f_i:

$$h(0) = f(0)\, g(0)$$
$$h(1) = f(0)\, g(1) + f(1)\, g(0)$$
$$h(2) = f(0)\, g(2) + f(1)\, g(1) + f(2)\, g(0)$$
$$h(3) = f(0)\, g(3) + f(1)\, g(2) + f(2)\, g(1) + f(3)\, g(0)$$
etc.

For physical reasons $h(0) = g(0) = 0$; the system then reduces to:

$$h(1) = f(0)\, g(1)$$
$$h(2) = f(0)\, g(2) + f(1)\, g(1)$$
$$h(3) = f(0)\, g(3) + f(1)\, g(3) + f(2)\, g(1)$$
etc.

So n equations with n unknowns are left and the system is consequently mathematically solvable. However, the solution which is found is physically not meaningful. It is easily seen, that starting at the first equation, an unknown f_i is explicitly found from every equation. In this procedure the large experimental error inherent in low g and h values accumulates, causing an ever stronger oscillation in the f values; the system is said to be unstable (12). Brie and co-workers describe two methods to overcome the physical insolvability of the system. The first method utilizes "state function theory" (12, 13). The transfer function of the system has to be deduced from a representation of the response curve in exponentials. In the second method an optimal time domain matrix [D] is constructed, which transposes the experimental curve into the thermogenesis:

$$\bar{f} = [D]\, \bar{h}$$

This mathematically much simpler method is only slightly less accurate than the method using state function theory. A smoothing procedure is required to prevent excessive fluctuations in f.

The methods have been tested for artificial functions containing no random error in a fictitious calorimeter (2). Generally the deviation between input and calculated thermogenesis did not exceed 2%; for unfavourable functions (block pulses e.g.) the deviation amounted to 6% at most. It is stated, that at an experimental precision of 0.01% the deviations in the thermogenesis are limited to about 6 percent.

The limit of precision of the experiments performed with the calorimeter described in Chapter II is set by the recorder and amounts to about 0.5% full scale. The relative error in the experimental curve may amount to some percents, therefore. This means that the error is a hundred times greater than the one which is included in the imaginary experiments of Brie. Application of his methods might have been useless on account hereof.

In the present work the solution of f from the convolution product $h(x) = f(x) * g(x)$ has been performed by means of Fourier analysis and synthesis. The method comprises the calculation of the Fourier transforms of both the experimental and the response curve. The response curve needs not be analysed in component terms, which is a distinct advantage of practical nature above all methods mentioned by Gravelle. Moreover, the need to describe the calorimeter in terms of a definite model (*e.g.* that of Laville) becomes superfluous.

Fourier analysis and synthesis is often applied in the calculation of line shape correction for X-ray diffraction patterns. Recently the method has been mentioned by Rojas (14) as a means to correct thermograms. The general procedure is given by Stokes (15) and will be summarized here.

For physical reasons the functions h, g and f must be integrable *i.e.* the integrals

$$\int_{-\infty}^{+\infty} f(x)\,dx, \quad \int_{-\infty}^{+\infty} h(x)\,dx \quad \text{and} \quad \int_{-\infty}^{+\infty} g(x)\,dx$$

have finite values. In practice a limited time interval only is relevant. The value for all three functions is negligible for times greater than, say a/2 and zero for $t < 0$. The concerned functions may be written as their Fourier series:

$$f(x) = \sum_{t=-\infty}^{\infty} F(t) \exp(-2\pi i x t/a) \qquad [3]$$

$$h(x) = \sum_{t=-\infty}^{\infty} H(t)\ \exp(-2\pi ixt/a) \qquad [4]$$

$$g(x) = \sum_{t=-\infty}^{\infty} G(t)\ \exp(-2\pi ixt/a) \qquad [5]$$

The convolution product becomes:

$$h(x) = \int_{-a/2}^{a/2} f(y)\ g(x-y)\,dy \qquad [6]$$

The complex Fourier coefficients H(t) are given by:

$$H(t) = \frac{1}{a} \int_{-a/2}^{a/2} h(x)\ \exp(2\pi ixt)/a)\,dx \qquad [7]$$

Similar expressions are valid for G(t) and F(t). If F, G and H from equations [3], [4] and [5] are substituted into [6] one obtains:

$$h(x) = \sum_{t}\sum_{t'} F(t)\ G(t') \int_{-a/2}^{a/2} \exp\{-2\pi iy(t-t')/a\}\exp(-2\pi ixt'/a)\,dy$$

If one considers that the integral is zero for $t \neq t'$ and that it equals a for $t=t'$, it may be written:

$$h(x) = a \sum_{t} F(t)\ G(t)\ \exp(-2\pi ixt/a)$$

Comparing this equation with [4] one concludes that

$$H(t) = a\ F(t)\ G(t) \quad \text{or} \quad F(t) = \frac{1}{a}\,\frac{H(t)}{G(t)} \qquad [8]$$

In words equation [8] states that the Fourier transform of the thermogenesis is the quotient of the Fourier transforms of the thermogram and the response curve respectively.

If [8] is substituted into [3] one obtains:

$$f(x) = \frac{1}{a} \sum_{t=-\infty}^{\infty} \frac{H(t)}{G(t)} \exp(-2\pi ixt/a) \qquad [9]$$

This formula explicitly expresses f(x) as a function of the Fourier transforms H(t) and G(t), which may be derived from the experimental curves h and g. In fact [9] represents the inverse Fourier transform of F(t).

Because H and G are complex quantities, F has also a real and an imaginary part, derived as follows:

$$aF(t) = \frac{H(t)}{G(t)} = \frac{H_r(t) + iH_i(t)}{G_r(t) + iG_i(t)}$$

$$F_r = \frac{H_rG_r + H_iG_i}{G_r^2 + G_i^2} \quad \text{and} \quad F_i = \frac{H_iG_r - H_rG_i}{G_r^2 + G_i^2}$$

From equation [3] it follows:

$$f(x) = \sum_{t=-\infty}^{\infty} \{F_r(t) + iF_i(t)\} \{\cos(2\pi xt/a) - i \sin(2\pi t/a)\}$$

$$f(x) = \sum_{t=-\infty}^{\infty} F_r(t) \cos(2\pi t/a) + F_i(t) \sin(2\pi xt/a) + i \{F_i(t) \cos(2\pi xt/a) - F_r(t) \sin(2\pi xt/a)\}$$

Upon summation the imaginary terms vanish because:

$$F_i(t) \cos(2\pi xt/a) = -F_i(-t) \cos(-2\pi xt/a)$$

and

$$F_r(t) \sin(2\pi xt/a) = -F_r(-t) \sin(-2\pi\ xt/a)$$

It remains:

$$f(x) = \sum_{t=-\infty}^{\infty} F_r(t) \cos(2\pi xt/a) + F_i(t) \sin(2\pi xt/a)$$

The Fourier transformation calculations could be performed on a PDP 8/I computer with Fortran II as programming language. A SABR-coded

Fast Fourier Transform subroutine written by Cederquist and made available through Decus Program Library (16) was used. The subroutine computes the direct or inverse transform of a definite number of complex points; these numbers have to be a pure power of two with a maximum of 2^9 or 512. The points have to be sampled at equidistant intervals.

The maximum number of points to be transformed limits the total time interval on which the correction procedure can operate. Dependent upon the chosen period of sampling, the total length of the correction period is determined. The period of sampling (10 or 20 sec) was chosen on the ground of the response velocity in question. In all instances the h function had to be truncated before it had fallen below the detection limit. No method was available to decide *a priori* whether the neglect of the function values omitted would affect the fundamental usefulness of the correction procedure, nor if the sampling period was sufficiently short to contain all information.

III.4 TESTING OF THE FOURIER ANALYSIS

For reasons of security it was thought desirable to subject the Fourier analysis procedure to a practical test in order to verify its utility. The purpose of the test should be to learn whether the influence of some possibly disturbing factors would be prohibitively strong:

1) The random experimental error in the curve is about 0.5 percent full scale. Brie (2) mentions for his correction procedures, that an experimental error of 0.01 percent causes deviations of about 2 percent in the thermogenesis. So alertness in this respect is advisable.
2) Truncation of the experimental functions might be disastrous, because a part of the information is ignored.

The Joule-effect was chosen as a means to produce heat, because it is reproducible and relatively simple to establish with a reasonable accuracy.

The experimental arrangement for the test procedure was as follows. A solid copper cylinder which was internally equipped with an electrical resistor functioned as a heat source in one of the reaction vessels. The other vessel contained a similar block. At both sides covers and glass tubes were in their normal position. By choosing the correct dimensions for the cylinder, the longest time constant of the response curve was made about equal to the one for reaction vessel plus adsorbent filling; this is about 7 minutes. An electrical current source supplied energy to the resistor; by con-

tinuously measuring the voltage over this resistor the generated Joule-effect could be calculated. In this way a well defined heat production could be established.

Isolation section and reaction vessels were evacuated. The heat flow was sampled every 10 seconds. Temperature was 30°C.

Firstly, it was verified whether the calorimeter could be considered to be a linear system. To this end the sensitivity of the calorimeter in the test arrangement was measured separately. The sensitivity in stationary situations appeared to be independent of the input power up to at least 260 mW. Its magnitude was 19.04 μW/μV (see Fig. III.6), somewhat smaller than found earlier with a different electrical resistor. The lower sensitivity can be explained by the slower response velocity of the system. This causes a higher temperature in the resistor and consequently a higher gradient in the electrical leads to the resistor and therefore, a lower efficiency in the heat flow measurement. A loss by radiation may also be of some influence.

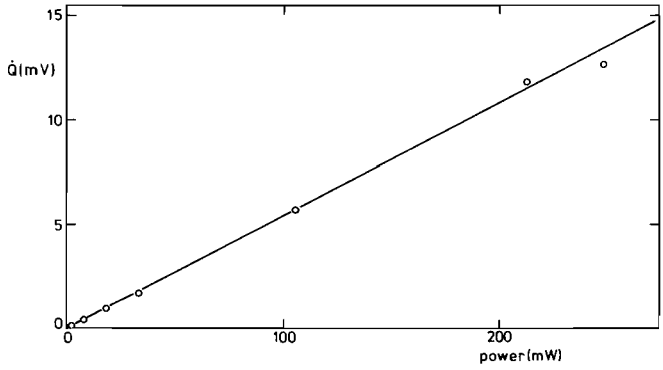

Fig. III. 6

Sensitivity measurement with an electrical resistance of 218 Ω; the sensitivity amounts to 19.04 W/V with a standard deviation of 0.31 W/V.

The additivity of signals was checked by an experiment shown in Fig. III.7. A 5 minutes lasting block pulse (fa) was recorded entirely; this curve is named h_a. After this two similar pulses were dosed with an interval of one minute in between them. The resulting thermogram (h_b) should coincide with the h-function calculated from addition of two h_a curves with a mutual time shift of 6 minutes. Additivity appears to apply, which follows

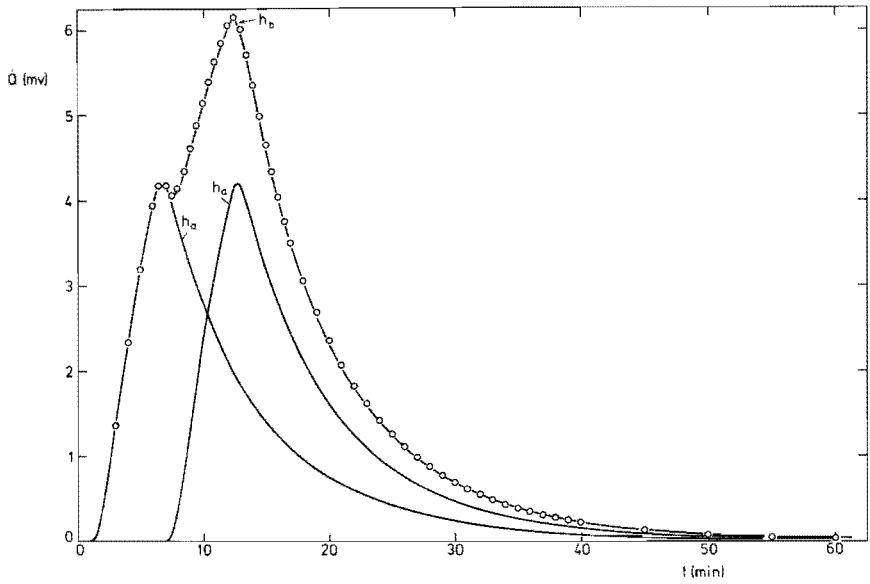

Fig. III.7

Heat fluxes appear to be additive. h_a Is the thermogram of one block pulse of shape f_a; h_b (full line) is the calculated sum of two h_a curves. The points represent the thermogram of two subsequent block pulses of shape f_a.

from the coincidence of h_b with the summation of the two subsequent h_a's.

The linearity of the system being confirmed within the boundaries of experimental precision a number of different f- and g-functions were generated:

1) With regard to g-functions the "dosing"-time was varied between 1 and 20 seconds. Within one dosing time pulses of different height were put in.
2) With regard to f a number of rather complex functions were presented to the measuring system:
   a. single block pulses, varying in height (1 to 280 mW) and width (5 to 10 minutes);
   b. a sequence of block pulses with a width of 5 minutes, alternating with very low heat development levels of the same width; the pulses continue during the entire interval measured;
   c. similar functions as measured in b, but with a smaller width (2 and 0.5 minutes);
   d. a high block pulse (120 mW), immediately followed by two small ones at a low level.

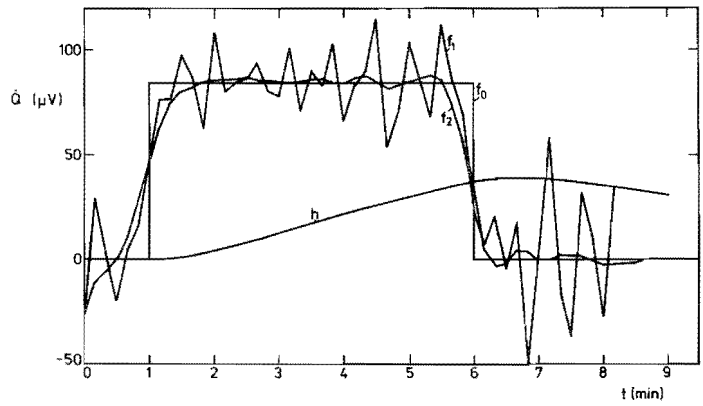

Fig. III. 8a

Reconstruction of a known thermogenesis consisting of one blockpulse.

f_0 original thermogenesis

h part of the recorded thermogram

f_1 reconstructed thermogenesis; number of smoothings: h one time, f_1 unsmoothed.

f_2 reconstructed thermogenesis; number of smoothings: h one time, f_2 four times.

All sampling times are included in the presentation of f_1 and f_2

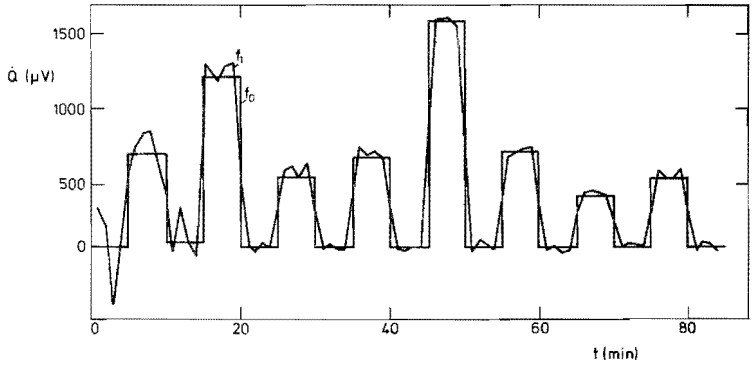

Fig. III. 8b

Reconstruction of a known thermogenesis consisting of a series of blockpulses; pulse widths are 5.0 min.

f_0 original thermogenesis

f_1 reconstructed thermogenesis

Because rather strong oscillations appeared to occur in the calculated thermogenesis curves, smoothing was applied. The number of smoothings was varied in some cases to estimate the effect of smoothing. The procedure is described in section III.6.

The consequence of truncation of the thermogram was investigated by cutting-off the experimental curve of one single block pulse, after definite fractions of the total heat amount had been recorded.

Figures III.8a-d show the reconstruction of a representative number of the thermogenesis curves carried out with a response curve that was found by a "dosing pulse" of about one second.

In Fig. III.8a the reconstruction of one single block pulse is given in its dependence upon the number of smoothings. The applied g-curve has a dosing time of 1.5 sec and the total amount of released heat is 20 mJ. The smoothed f-functions are satisfactory approximations of the real thermogenesis. Except for points at the very beginning there does not exist an influence in the final result, whether a smoothing treatment is given to h or to f, provided that the total number of smoothings remains constant. On account of the result found with this experiment a standard smoothing routine was chosen, that has been applied to nearly all kinetic experiments: smoothing of h was carried out one time and f was smoothed four times. The consequence is that sharp angles are rounded over a period of 0.5 minute. The deviations amount to about 3% at most.

The sequence of pulses (Fig. III.8b) over the entire interval is fairly well found back; the starting phase possesses rather large oscillations. The final pulses are remarkably well reconstructed. This might excite some surprise, because the thermogram has been cut off shortly hereafter, meaning that certainly not all the heat of these pulses has been taken into account in the corrective calculation. Correction of the same h-curve with a response curve of 10 sec and an amount of released heat of 12 J gives rise to an f_1-curve that is nearly identical.

The reconstruction of fast changing input signals is shown in Fig. III.8c (another instance is found in Fig. III.11). The pattern of the sequence of pulses with a width of half a minute is seen to be preserved, although the quantitative precision is lost. In the calculation the smoothing procedure has been carried out only once in order not to lose detailed information. Because one observation is made in every 10 seconds, only three sampling points cover each pulse.

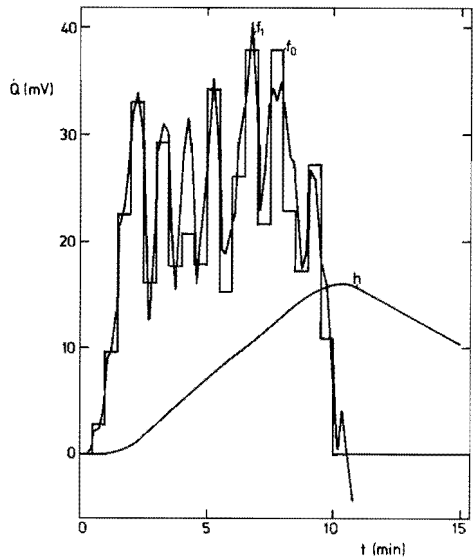

Fig. III. 8c

Reconstruction of a known thermogenesis; pulse widths are 0.5 min.

f_0 original thermogenesis

h recorded thermogram

f_1 reconstructed thermogenesis

The input presented to the calorimeter in the experiments shown in Fig. III. 8d is the most tedious one. The small heat evolutions following the big pulse are completely overshadowed in the thermogram. Nevertheless the two low levels are still recognisable. The curve f_1 was obtained by performing the smoothing procedure ten times. The sharp angles become more gently curved, but the f values can be seen to be "scrambled" over time intervals of 1.5 minutes at most. Usually calculated high pulses show some overshoot (see Fig. III. 12), which appeared to be a normal feature for thermogenesis curves found by Fourier analysis. Brie (2) also mentions this effect for his procedures. The overshoot stretches over only three to four time units.

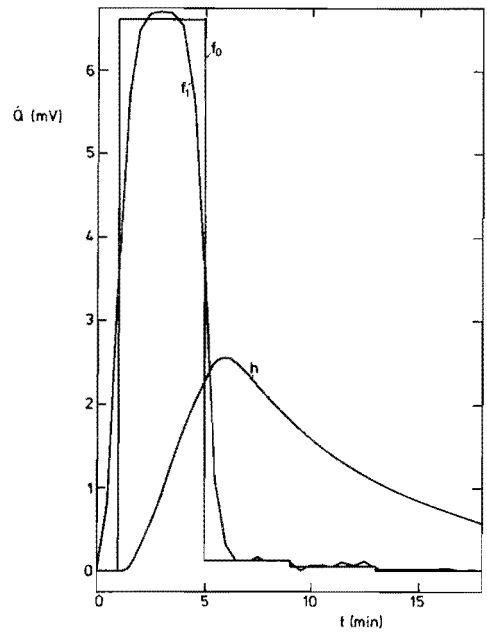

Fig. III. 8d

Reconstruction of a known thermogenesis consisting of a high pulse followed by two small pulses.

f_0 original thermogenesis

h part of recorded thermogram

f_1 reconstructed thermogenesis; f_1 has been smoothed ten times.

The effect of truncation of the thermogram is illustrated in Figures III. 9a, b and c. The input is a single block pulse of 10 minutes width. An integrated version of the thermogram is shown in Fig. III. 10. The reconstruction of the thermogenesis appears not to be affected when the relative amount of total heat, that is taken into account in the calculation, is decreased to 65 percent (see Fig. III. 9a and b). The oscillation becomes somewhat stronger. If the thermogram is truncated before the pulse has ended, the part before this point is not affected seriously. Fig. III. 9c shows that truncation at ten minutes leaves the reconstructed thermogenesis nearly unchanged until 8.5 minutes.

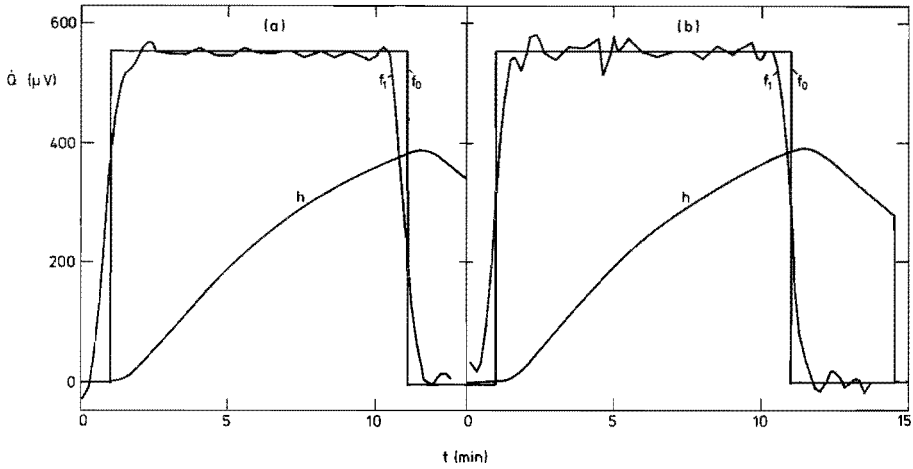

Fig. III. 9a and b

Reconstruction of a known thermogenesis, using the entire thermogram (a) and using the heat thermogram after truncation at 14.5 min (b).

f_0 original thermogenesis

h recorded thermogram

f_1 reconstructed thermogenesis

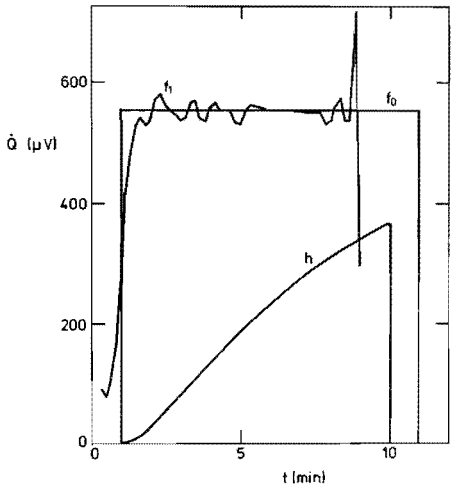

Fig. III. 9c

Reconstruction of the same blockpulse of Fig. III. 9a and b; the thermogram (h) was truncated at 10 min.

f_0 original thermogenesis

h recorded thermogram

f_1 reconstructed thermogenesis

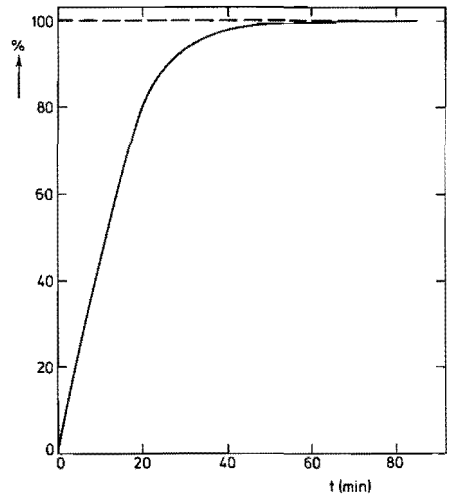

Fig. III. 10

Integrated thermogram of the block pulse used in the calculations illustrated in the Figures III. 9a, b and c.

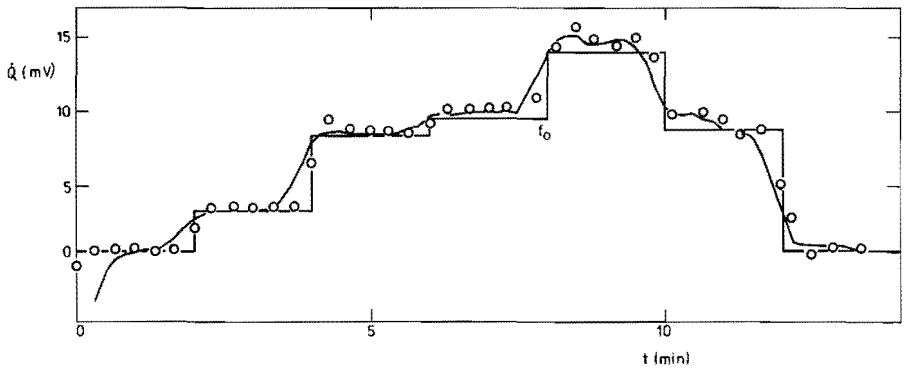

Fig. III. 11

Two reconstructions of one thermogenesis (f_o); corrected with a response curve determined with a block pulse of 1 sec (o) and corrected with a response curve determined with a block pulse of 20 sec (—).

The influence of the pulse width used in the finding of the response curve is limited, as already said. Variation between 1 and 20 seconds appears to lead to similar results (see Fig. III.11), except in the first four points. The approximation of a Dirac pulse apparently is not critical.

From these test experiments carried out on a thermally well defined system it may be concluded that the method of correction with the Fourier analysis operates satisfactorily for experiments obtained with the calorimeter of Chapter II. The random error of 0.5 percent is sufficiently small to suppress the resulting oscillation by smoothing without losing essential information. Truncation of the thermogram does not have a predominant influence upon the result. This is true, even when only a relatively small fraction of the total amount of heat is included into the calculation. A substantial broadening of the pulse that generates the response curve, does have only a minor influence upon the calculated f-functions.

The more gently curved thermogenesis functions of the chemical reaction system may be expected to be more suitable for the correction procedure. The limiting factor for the precision of correction of these curves must probably be found in the correctness of the response curves.

III.5 THE DETERMINATION OF THE RESPONSE CURVE

The response curve is a characteristic function of the calorimeter plus sample. Essentially two different approximations may furnish its pattern. Starting from a thermal model of the calorimeter, it is possible to describe the temperature dynamics by means of the law of Fourier

$$\frac{\delta\theta}{\delta t} = \frac{\lambda}{\rho c_p} \nabla^2\theta + \frac{W}{\rho c_p}$$

in which W is the heat generation; the other symbols have their usual meaning.

Provided that all thermal parameters in the model are known with a sufficient degree of accuracy, the response curve can be calculated by performing a hypothetical experiment. However, in many cases these parameters are not known or are hard to be determined. This is generally true in work on adsorbents and catalysts. In this respect the other approximation of the problem, a calibration method, is to be preferred; calibration accounts implicitly for all known or unknown parameters which are relevant

to the heat flow. In contrast to the explicit calculation method, however, a real experiment has to be performed. This experiment has to meet at least two requirements:

- a heat flow pulse of sufficiently short duration (Dirac function) has to be fed to the calorimeter contents;
- the path of the heat flow in the calibration experiment and the experiment proper must be very similar.

Both conditions are formulated not too strictly, because in practice valuable corrections have appeared to be possible, although g-curves are unevitably imperfect. According to Naslin (17) the demand concerning the duration of the heat flux pulse must be seen against the response velocity of the system. From the experiments carried out with electrical pulses, it has appeared that dosing times of 20 sec for a response curve with a time constant of 7 minutes are not too long.

Strictly speaking the only perfect measurement of a response curve of a calorimetric arrangement is hidden in the very experiment itself. When trying to find it, however, one closes a vicious circle. In order to overcome this problem one has to abandon perfection in the response curve in at least one of the two aspects mentioned. For each type of reaction an appropriate procedure might be thought of to approach the real g-curve as closely as possible. In catalyst investigations the g-curve is often measured by means of a heat flow pulse in an electric resistance wire that is added to the solid bed (2). The objection is obvious; the place of origin of heat is shifted from the adsorbent to a localized power centre that is absent in the experiment proper. The thermal paths are strongly different.

For the kind of experiment described here a different way of determining g is applied. Before every kinetic experiment the g-curve of the sample was registrated by means of a cyclohexane adsorption experiment. This method aimes at identical paths but is less good fit to the demand of a Dirac function.

A block-pulse heat evolution is approached by dosing cyclohexane to the adsorbent during a short time. Cyclohexane is adsorbed physically; it is distributed quickly and homogeneously over the adsorbent surface. On account of the experience gained with the test experiments a dosing time of 5 to 15 seconds was judged to be sufficiently short. After the curve had been recorded, a similar experiment could be carried out to measure a second g-curve, now originating from a desorption effect.

Although the adsorption pulse method is essentially better than the electrical pulse method, the resemblance between the thermal paths in cyclohexane and sarin adsorption has its limitations. In any mathematical model for the heat flow (thermal path) sarin and cyclohexane are represented by different parameters, causing different overall conductivity and capacity. This factor has been weighed experimentally and appeared to be very small. Two g-curves were recorded from one sample, one by adsorption of 95 mg of cyclohexane and the other by a partial desorption (80%) of this amount. Though a considerable mass difference in the final adsorbed phases does exist, the cumulative heat development curves do not show a difference that cannot be explained by the normal experimental error. So the replacement of an adsorbed amount of cyclohexane by sarin is very unlikely to significantly alter the response curve visibly. Influence of the different vapour pressures as dependent on the adsorbed amounts might have been expected. The vapour phase amounts being small, their influence should be found in the effect upon conductivity and not upon capacity. The absence of deviation, however, proofs that no significant difference in the overall heat conductivity occurs.

The role of the gas phase in the overall heat conductivity has been examined in a separate experiment. After a cyclohexane adsorption, helium was added up to a total final pressure of 12 Torr. No change in the longest time constant of the response curve was observed. Apparently the amount of helium does not affect the conductance of the adsorbent bed to a degree as to change the response velocity.

For this reason it may be concluded that the vapour phase conduction in case of sarin adsorption will not give rise to a response curve deviating from the one found by cyclohexane adsorption.

With two g-curves, one originating from adsorption of cyclohexane and the other from desorption, the correction procedure was carried out on a sarin adsorption experiment on the same sample. The corrected curves do not deviate mutually more than 4% (see Fig. III.12). Even more important is the fact that the general shape in both cases is the same; the strong effect caused by adsorption is reconstructed similarly.

A second limitation in the resemblance between cyclohexane and sarin adsorption is the inhomogeneity in sarin distribution over the surface. From experiments carried out with radioactive sarin (see Chapter IV) it appeared that the sarin adsorption process in a full cylindrically shaped adsorbent

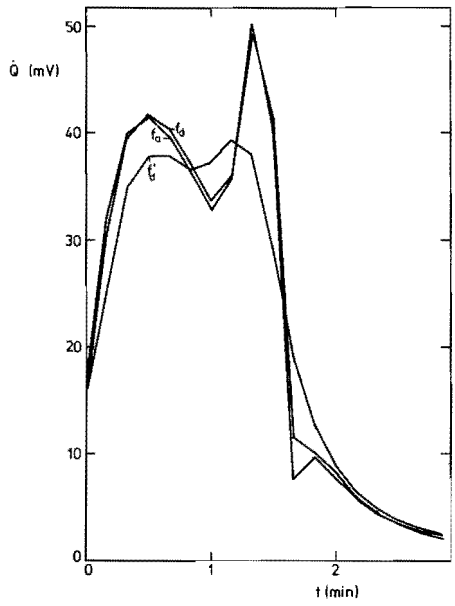

Fig. III. 12

Three reconstructions of the first stage of a sarin decomposition experiment on alumina. Corrections were made with response curves determined by adsorption (f_a) and desorption (f_d) of cyclohexane; f_d' represents the four times smoothed curve f_d.

bed takes place unevenly. A part with a high sarin concentration (near the vapour inlet) co-exists along with a fraction that is totally uncovered with adsorbate. A g-curve, determined by means of cyclohexane adsorption, seems to be unreliable for adsorbents piled up in a full cylindrically shaped bed; consequently, correction for the experiments involved has not been made. The problem of the inhomogeneous sarin adsorption is much less serious when the adsorbent is piled up against the vessel wall. The thickness of the layer is about 1 mm and the dimensions of the granules vary between 0.25 and 0.50 mm. Only a very slight gradient of vapour pressure does exist over this layer. Except in cases of a very low surface coverage the adsorption may be assumed to be homogeneous over the granules.

III.6 SMOOTHING

Figure III.8a shows an unsmoothed thermogenesis curve obtained by means of Fourier analysis. Its fluctuating character is salient. In order to remove these fluctuations without losing information it was judged useful to smooth the curve. Two smoothing procedures were available.

The first method is based on Fourier transformation and seemed very convenient for this reason. Rapid fluctuations (noise) in a function are reflected in non-zero values for high frequency numbers in its Fourier transform. If these values are set equal to zero the inverse transformation delivers the original function without noise. A practical application of this method is described by Hayes a.o. (18). Essentially the method comprises 1. a Fourier transformation of the function to be smoothed; 2. a smoothing function to truncate the high frequencies in the Fourier spectrum; 3. an inverse transformation to the time domain. However, in applying this method to the thermogenesis curves of sarin decomposition, erroneous results were obtained.

Another, mathematically simpler method, appeared to give satisfactorily smoothed thermogenesis curves. In this procedure the heat flux is given a new value for each sampled time. If n_i is the heat flux of point number i the new value is found from

$$n_i' = \frac{n_{i-1} + 2n_i + n_{i+1}}{4}$$

It is easily seen that the function integrated in the total time interval is not changed significantly.

The fluctuations in f originate from the experimental errors in the observed h-curve. It seemed to be useful, therefore, to apply the procedure first to the function h. In the standard correction routine, adopted for most of the experiments, h was one time and f was four times smoothed. From Fig. III.12 also a comparison can be made between the unsmoothed and the four times smoothed f-curve of a sarin adsorption experiment. From this figure it is seen that the relevant function shape remains unaffected by the smoothing procedure.

Unless otherwise stated, correction includes one smoothing procedure of the thermogram (h) and four of the calculated thermogenesis (f).

REFERENCES

1. C. Brie, J.-L. Petit, P.C. Gravelle, C.R. Acad. Sc. 273 (1971) 1.
2. C. Brie, Thèse, Lyon, (1971).
3. P.C. Gravelle, Adv. Catal. 22 (1972) 191.
4. G. Laville, C.R. Acad. Sc. 240 (1955) 1060.
5. Y. Thouvenin, C. Hinnen, A. Rousseaux, Colloq. Int. Cent. Nat. Rech. Sci. 156 (1967) 65.
6. B. Valeur, J. Moirez, J. Chim. Phys. 70 (1973) 500.
7. R. Hooke, T.A. Jeeves, J. Assoc. Comp. Mach. 8 (1962) 212.
8. E. Calvet, F.M. Camia, J. Chim. Phys. 55 (1958) 818.
9. J.C. Garrigues, R. Roux, A. Valette, Colloq. Int. Cent. Nat. Rech. Sci. 156 (1967) 357.
10. F.M. Camia, Journées Int. Transm. Chaleur, C.R., Paris 1961, (1962) p. 703.
11. C. Brie, M. Guivarch, J.-L. Petit, Proc. 1st Int. Conf. Calorimetry and Thermodynamics, Warschau (1969).
12. R.C. Dorf, "Time-domain analysis and design of control systems", Addison-Wesley, Reading, Mass. (1964).
13. D.G. Schultz, J.L. Melsa, "State functions and linear control systems", McGraw-Hill; New York (1967).
14. E. Rojas Blasi, Thesis, Barcelona (1971).
15. A.R. Stokes, Proc. Phys. Soc. London, 61 (1948) 382.
16. G. Cederquist, Cooley Electronics Laboratory, University of Michigan, Ann Arbor, Michigan 48105.
17. P. Naslin, "Les régimes variables dans les systèmes linéaires et non linéaires", Dunod, Paris (1962), p. 83.
18. J.W. Hayes, D.E. Glover, D.E. Smith, Anal. Chem. 45 (1973) 277.

CHAPTER IV

MOBILITY OF ADSORBED SARIN

IV.1 INTRODUCTION

From the thermokinetic investigations described in the Chapters V and VI the problem arose, whether adsorbed sarin is mobile or not.

If adsorbed sarin is mobile, it is principally possible that the sarin molecules, after being adsorbed, redistribute over the surface to positions that are energetically more favourable. The duration of the accompanying heat effect is dependent upon the kinetics of this redistribution process. During this period the heat flow pattern drawn by the decomposition of sarin might be disturbed, so that no unequivocal information on the reaction kinetics is obtained. Clearly this problem is connected to the lack of specificity of the calorimetric technique.

The purpose of the experiments described in this chapter was to estimate the mobility of adsorbed sarin. A method that utilizes radioactive sarin was developed. The principle of the method is as follows.

If a vapour is dosed onto a serried adsorbent bed, it is likely to be adsorbed first in the upper layer and gradually in lower parts. If the dosing is stopped at a moment the distribution is still uneven, it depends upon the type of adsorption what happens to the adsorbate. If the adsorption is immobile, the distribution does not change. In case of mobile adsorption the vapour is redistributed over the surface under influence of the two-dimensional pressure. If the adsorbate is radioactive, the local radiation intensities generally change. The variation of these intensities gives an indication of the mobility.

IV.2 EXPERIMENTAL

Adsorbents and adsorbate

Three adsorbents were investigated: carbon black (Regal 400), carbon black impregnated with chromium oxide (2.9% weight percent chromium) and Ketjen alumina. Further properties of these adsorbents are given in Chapter V.1.2. All samples were grained; sieve fractions between 0.25 and 0.50 mm were used.

^{32}P sarin was synthetized in the Chemical Laboratory TNO according to a procedure described by De Borst (1). The specific activity was approximately 25 μCi/g.

Procedure

The experimental setup is schematically shown in Fig. IV.1. It comprised a vacuum pumping system consisting of a rotary pump (A), a mercury diffusion pump (B) and a liquid nitrogen trap (C), an adsorbent vessel (G), a Geiger-Müller counter (K), a dosing vessel for liquid radioactive sarin (F) and pressure gauges (D, E). A cooling device (H) provided the possibility to establish low relative vapour pressures.

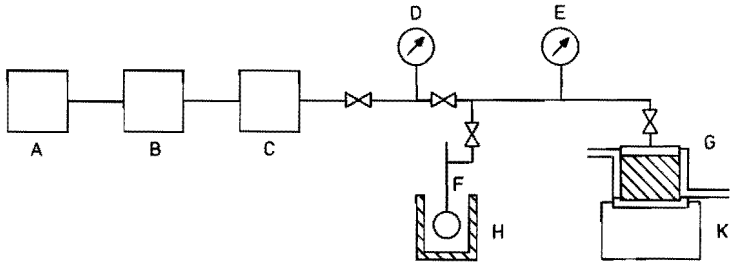

Fig. IV.1

Schematical view of the adsorption apparatus (see text for explanation).

The adsorbent vessel, described in (2), was constructed in a way to ascertain a fixed and reproducible geometry of the adsorbent bed with respect to the window of the GM counter.

The dosing procedure was identical to the one utilized in thermoki-

netic measurements. The adsorbent was evacuated to a pressure lower than 10^{-4} Torr. During a short time sarin was admitted; the vapour was generated from the previously evacuated and weighed dosing vessel containing ^{32}P sarin. Without further addition of sarin vapour, the radioactivity was measured as a function of time. The dosing vessel was cooled down to $-10^{o}C$ during an hour to condense gaseous sarin from the room connecting adsorbent and dosing vessel. The decrease in weight of the vessel gave a measure of the amount adsorbed sarin.

The measured radioactivity was corrected for background, dead time of the counter and decrease in specific activity as a result of the decay of ^{32}P.

IV.3 RESULTS AND DISCUSSION

The experimental parameters of the measurements are summarized in Table IV.1.

Table IV.1

Experimental parameters of ^{32}P sarin adsorption for mobility measurements.

	Cr contents (%)	dosing time (min)	bed height (mm)	W_a sarin (mg)	overall coverage (%)
carbon black	0	1	10	63	33
	0	1	20	35	9
	0	1	30	30	5
	2.9	4.5	11	5	2.5
alumina	0	0.85	11	32	9

For the carbon adsorbents the change in measured radioactivity as a function of time is given in Figures IV.2a,b and c. It is seen that the pure carbon black samples show an increase in activity with time. Apparently the sarin molecules are initially adsorbed in the upper layer of the carbon bed and migrate gradually downward. Two effects are responsible for the increase in counting efficiency: (a) the geometry becomes more favourable and (b) the average height of the absorbing layer decreases.

From the experiment with a bed height of 3 cm it is seen clearest

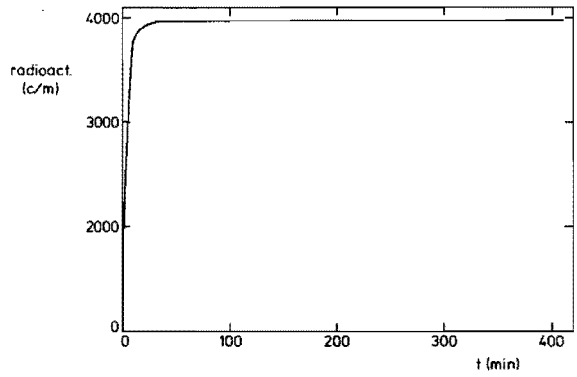

a

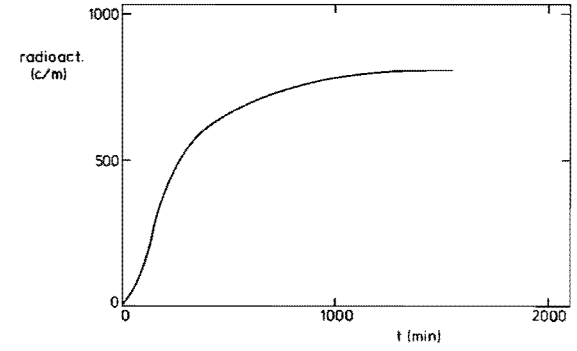

b

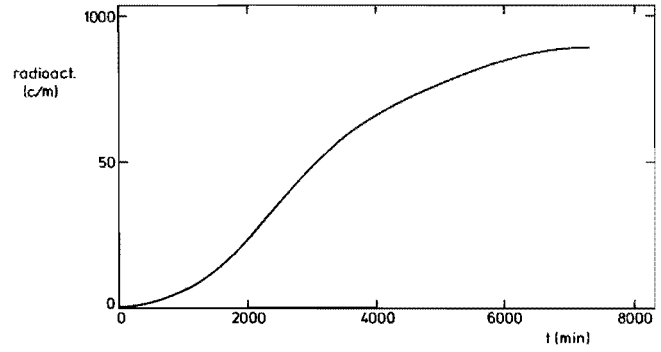

c

Fig. IV.2

^{32}P sarin adsorption on carbon black. Increase of measured activity as a function of time: a) bed height 10 mm, α = 0.33; b) bed height 20 mm, α = 0.09; c) bed height 30 mm, α = 0.05.

that the migration over the carbon surface only very slowly establishes a homogeneous distribution.

If a chromium oxide impregnation is added to the carbon, the mobility vanishes as is seen from Fig. IV.3.

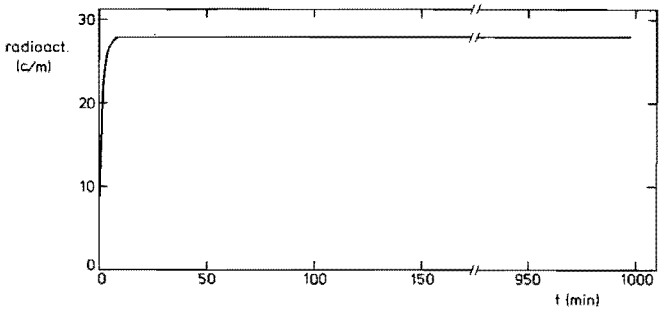

Fig. IV.3
^{32}P sarin adsorption on carbon black impregnated with chromium oxide; bed height 11 mm, α = 0.025.

Sarin adsorbed on alumina was expected to be immobile. Therefore, it was tried to find first a critical bed height which was favourable to detect sensitively the movement of sarin to lower layers.

In a separate vessel ^{32}P sarin was dosed to a large amount of alumina up to an overall coverage of 50%. The adsorption vessel was filled stepwise with this material, while between two subsequent steps the radioactivity was measured; the results are shown in Fig. IV.4. It appeared that contaminated alumina above a total height of about 14 mm does not contribute to the signal in the GM counter observably.

It appeared favourable to choose a bed height of about 10 mm. In a region at this distance to the GM window, a possible movement of sarin downward is detectable, while a dosage of sarin to the adsorbent may be least expected to cover the alumina directly to an even distribution. Fig. IV.5 shows the result of a dosage of 32 mg ^{32}P sarin to 3.3 g of alumina, constituting a total bed height of 11 mm; the total surface area amounts to about 590 m^2. According to Lippens (3) the surface area of one molecule in an adsorbed monomolecular layer is given by:

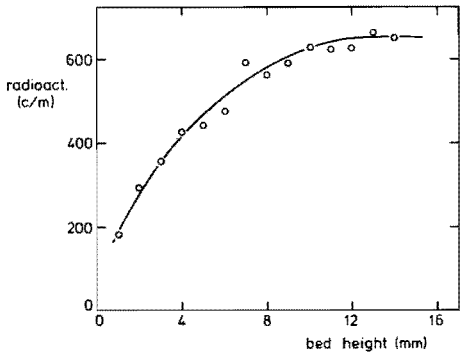

Fig. IV.4

Determination of the critical bed height for alumina; the surface of the adsorbent is covered to about 50% with ^{32}P sarin.

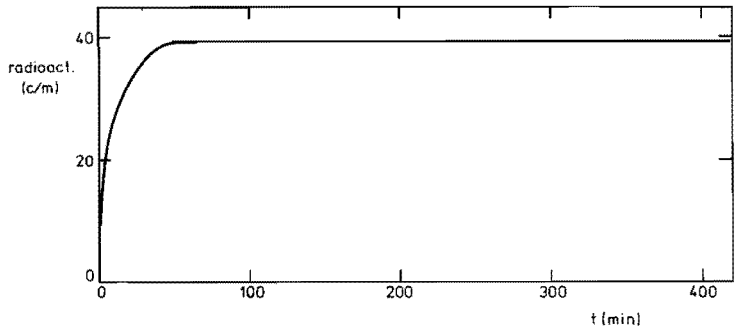

Fig. IV.5

^{32}P sarin adsorption on alumina; bed height 11 mm, α = 0.09.

$$S = 1.530 \quad \sqrt[3]{M^2 V_{sp}^2} \quad \text{Å}^2$$

where M is the molecular weight and V_{sp} the specific volume of the adsorbate in liquid phase expressed in ml/g. Because for sarin M = 140 and V_{sp} = 1.09 ml/g the molecular area amounts to 44 Å^2. In a monomolecular layer 1 mg sarin covers a surface area of 1.7 m^2.

If the adsorbed 32 mg sarin constitute a monomolecular layer in the upper part of the bed, the coverage is confined to the highest layer

of 1 mm thickness. In view of the relatively low initial increase in activity, the fraction adsorbent which is actually covered, seems to be small indeed; a rather sharp line divides the covered and uncovered alumina. Notwithstanding this high concentration gradient, no increase in radioactivity was detected at all. This proves unequivocally that the adsorption of sarin is immobile.

This conclusion agrees with the result of an experiment performed in the calorimeter, in which 80 mg ^{32}P sarin was dosed to a 20 mm high alumina bed. After the thermokinetic curve of this experiment had been recorded during 48 hours, the bed was separated into three equal layers. The radioactive intensities of these three fractions had a ratio of 81:12:7 (from upper to lower layer), showing that the adsorption had been limited largely to that part of the adsorbent where the adsorbate entered the bed.

IV.4 CONCLUSION

Adsorbed sarin is immobile on the oxidic surfaces of alumina and carbon black impregnated with chromium oxide. Sarin possesses relatively small mobility on a carbon black surface.

REFERENCES

1. C. de Borst, CL-Report 1973-5, Chemical Laboratory TNO, Rijswijk, The Netherlands (1973).
2. J. Medema, J.J.G.M. van Bokhoven, "Protection against toxic compounds", Chemical Laboratory TNO, Rijswijk, The Netherlands (1973), p. 71.
3. B. Lippens, Thesis, Delft (1961), p. 110.

CHAPTER V

THERMOKINETICS OF SARIN DECOMPOSITION

This chapter describes the experimental procedure that is followed to obtain thermokinetic data on the decomposition of adsorbed sarin. Apart from adsorption the heat development may be considered to originate from only one decomposition reaction.

The presentation of the results inevitably anticipates to some extent the interpretation of the kinetic information.

V.1 EXPERIMENTAL

V.1.1 Procedure during the thermokinetic experiments

A complete thermokinetic experiment comprises subsequently the following steps:

a. Pretreatment of the sample
b. Installation and equilibration of the calorimeter
c. Determination of response curve
d. Dosing of sarin
e. Measurement of heat development.

Ad a. The vessels were filled with powdered adsorbent. In case of alumina a powder was used with particle dimensions between 0.25 and 0.50 mm. The grain dimensions of other adsorbents were smaller than 0.50 mm and had no well defined lower limit. When vacuum heat pretreatment was desired the vessels were placed into an oven and directly connected to the

vacuum system. Pretreatment temperature was limited to about 150°C on account of the rubber "O" rings between vessel and cover.

Ad b. After the vessels with their connecting tubes had been placed into the calorimeter, the instrument was installed in a water bath thermostat and the vacuum lines to isolation vacuum and to the vessels were coupled to the pumping system. Temperature equilibration was enhanced by establishing thermal contact between outer and inner wall by opening the "heat valve" (see Chapter II.5). The equilibrium situation was usually attained within 18 hours dependent upon reaction temperature. Simultaneously the reaction vessels were evacuated down to a pressure of about 10^{-4} Torr. Then the reaction vessels were closed to stop the water desorption.

Ad c. The response curve was measured by a shortly lasting dosage of cyclohexane to the adsorbent. Dosing times were confined between 5 and 15 sec. After the response curve was recorded the cyclohexane was desorbed by evacuation and equilibrium situation was established again.

Ad d. Sarin was dosed to one of the samples by creating a vapour pressure above this sample. The vapour was generated from the weighed evacuated dosing vessel. Dosing times varied usually between 1 and 3 minutes and were ended by closing valve V shown in Fig. II.6; the dead volume behind this valve is about 20 cm^3. After the dosage the sarin vessel was cooled to about -15°C in order to condense sarin vapour. The new weight of the vessel plus contents gave a measure for the amount adsorbed. Correction was made for the fraction sarin still remaining in the vacuum line; probably this fraction had been adsorbed on the walls. The absolute accuracy amounts to $\pm$ 1 mg. The adsorbed quantity was usually contained within the range 30 to 100 mg.

Ad e. The heat development measured by the thermopile was registrated on a recorder with a most sensitive range of 20 μV and on punch tape. Sampling times for the puncher were taken as 10 seconds, 1, 10 or 60 minutes, dependent upon the slope of the measured curve. The diagram below shows the registration process schematically:

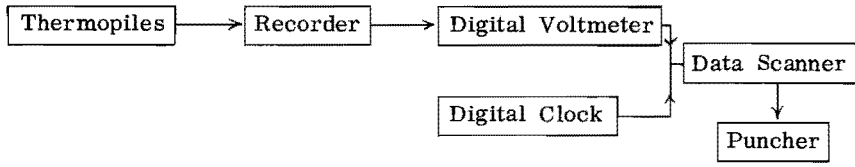

An experiment lasted in most cases between 24 and 48 hours. After one sample had been used, the activity of the reference sample was measured similarly.

Influence of type of heat flow meter

The replacement of the flat heat flow meters by the cylindrical ones affected the procedure in two respects:

a. Whereas in case of the flat heat flow meters it was possible to instal the reaction vessel plus glass tube without exposing the contents to air, a very short exposure had to be allowed when the cylindrical heat flow meters were used. However, the effect of this short contact can be estimated to be negligibly small. The volume that is inevitably filled with air is exactly the dead volume. If all the water vapour from this amount of air would have been adsorbed by the sample, the relative increase in weight would not have surpassed approximately 1%, which corresponds to a change in effective preheating temperature of less than 2^{o}C (see Fig. V. 1).

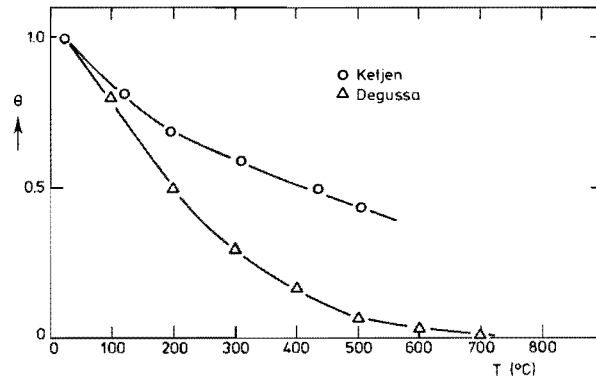

Fig. V. 1

Surface coverage with chemisorbed water as a function of temperature for Ketjen and Degussa alumina.

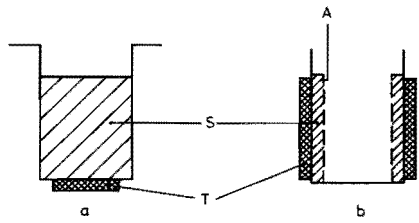

Fig. V.2a and b

Shape of the adsorbent bed normally used with flat (a) and with cylindrical (b) heat flow meters; S adsorbent, A monel gauze, T thermopile.

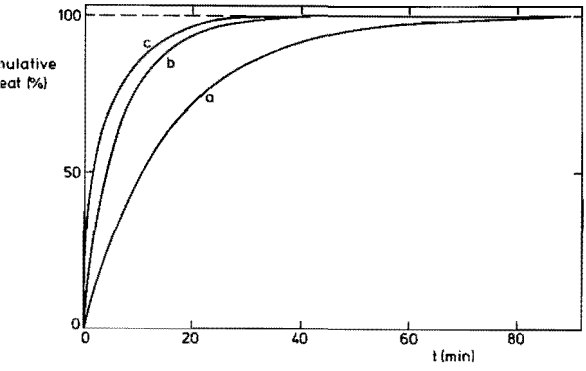

Fig. V.3a

Cumulative response curves measured with short dosages of cyclohexane on alumina samples; for sample position as shown in Fig. V.2a for flat (a) and cylindrical (b) heat flow meters; for sample position as shown in Fig. 2b for cylindrical heat flow meters (c).

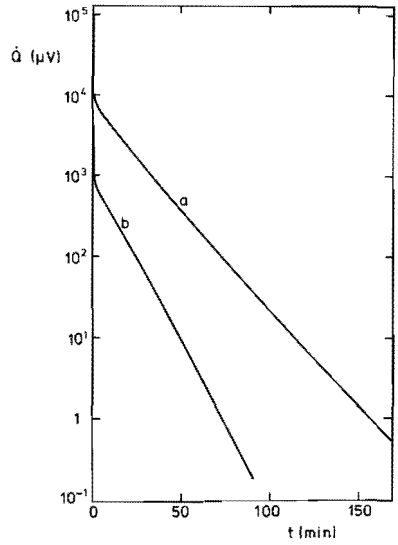

Fig. V.3b

Two differential response curves: (a) associated with flat heat flow meters and adsorbent bed shape shown in Fig. V.2a; (b) associated with cylindrical heat flow meters and adsorbent bed shape shown in Fig. V.2b.

b. When the flat heat flow meters were used, the adsorbent was piled up as a full cylindrical bed covering the whole bottom. In case of the cylindrical meters the adsorbent was piled up against the vertical wall (see Fig. V.2a and b). The advantages are, firstly, a shorter average thermal path between adsorbent and vessel and, secondly, a decrease in the amount of adsorbent resulting in a decrease in heat capacity. On account of these factors the response curve as it is measured by cyclohexane adsorption, is substantially faster. This is shown in Fig. V.3a and b. The quantity of sarin that was adsorbed was not affected by the decrease in adsorbent, because at favourable amounts of adsorbed sarin (30 to 100 mg) a relatively large fraction of the adsorbent is not involved in the adsorption process (see Chapter III.5).

For a number of experiments performed with the cylindrical heat flow meters the response curve was measured and corrections could be made. Experiments carried out with the flat meters could not be corrected at all (see Chapter III).

Data processing

A PDP8/I computer being available, the punch tape enabled an easy use of computer programmed procedures for plot subroutines and calculations. Appropriate programs were written. Linear or logarithmic plots of heat flow against time and linear plots of heat flow against reciprocal time, were rapidly drawn on a scope output device by the program "PLOCON". Amounts of heat developed between defined limits could be figured by means of the program "HEAT", which utilizes the trapezoidal rule. The total correction procedure by means of Fourier analysis was performed by the program "FOURTS" and took about 25 minutes of time, input and output times included. The Fast Fourier Transform subroutine which was required for this, was available, as mentioned before in Chapter III.3.

A separate program converted the raw calorimetric data, which were annotated in *bcd* code, into appropriate ASCII coded files that could be handled by the other programs.

V.1.2 Materials

Adsorbents

Two types of alumina were investigated: Ketjen (K) alumina and Degussa (D) alumina.

The alumina made available by Ketjen (AKZO Chemie Nederland, Amsterdam, The Netherlands) had a γ-type crystal structure. The specific surface area was 280 m^2/g. The material consisted of pellets which were grained to a powder; the sieve fraction between 0.25 and 50 mm was used.

The alumina obtained from Degussa (Frankfurt, Germany) was characterised by the manufacturer as type C; it consisted mainly of crystallites of the γ-structure, although the presence of some δ-alumina was shown by X-ray diffraction. The specific surface area was 110 m^2/g. Before use the aerogel like material was pressed into discs, which were broken into pieces of about 0.1 mm. Both aluminas were not further calcined befure use.

Magnesia was prepared from inactive MgO according to a method described by Baird and Lunsford (1). Calcination temperature was limited to 400°C, providing a specific surface area of 180 m^2/g.

Carbon black was obtained from Cabot (Berre-l'Etang, France); it is known commercially as Regal 400. Impregnation with chromium oxide was performed by contacting the material with a Chromium(VI)oxide solution in water. After filtration it was dried in vacuum at room temperature. The surface area of the carbon black amounted to 115 m^2/g and was hardly affected by the chromium oxide impregnation.

Both magnesia and carbon black samples were used as a finely divided powder.

Adsorbates

The organophosphorus compounds were synthetized in the Chemical Laboratory TNO according to procedures described in (2). The purity of the samples was 99 percent at least.

V.2 RESULTS

An adequate description of the calorimetric results requires qualitative information on the reaction system (see Chapter II. 1). This information is available from an infrared study of sarin adsorbed on alumina and magnesia (3). Additional information as to the nature of the reaction was obtained from comparative quantitative experiments with the calorimeter.

The nature of the reaction being identified, it is possible to give a description of the reaction kinetics directly from the thermokinetics.

V.2.1 Identification of the reaction

The infrared study by Kuiper (3) has revealed the behaviour of sarin adsorbed on alumina and magnesia. His conclusions relevant in this context are:

1. Sarin is adsorbed onto the surface via its phosphoryl oxygen.
2. A relatively slow defluoridation of adsorbed sarin molecules occurs. Adsorbed isopropyl methylphosphonic acid (hydroxysarin) and adsorbed hydrogen fluoride are the products.

Except by defluoridation, adsorbed sarin can decompose also by dealkylation of the isopropyl group, propene being liberated as a gaseous reaction product. The kinetics of this reaction have been described by Kuiper also (3). The rate of this reaction is extremely low; during a week only a few percents of the adsorbed sarin decomposes by dealkylation. Dealkylation experiments have been performed also with other phosphorus compounds resembling sarin: isopropyl dimethylphosphinate (IDMP), diisopropyl methylphosphonate (DIMP), diisopropyl phosphorofluoridate (DFP). The relatively fastest reaction has been observed for DFP; this compound dealkylates about 8 times faster than sarin.

In order to establish whether dealkylation contributes significantly to the total heat evolution in sarin decomposition, calorimetric experiments were carried out with the organophosphorus compounds mentioned above. In addition the decomposition of dimethylphosphinoic fluoride (DMPF) was investigated. The two compounds containing fluorine, DFP and DMPF, caused heat evolutions comparable in magnitude to that for sarin. The two compounds without fluorine, IDMP and DIMP, showed a heat effect that is smaller by a factor 20 with respect to sarin. Apparently a substantial heat

evolution is connected to the presence of fluorine in the compound. Two possible explanations present themselves: the fluorine is responsible for the heat evolution indirectly by a promoting influence upon dealkylation or, secondly, defluoridation is the source of heat evolution. The first possibility may be precluded on account of the experiments on DFP that show that an 8 times faster dealkylation is coupled to a smaller heat evolution. Therefore it may be concluded that the contribution of dealkylation to the heat effect is very small. For this reason it seems to be justified to interpret the thermograms as kinetic curves of the defluoridation reaction only.

V.2.2 Description of results

A. Results obtained with flat heat flow meters

The experiments mentioned in this paragraph are related to alumina and were all performed at $30^{o}C$.

A response curve of the calorimeter, equipped with the flat heat flow meters, was measured by means of cyclohexane adsorption and is shown in Fig. V.3b. The heat effect due to adsorption falls below the detection limit not before 200 minutes. Correction being impossible for these experiments (see Chapter III.5), the period for neat information regarding the reaction kinetics, starts at 200 minutes. Consequently the results mentioned below are related to this period only.

In order to find a kinetic order for the reaction, a number of relations between reaction rate and time were tested

Order	$\dot{Q}$ (= reaction rate x ΔH_r)
0	k
1	e^{-kt}
2	$\frac{k}{(kt+D)^2}$

None of these kinetic equations fitted the experimental results.

A satisfactory description of the results appeared to be possible, if they were interpreted in terms of Zeldovich kinetics (4). The characteristic equation for Zeldovich kinetics in adsorption processes may be formulated in its integrated form as (see Chapter VI.2)

$$q = \frac{1}{\alpha} \ln (t+t_o) - \frac{1}{\alpha} \ln t_o \qquad [1]$$

if q is the amount adsorbed at time t, and α and t_o are constants. If equation [1] is differentiated with regard to time, one obtains:

$$\frac{dq}{dt} = \frac{1}{\alpha(t+t_o)}$$

For sufficiently large times the rate of adsorption is practically proportional to the reciprocal value of time.

If the rate of sarin decomposition is plotted against reciprocal time, a proportional relation appears to exist (see Fig. V.4). This proportionality is very accurate in most cases; occasionally a slight curvature to or from the reciprocal time axis is observed.

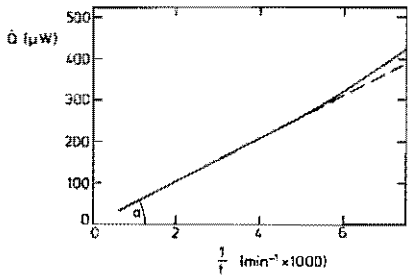

Fig. V.4

Measured heat flow as a function of reciprocal time for a sarin adsorption on alumina pretreated at 28°C; W_a = 46.0 mg, T_r = 28°C. The calorimeter was equipped with flat heat flow meters.

The hyperbolic relation between reaction rate and time is best expressed by the quantity A, defined by

$$A = \frac{\dot{Q} \times t}{M_a} \qquad (M_a \text{ the number of adsorbed mmole})$$

in the time interval where it is constant. A appears to be independent of the amount adsorbed; this is illustrated in Fig. V.5.

The Zeldovich kinetics of the reaction system may be plotted in a way showing A more directly; this is done in Fig. V.6. The product $\dot{Q} \times t$

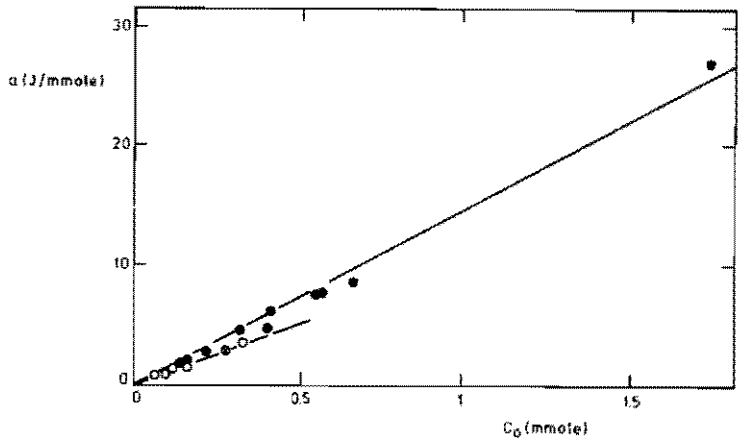

Fig. V.5

The slope a (see Fig. V.4) as a function of amount adsorbate;

(o) sarin; alumina pretreated at 80°C

(•) sarin; alumina pretreated at 27°C

(•) DFP ; alumina pretreated at 27°C.

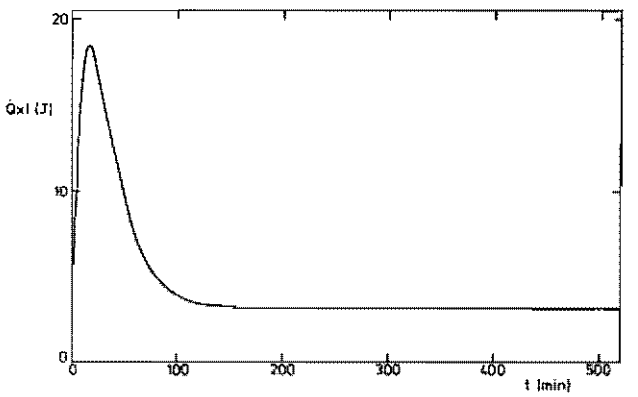

Fig. V.6

The same experiment of Fig. V.4 presented in $\dot{Q} \times t$ *versus* t plot.

yields a horizontal line when it is plotted against time for t $>$ 200 min. The values of these products (A) for different adsorbates and differently pretreated alumina samples are gathered in Table V.1.

Table V.1

The value for A for several compounds on Ketjen alumina; reaction temperature is 28°C.

adsorbate	pretreatment of Al_2O_3	A (J/mmole)
IMPF	3 hr vac at 80°C	10.3
IMPF	vac at 28°C	14.0
IMPF	HF; vac at 28°C	4.9
DMPF	vac at 28°C	18.6
DFP	vac at 28°C	9.3

Previous evacuation of the adsorbent at 80°C during 3 hours causes this slope to decrease from 14.0 to 10.3 J/mmole. Previous adsorption of hydrogen fluoride does not affect the proportional relation between rate and reciprocal time, but only the value of constant A. Two other phosphorus fluorides have been tried: dimethylphosphinoic fluoride (DMPF) and diisopropyl phosphorofluoridate (DFP). Both showed a decomposition according to Zeldovich kinetics.

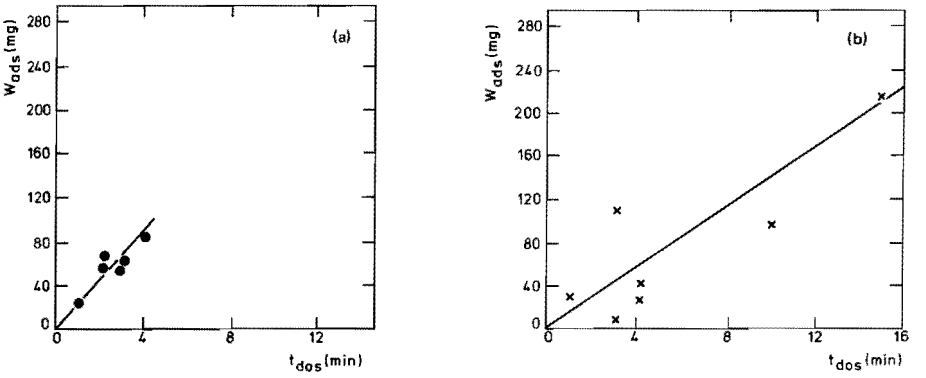

Fig. V.7

Amount of adsorbed sarin as a function of dosing time for left (a) and right (b) reaction vessel; the calorimeter was equipped with flat heat flow meters.

From the Figures V.7a and b it may be seen that the amount of adsorbed sarin is proportional to the dosing time. This is consistent with the results of the radioactive sarin experiments (see Chapter IV.3). The large scattering in the results must probably be ascribed to the strong influence of the inevitably varying vacuum conditions upon adsorption velocities.

B. Results obtained with cylindrical heat flow meters

A representative response curve of the calorimeter, equipped with the cylindrical heat flow meters was already shown in Fig. V.3b. The heat effect of adsorption is terminated considerably earlier relative to the situation in which flat heat flow meters are used. The time from which direct information on the reaction kinetics could be obtained was lowered to about 90 minutes.

Most experiments were performed on Ketjen alumina; for reasons of comparison, also some other adsorbents were examined: Degussa alumina, magnesia, and carbon black impregnated with chromium oxide.

Fig. V.8 shows the general shape of an uncorrected sarin decompo-

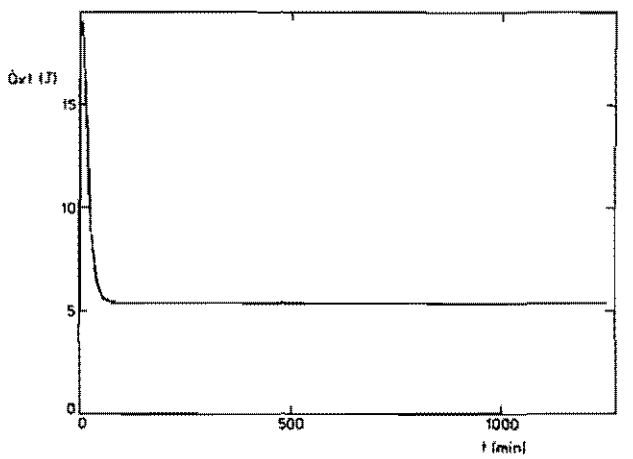

Fig. V.8

Product of uncorrected heat flow and time as a function of time for a sarin adsorption on alumina pretreated at 37°C; T_r = 37°C, W_a = 58.0 mg; the calorimeter was equipped with cylindrical heat flow meters.

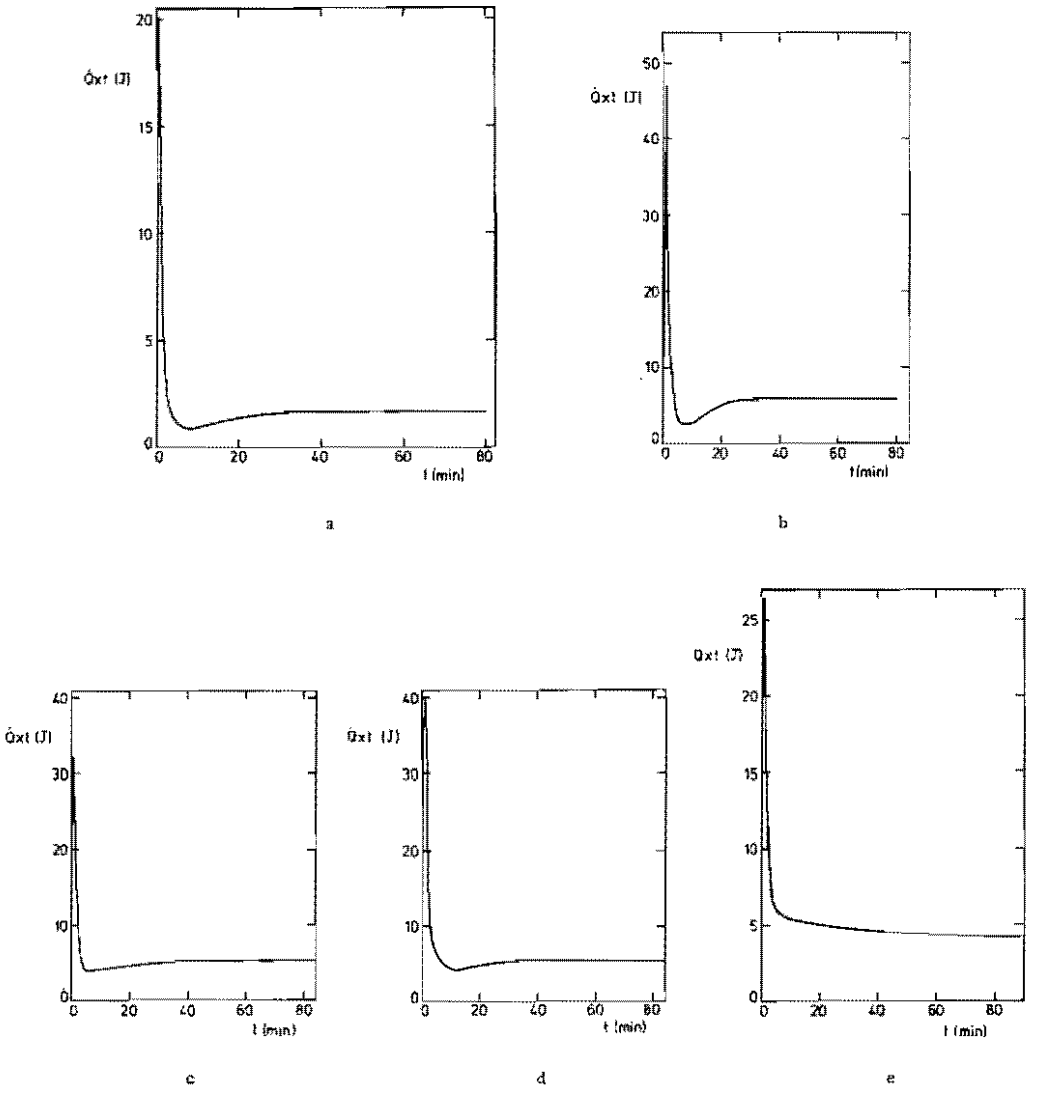

Fig. V.9

Product of corrected heat flow and time for sarin decompositions on alumina samples pretreated at 120°C.

a. T_r = 0°C; W_a = 39.0 mg

b. T_r = 10°C; W_a = 77.5 mg

c. T_r = 20°C; W_a = 56.5 mg

d. T_r = 30°C; W_a = 67.0 mg

e. T_r = 40°C; W_a = 44.0 mg

sition experiment. The hyperbolic relation between $\dot{Q}$ and t appears to be valid for $t \geq 90$ min. The rise in the product $\dot{Q} \times t$ for $t < 90$ min is evidently due to the adsorption heat.

The corrected thermograms of the experiments performed at different temperatures on alumina pretreated at 120°C are shown in Fig. V.9a to e.

The heat of adsorption appears to have been pushed back to times smaller than 5 to 15 min. The hyperbolic relation between $\dot{Q}$ and t may be seen to extend over times down to 80 to 5 minutes, dependent upon temperature. The lower limit of this interval has become visible for the lower reaction temperatures.

The quantity A is shown as a function of reaction temperature in Table V.2 for samples preheated at 75°C or higher. The average A value for similarly pretreated samples examined with the flat heat flow meters at T_r = 30°C fits reasonably well into this series (see Table V.1).

Table V.2

A-values for (K) alumina samples preheated at 75°C or higher at different reaction temperatures (T_r)

T_r (°C)	A (J/mmole)
0	11.1
10	10.5
20	11.0
30	11.3
40	12.7

Table V.3

A-values for (K) alumina samples pretreated at reaction temperature (T_r)

T_r (°C)	A (J/mmole)
10	8.3
10	10.7
10	12.3
37	12.9
37	13.4

The A values found for samples evacuated at reaction temperature show a rather large scattering and are somewhat lower than might have been expected from the data obtained with the flat heat flow meters. They are shown in Table V.3. Contrary to the results obtained with the flat heat flow meters there seems to be no significant difference between the preheated samples and the samples evacuated at reaction temperature. This might be ascribed to a higher evacuation efficiency for the annularly packed beds.

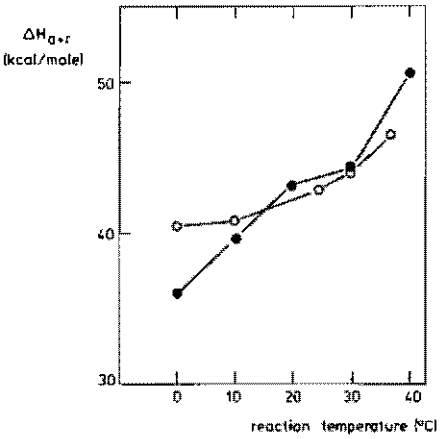

Fig. V.10

Integral amount of heat registrated up to 90 min for sarin decompositions on alumina samples; (●) samples pretreated at temperatures between 75°C and 120°C, (○) samples pretreated at reaction temperature.

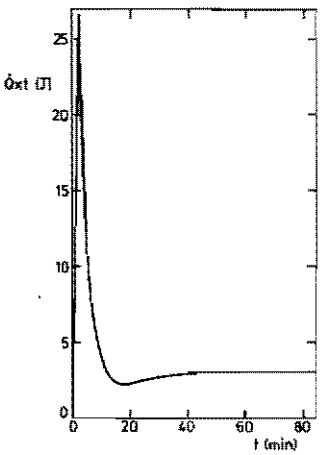

Fig. V.11

Product of corrected heat flow and time as a function of time for a sarin decomposition on alumina that is previously doped with HF; pretreatment and reaction temperature 20°C; W_a = 52.0 mg.

In Fig. V.10 the integral amount of heat registrated after 90 min is plotted as a function of reaction temperature for preheated samples. This quantity (ΔH_{a+r}) comprises all heat of adsorption plus a fraction of the heat of reaction. At higher temperature the reaction contributes obviously more heat.

The corrected thermogram of sarin decomposition on alumina previously covered with gaseous hydrogen fluoride is shown in Fig. V.11. HF appears to inactivate the surface for sarin decomposition.

Degussa alumina

In order to obtain an impression of the relation between activities of (K) and (D) alumina three experiments were performed on (D) alumina at 30°C. The samples were pretreated differently: evacuation at 120 and 30°C, HF poisoning and evacuation at 30°C. The former two samples led to the same results as (K) alumina (see Fig. V.12), the latter showed no long-lasting heat effect at all.

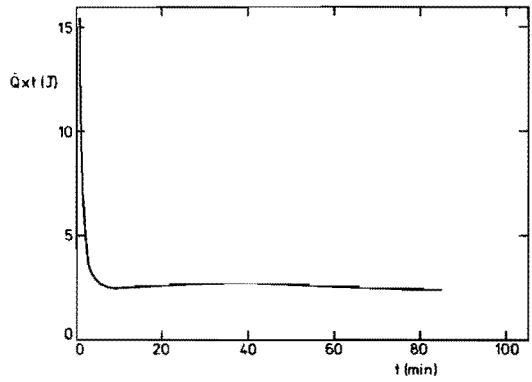

Fig. V.12

Product of corrected heat flow and time as a function of time for a sarin decomposition on Degussa alumina; pretreatment and rection temperature 30°C, W_a = 34.5 mg.

Values for the quantities A and ΔH_{a+r} are given in Table V.4. The overall coverages were somewhat higher than for (K) alumina: 50 to 60% of a monolayer compared to 20 to 40% for (K) alumina.

Table V.4

The quantities A and ΔH_{a+r} for sarin decomposition on (D) alumina at $T_r = 30^{\circ}C$.

Pretreatment	(A J/mmole)	ΔH_{a+r} (kcal/mole)
vac at T_r	10.7	46.9
vac at 120°C	9.3	47.8
HF; vac at T_r	n.a.	27.5

Magnesia

Magnesia was examined in order to get insight into the influence of surface basicity upon the rate of decomposition. Experiments were all performed on samples evacuated at reaction temperature. T_r was varied between 0 and 30°C. Zeldovich kinetics appeared to hold for magnesia. Two thermokinetic curves could be corrected for thermal inertia; the sampling period was taken as 20 sec. The results are shown in Fig. V.13 a and b.

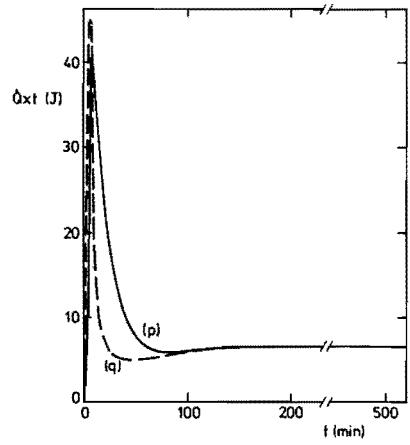

Fig. V.13a

Product of heat flow and time for sarin decomposition on a magnesia sample pretreated at reaction temperature; $T_r = 10^{\circ}C$, $W_a = 93.0$ mg; (p) uncorrected, (q) corrected curve.

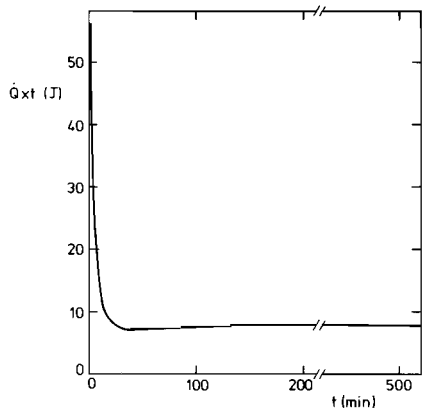

Fig. V.13b

Product of heat flow and time as a function of time for a sarin decomposition on a magnesia sample pretreated at reaction temperature; $T_r = 30^oC$, W_a = 88.0 mg.

For the experiment performed at 10^oC the uncorrected curve is shown also. In this curve the time limit for the hyperbolic relation between rate and time is visible already. Correction seems to be less successful than in case of alumina; this might be explained by a greater difference in thermal paths for heat evolutions by sarin and cyclohexane adsorptions. However, another explanation may be found in the presence of a rapid reaction that does not obey Zeldovich kinetics. Other indications pointing to such a reaction are found in the A and ΔH_{a+r} values for $T_r = 0^oC$; these values together with those of other experiments have been collected in Table V.5.

Table V.5

Characteristic quantities for decomposition reactions on magnesia.

Adsorbate	Reaction temp. (°C)	θ overall (%)	A (J/mmole)	ΔH_{a+r} (kcal/mole)
IMPF	0	54	15.8	39.8
	0	24	17.4	42.3
	10	44	9.7	-- *
	10	36	-- *	44.1
	10	43	9.3	48.4
	20	49	-- *	50.5
	30	42	12.4	53.5
DMPF	10	8	-- *	48.5

* not measured.

Carbon black

The activity of carbon black for sarin decomposition is negligibly small. This is seen in Fig. V.14 where the heat effects of cyclohexane and

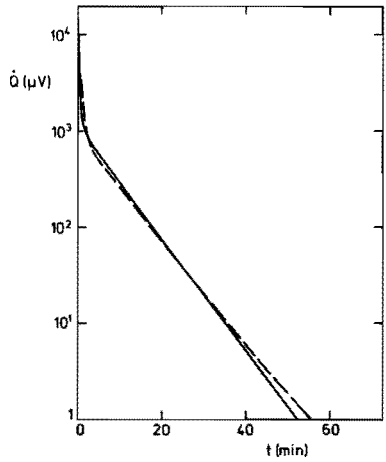

Fig. V.14

Logarithmic plots of heat developments resulting from cyclohexane (solid line) and sarin (dotted line) adsorptions on the same sample of carbon black. The sample was evacuated between the two adsorptions.

sarin are compared; the shapes of the signals are very much the same. The small mutual deviation may be ascribed to a difference in thermal paths, arising from a different initial distribution over the bed. Another explanation may be found in the redistribution of sarin over the carbon bed (see Chapter IV.2).

If the carbon is impregnated with chromium trioxide, a decomposition according to Zeldovich kinetics is observed. The activity increases with increasing chromium contents, although it is still relatively low at a chromium percentage of 6. One of the uncorrected curves is shown in Fig. V.15. Other relevant quantities have been listed in Table V.6.

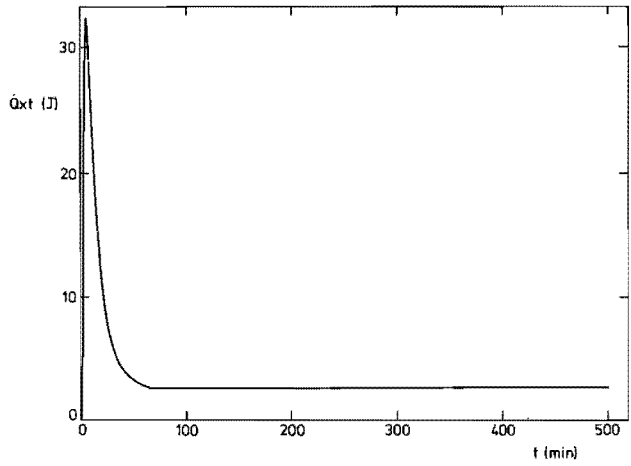

Fig. V.15

Product of heat development and time as a function of time for a sarin decomposition on carbon black impregnated with chromium oxide (6.2 weight percent chromium). Pretreatment and reaction temperature 25°C; W_a = 72.0 mg.

Table V.6

Characteristic quantities for sarin decomposition on carbon black, impregnated with chromium (VI) oxide; samples are pretreated at T_r.

% Cr	T_r (°C)	$\theta_{overall}$ (%)	A (J/mmole)	ΔH_{a+r} (kcal/mole)
0	28	35	n.a.	15.7
4.1	28	41	2.1	24.8
6.2	25	27	5.0	29.5

REFERENCES

1. M.J. Baird and J.H. Lunsford, J. Catal. 26 (1972) 440.
2. J. Houben and Th. Weijl, "Methoden der Organischen Chemie", I: Organischen Phosphorverbindungen, Georg Thieme Verlag, Stuttgart, 1963.
3. A.E. T. Kuiper, Thesis, Eindhoven (1974).
4. C. Aharoni and F.C. Tompkins, Adv. Catal. 21 (1971) 1.

CHAPTER VI

DISCUSSION OF RESULTS IN TERMS OF VARIATION IN THE ACTIVATION FREE ENERGY

In this chapter an attempt is made to find a kinetic model for the defluoridation reaction of sarin adsorbed on alumina. The starting point for the discussion is the experimental fact that the reaction obeys Zeldovich-Roginskii kinetics (see Chapter V.2.2).

The chapter opens with the description of the possible reaction mechanisms in order to clarify the rate limiting step and the relevant activated complex. These are indispensable for an appropriate explanation of the fundamental kinetic parameters. The second section shortly reviews some general characteristics of Zeldovich kinetics. In the third section a model is postulated as a basis for the explanation of the Zeldovich kinetics of sarin decomposition; the related rate equation is derived. After a confrontation of this model with the experimental results (section 4) the usefulness of the model and the implications will be discussed in the last section of this chapter.

VI.1 MECHANISMS FOR THE DEFLUORIDATION OF ADSORBED SARIN

Data on the adsorption process and the structure of adsorbed sarin on alumina are available from a study by Kuiper (1). The act of adsorption may be considered to occur in two steps:

1. a hydroxyl group is expelled from an adsorption site and an aluminium ion is exposed;
2. a sarin molecule adsorbs via its phosphoryl oxygen onto the created Lewis acid site.

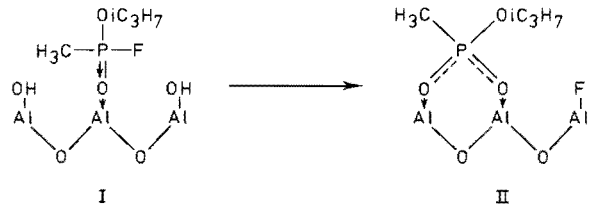

I II

Fig. VI. 1

The adsorption structures of sarin (I) and of defluoridated sarin (II).

Fig. VI. 1 shows the adsorbed molecule (structure I). Structure I is slowly replaced by structure II, indicating the course of the defluoridation reaction. Besides structure II adsorbed hydrogen fluoride is formed.

An attempt to formulate a possible mechanism for the defluoridation of adsorbed sarin may be based on comparison with homogeneous hydrolysis of phosphate esters. Many investigations on homogeneous substitution reactions of organophosphorus compounds have been made; they are collected and discussed in literature (2, 3). The following results from these investigations seem to be relevant to provide a framework for the formulation of a mechanism of defluoridation of adsorbed sarin.

1. The first step in hydrolysis of phosphate esters is the uptake of a hydroxyl ion or water molecule into the coordination of the central phosphorus; the geometry of the coordination changes from a tetrahedron to a trigonal bipyramide.
2. Permutational (or skeletal) isomerisation may occur; the two apical ligands change position with two of the three equatorial ligands.
3. Ligands may show a preference for the occupation of apical or equatorial positions. Strongly electronegative groups reside preferently in apical position. The hydroxyl ion is rather indifferent to the place it occupies. The oxide anion shows a distinct preference for the equatorial position. Steric-hindrance being greatest in apical position, large groups have a tendency to reside in equatorial positions.
4. Groups enter or depart via apex positions; apex ligands are generally more reactive than equatorial ligands.

If the same features characterise the hydrolysis of adsorbed sarin, the following initial and final steps seem plausible:

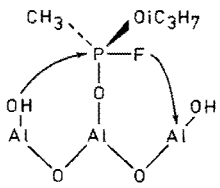

Fig. VI. 2a

In a concerted mechanism the surface-hydroxyl and the fluoride ion move simultaneously to, respectively from the phosphorus.

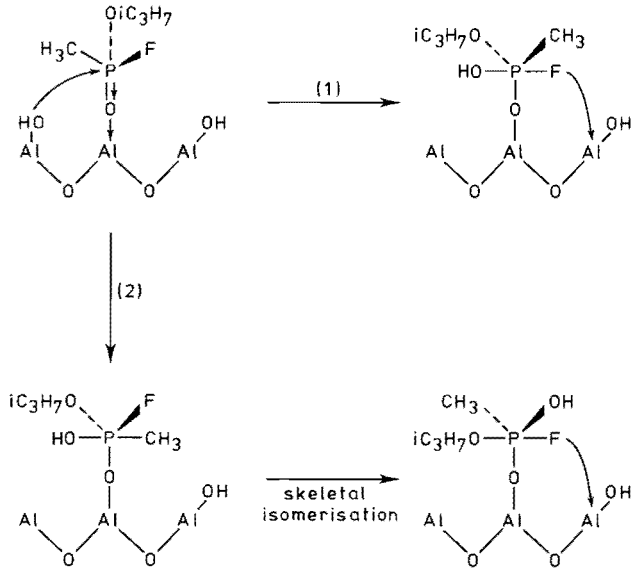

Fig. VI. 2b

Possible mechanisms implying relatively stable intermediates of five-coordinate phosphorus; after the entrance of a hydroxyl the fluorine resides in apical (path 1) or in equatorial (path 2) position. In the latter case the fluorine may reach apical position by skeletal isomerisation.

- a neighbouring hydroxyl ion is taken up into the coordination of the central phosphorus in apical position;
- the fluoride departs from apical position to the surface.

If the steps take place simultaneously, the reaction is said to follow a concerted mechanism (Fig. VI. 2a). It is seen that the reaction comprises the simultaneous loosening of two hydroxyl ions from the surface, which most probably gives rise to a high activation energy.

Five-coordinate phosphorus compounds are relatively stable, particularly if they possess two or more P-O bonds (3). After uptake of a hydroxyl, the phosphorus complex possesses three P-O bonds and might have, therefore, a substantial life time. Permutational isomerisation might occur and a different mechanism is possible. Various possibilities may be distinguished.

The hydroxyl may enter the complex opposite to the fluorine, which, as a consequence, resides in an apex. It is in a position to depart immediately (path 1 in Fig. VI. 2b). The situation differs from the concerted mechanism in that the fluoride may be bonded by the aluminium ion that remains exposed after having lost its hydroxyl group. Alternatively the hydroxyl may enter the phosphorus coordination opposite to the methyl or isopropoxy group, the fluoride assuming a less probable equatorial position (path 2 in Fig. VI. 2b). By isomerisation the fluoride may reach an apical position from which it leaves the complex.

From i.r. (1) there are no indications for the presence of a five-coordinate phosphorus complex. With the information available so far it cannot be decided which mechanism actually takes place.

If the reaction proceeds in two stages the rate determining step must be the uptake of a hydroxyl by the phosphorus. This is evident from the experience that substitution reactions at four-coordinate phosphorus run faster if the entering nucleophilic ligand is more basic (2). The absence of indications for five-coordinate phosphorus in the infrared spectra is in agreement with this. If the mechanism is concerted, the uptake of a hydroxyl is obviously involved in the rate determining step.

The two mechanisms have much in common. In both cases the rotational degree of freedom about the Al-O-P axis is lost in the formation of the activated complex. The formation of the activated complex implies for both mechanisms the conversion of a tetrahedron to a trigonal bipyramide. Bond angles as well as bond lengths are changed.

VI.2 GENERAL REMARKS ON ZELDOVICH-ROGINSKII KINETICS

Extensive reviews on Zeldovich-Roginskii kinetics have been published by Low (4) and by Aharoni and Tompkins (5). Often but incorrectly this type of kinetics is designated as Elovich kinetics. It will be called here shortly "Zeldovich kinetics". Low collected a great many kinetic data on chemisorption processes from literature and described them uniformly by means of Zeldovich plots. Aharoni and Tompkins lay more stress on theoretical concepts behind the experimental law.

Most chemisorption processes obey the experimental logarithmic rate law which is essential for Zeldovich kinetics:

$$\frac{dq}{dt} = ae^{-\alpha q} \qquad [1]$$

where q is the amount adsorbed at time t, while a and α are constants, valid for one experiment. In its integrated form equation [1] may be written as

$$q = \frac{1}{\alpha} \ln (t+t_o) - \frac{1}{\alpha} \ln t_o \qquad [2]$$

where the constant $t_o = 1/\alpha a$. Equation [2] is usually utilized to test whether Zeldovich kinetics are applicable. The value of t_o is adapted in order to obtain the best linearity in a q against ln t plot.

Aharoni and Tompkins mention a number of physical models that have been proposed to explain the experimental Zeldovich equation. Essential for some models is a surface inhomogeneity. This nonuniformity of surface sites may be an intrinsic property of the adsorbent, but may also be induced by the very adsorption process itself.

Most explanations depart from the isothermal rate equation:

$$\frac{dq}{dt} = K(p)\, n \exp(-E/RT) \qquad [3]$$

where K(p) is a constant accounting for pressure influences and condensation coefficient, n is the number of available adsorption sites and E is the activation energy for adsorption. Starting from equation [3] it is possible to derive the Zeldovich equation assuming one or both of the following prepositions (5):

1. the number of sites available for adsorption decreases exponentially with the number of occupied sites;
2. the activation energy involved in the adsorption process varies with coverage. This variation may be either intrinsic or induced by the adsorption process.

Variation in site number may be applicable to adsorbents with semiconducting properties. Cimino a. o. (6) explain the Zeldovich kinetics for hydrogen adsorption on zincoxide in this way. Taylor and Thon (7) had previously applied Volkenshteins (8) theory that states that adsorption sites may be generated by the very act of adsorption.

Variation in activation energy, which was first proposed by Halsey (9), requires an assumption concerning the actual shape of the distribution function of activation energy. For the sake of mathematical simplicity a rectangular distribution is often chosen.

It may be noted here that a variety of processes other than chemisorption obey Zeldovich kinetics. McLintock (10) mentions among others: oxidation of metals, coals and charcoals, and decomposition of surface formate on nickel.

The mere applicability of Zeldovich kinetics gives no indication as to the mechanism of the involved process (11). Variation of the experimental parameters of the process is absolutely necessary to obtain information for a reliable construction of a physical model. Although the general validity of the logarithmic rate law suggests a universal mechanism, the Zeldovich equation has to be considered to be no more than an appropriate means to correlate adsorption data (12).

The model departing from a variation in activation energy will appear to offer a basis for the explanation of the Zeldovich kinetics of sarin decomposition.

VI.3 KINETIC MODEL

VI.3.1 Basis for a kinetic model

As was mentioned in section 1 of this chapter a distribution in activation energy is sometimes assumed to explain Zeldovich kinetics for chemisorption. A distribution of activation free energies is an essential part of the model that is postulated here to explain the kinetics of the defluoridation

reaction of sarin on alumina. The similarity of the kinetics on the other oxidic surfaces investigated, suggests that the model has equal validity for those adsorbents. The model is characterised by the following features:

1. Adsorbed sarin molecules are immobile.
2. The molecules decompose by a defluoridation reaction; the activation free energy involved in this reaction is not equal for all reacting molecules; on an average it increases in the course of the reaction.
3. For each fraction of molecules with the same energy for decomposition the reaction is first order in sarin and zero order in any other species.
4. The reaction enthalpy may be taken to be equal for all molecules.

Ad 1. Immobility of adsorbed sarin.

From Chapter IV it is known that sarin molecules are immobile after adsorption on an oxidic surface. The uneven macroscopic distribution over the adsorbent bed is closely related to this immobility. The distribution over the different surface sites, however, is independent of the overall surface coverage.

Ad 2. Heterogeneity of the surface.

Heterogeneity of surface sites on alumina is expressed in such quantities as differential heat of adsorption and variation in surface acidity. With respect to sarin decomposition a scatter in strength of basic sites seems to be of particular interest, although a change in activation energy caused by the very reaction cannot be precluded *a priori* (induced heterogeneity).

In order to test the model a definite distribution function for the activation free energy has to be chosen, whether this distribution exists at the beginning of the reaction or develops gradually in the course of the reaction. For the sake of mathematical simplicity a block shaped distribution function will be assumed first: all activation free energies between the limits G_1 and G_2 are supposed to occur with equal frequency. This choice is referred to as the "simple model" by Peers (13). The choice of this function is arbitrary, but it will be seen to be justified substantially from experimental evidence.

Ad 3. Order of the reaction.

First order kinetics in sarin for each fraction of molecules on a

"patch" with one definite activation free energy, seems to be likely on basis of the mechanisms proposed in the foregoing section.

It would be more precise to state that the reaction is first order in "reaction centres": a reaction centre is thought to consist of an adsorbed sarin molecule plus neighbouring reactive hydroxyl groups. This centre reacts, if the activation free energy, specific to this centre, is overcome. On account of the feature mentioned in 1, however, the numbers of reaction centres and sarin molecules are identical.

For the sake of completeness the reaction rate equation will be calculated also for the case that the reaction would be second order in sarin.

Ad 4. Constant heat of reaction.

It is not the enthalpy of the rate determining reaction that is involved in the measurement, but the overall enthalpy of all steps that are passed through in the reaction sequence. This implies that the enthalpy measured differs from the enthalpy of the reaction proper.

Although a distribution in overall enthalpy is equally likely to exist as a distribution in activation energy, it cannot influence the kinetics of the reaction. If a constant activation energy is assumed, the measured reaction enthalpy is an average at every time of the reaction. If a distribution is assumed both in activation energy and reaction enthalpy, the calorimetrically measured kinetic curve is distorted in a way dependent on the coupling between the distributions. It is assumed that the coupling is random for all energies, which practically implies that the overall reaction enthalpy may be regarded to have a constant value.

VI.3.2 Derivation of the rate equation

The model given in the preceeding section permits a straight-forward derivation of the kinetic equation.

Let an amount sarin (C_o) be adsorbed at time $t = 0$ on a system of reactive sites that possess a block shaped distribution function in activation free energies ($\rho(G)$) between the extreme values G_1 and G_2. These values are connected with reaction rate constants K_1 and K_2 respectively:

$$K_1 = K_o C^{-G_1/RT} \quad \text{and} \quad K_2 = K_o C^{-G_2/RT}$$

The distribution function $\rho(G)$ must be normalised; integration between $G = 0$ and ∞ leads to the value one by definition. Hence

$$\int_{G_1}^{G_2} \rho(G)\, dG = 1$$

It follows that $\rho(G) = 1/(G_2-G_1)$ for $G_1 < G < G_2$ and $\rho(G) = 0$ outside this interval. The initial amount of sarin encountering an activation energy G is called C_G^o and is

$$C_G^o = \frac{C^o}{G_2-G_1} \qquad [4]$$

The dimension of C^o is that of moles.

Those molecules that experience an activation free energy G, decompose according to the kinetic equation:

$$-\frac{dC_G}{dt} = K_G C_G \qquad [5]$$

If $C_G(t)$ is solved

$$C_G(t) = C_G^o\, e^{-K_G t} \qquad [6]$$

After insertion of equation [6] into equation [5] the total velocity is found by integration of equation [6] over G between the limits G_1 and G_2; each C_G^o has to be multiplied by the distribution function

$$r = \int_{G_1}^{G_2} -\left(\frac{dC_G}{dt}\right) dG$$

$$r = \frac{C^o}{G_2-G_1} \int_{G_1}^{G_2} K_G\, e^{-K_G(t)}\, dG$$

Integration proceeds simpler if the integration variable G is replaced by K. If the relations $K = K_o \exp(-G/RT)$ and $dG = -(RT/K)\,dK$ are inserted, it follows:

$$r = \frac{-RTC^o}{G_2-G_1} \int_{K_1}^{K_2} e^{-Kt} dK \qquad [7]$$

$$r = \frac{RTC^o}{G_2-G_1} \frac{1}{t} (e^{-K_2 t} - e^{-K_1 t}) \qquad [8]$$

In the special case that $t = 0$ equation [10] reduces to

$$(-\frac{dc}{dt})_{t=o} = \frac{RTC^o}{G_2-G_1} \int_{K_1}^{K_2} dK$$

or

$$(-\frac{dc}{dt})_{t=o} = \frac{RTC_o}{G_2-G_1} (K_1-K_2) \qquad [9]$$

In order to test if the $\lim_{t\to o} (-\frac{dc}{dt})$ from equation [8] leads to equation [9] the exponentials were developed in series:

$$\lim_{t\to o} (-\frac{dc}{dt}) = \lim_{t\to o} \frac{RTC^o}{G_2-G_1} \frac{1}{t} \left\{1-K_2 t + \frac{(K_2 t)^2}{2!} - \ldots - (1-K_1 t + \frac{(K_1 t)^2}{2!} - \ldots)\right\}$$

$$= \lim_{t\to o} \frac{RTC^o}{G_2-G_1} \left\{(K_1-K_2) + \frac{t}{2!} (K_2^2 - K_1^2) + \ldots\right\}$$

$$= \frac{RTC^o}{G_2-G_1} (K_1-K_2)$$

The value corresponds indeed to the one found in equation [9]. If the reaction rate is integrated between $t = 0$ and ∞ the initial amount C^o must be found. Since (14)

$$\int_0^\infty \frac{1}{t}(e^{-K_2 t} - e^{-K_1 t})\,dt = \ln \frac{K_1}{K_2}$$

and

$\ln K_i = \ln K_o - G_i/RT$, this is easily verified.

A similar derivation for the rate equation for chemisorption processes has been given by Peers (13).

The thermogenesis ($\dot{Q}$) is related to the reaction rate by:

$$\dot{Q} = (-\frac{dc}{dt})\,(-\Delta H_r) \qquad [10]$$

From equations [8] and [10] it follows:

$$\dot{Q} = \frac{RTC^o(-\Delta H_r)}{G_2-G_1}\,\frac{1}{t}\,(e^{-K_2 t} - e^{-K_1 t})$$

The time dependency of the factor $(e^{-K_2 t} - e^{-K_1 t})$ is strongly influenced by the magnitude of K_1 and K_2. If K_1 is sufficiently large and K_2 sufficiently small there is a time interval in which $e^{-K_2 t}$ is still unity, while $e^{-K_1 t}$ practically equals zero already. In this time interval the factor $(e^{-K_2 t} - e^{-K_1 t})$ may be set equal to one and consequently the reaction rate is proportional to the reciprocal time:

$$r = \frac{RTC^o}{G_2-G_1}\,\frac{1}{t}$$

For times lower than this interval the reaction rate may be written as:

$$r = \frac{RTC^o}{G_2-G_1}\,\frac{1}{t}(1 - e^{-K_1 t}) \qquad [11]$$

The quantities r and rxt are illustrated graphically in Fig. VI.3a and b. $RTC^o/(G_2-G_1)$ will be named A' if C^o assumes unity value.

The rate equation may be derived similarly, if second order kinetics in sarin is assumed for the reaction on a patch with constant activation energy. The result is:

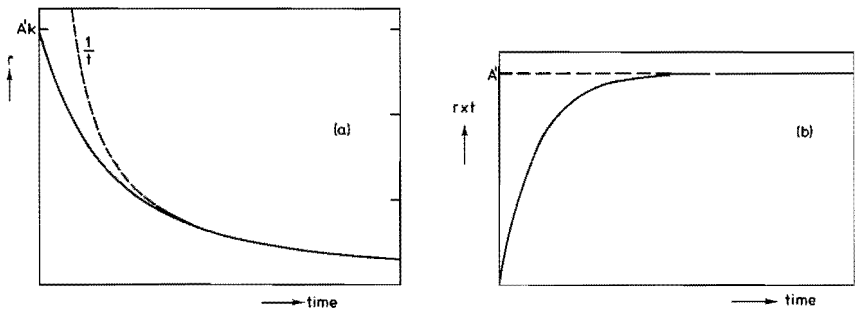

Fig. VI.3

General shape of a graphical representation of the functions $r = A'/t\{1-\exp(-K_1 t)\}$ (a) and $rxt = A'\{1-\exp(-K_1 t)\}$ (b).

$$r = \frac{RT(K_1-K_2)}{(K_2 t + \beta)\,(K_1 t + \beta)}$$

where $\beta = (G_2-G_1)/C^o$. If K_2 is sufficiently small the denominator may be written in good approximation as $\beta\,(K_1 t + \beta)$ for small t. Reaction rate becomes in this interval:

$$r = \frac{K_1 RT}{\beta\,(K_1 t + \beta)} \qquad [12]$$

This relation is exactly congruent to the differential representation of the Zeldovich equation (*cf* equation [2]). If $K_1 t \rangle\rangle \beta$, then the reaction rate is inversely proportional to time.

Relations similar to equation [12] are obtained if other concentration dependencies are choosen. They all show an inverse proportionality between rate and time in a smaller time interval, than when first order kinetics are assumed.

The characteristic hyperbolic relation between time and reaction rate, which was found experimentally in a broad time interval, is explained by the given model both for first and second order reaction. Discrimination between the first and second order kinetics is expressed in the fashion in which the relation deviates from the hyperbolic one outside the interval in question.

Anticipating the confrontation of the model with the experimental

results (see next section) it may be noted here that discrimination between first and second order kinetics is possible by means of those experiments that show as sufficiently large deviation from the hyperbolic relation at small times. The best fitting curves given by:

$$\dot{Q} \times t = A(1 - e^{-K_1 t})$$

and $$\dot{Q} \times t = At/(t + B)$$

were compared to the experimental curves in a $\dot{Q} \times t$ against t plot (see Fig. VI.9a). In all cases first order kinetics appeared to fit much better than second order. Therefore, only first order will be taken into account from now on. The reaction mechanism proposed in section VI.1 is consistent with first order kinetics.

VI.3.3 Application to experimental results

The kinetic model can be tested most completely on the series of experiments performed at different temperatures on Ketjen alumina pretreated between 80 and 120°C. Although the experiments on other adsorbents do not suffice to permit an equally reliable check, it is possible to recognise essential features of the model for these adsorbents as well.

a. Ketjen alumina

For a comparison of experimental results with rate equation [11] three factors may be discerned: (i) inverse proportionality between rate and time; (ii) proportionality between absolute temperature and rate; (iii) factor $(1-\exp(-K_1 t))$

(i) The validity of the inverse proportionality between time and rate was shown satisfactorily in Chapter V.

(ii) The temperature dependency of the rate is best clarified by the quantity A defined as

$$A = \frac{RT(-\Delta H_r)C^o}{G_2 - G_1} \quad \text{for } C^o = 1 \qquad [13]$$

The quantities A and A' differ a constant factor, *viz.* $(-\Delta H_r)$. After combination of equations [11] and [13] one obtains:

$$\dot{Q} = \frac{A}{t} \{1 - \exp(-K_1 t)\}$$

For samples pretreated at temperatures between 80 and 120°C the quantity A appears to show no significant differences. At a reaction temperature of 30°C the A values of samples pretreated at 120 and 80°C amount respectively to 11.3 ± 0.5 and 10.2 ± 1.7 J/mmole. These samples show equal activities as may be seen also from the quantity ΔH_{a+r} (Chapter V.2.2). Therefore, all A values of the related samples are collected in one plot (Fig. VI.4) of A *versus* temperature. A rather broad scattering is observed along the best fitting straight line through the origin; however, it is evident that the influence of reaction temperature is very weak.

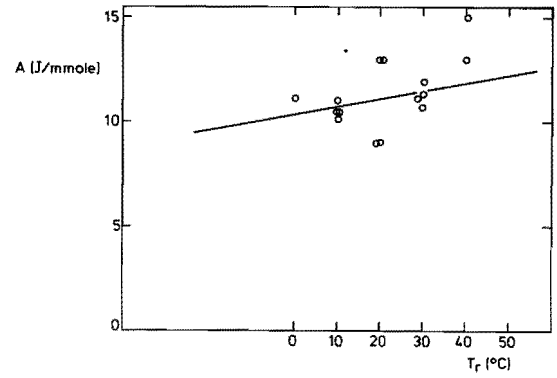

Fig. VI.4

Variation of the quantity A with reaction temperature for (K) alumina samples pretreated at temperatures between 75 and 120°C.

Although an accurate linear proportionality between rate and absolute temperature cannot be drawn from this graph, the experimental relation is certainly not contradictory to that following from the model as represented in equation [13].

(iii) For most samples pretreated at 120°C it is possible to find a reasonably fitting function of the form

$$r \times t = A' \{1-\exp(-K_1 t)\}$$

by choosing appropriate values for K_1. For reaction temperatures 0, 10 and 20°C the best fitting functions are shown in Fig. VI.5a to c. For one of the

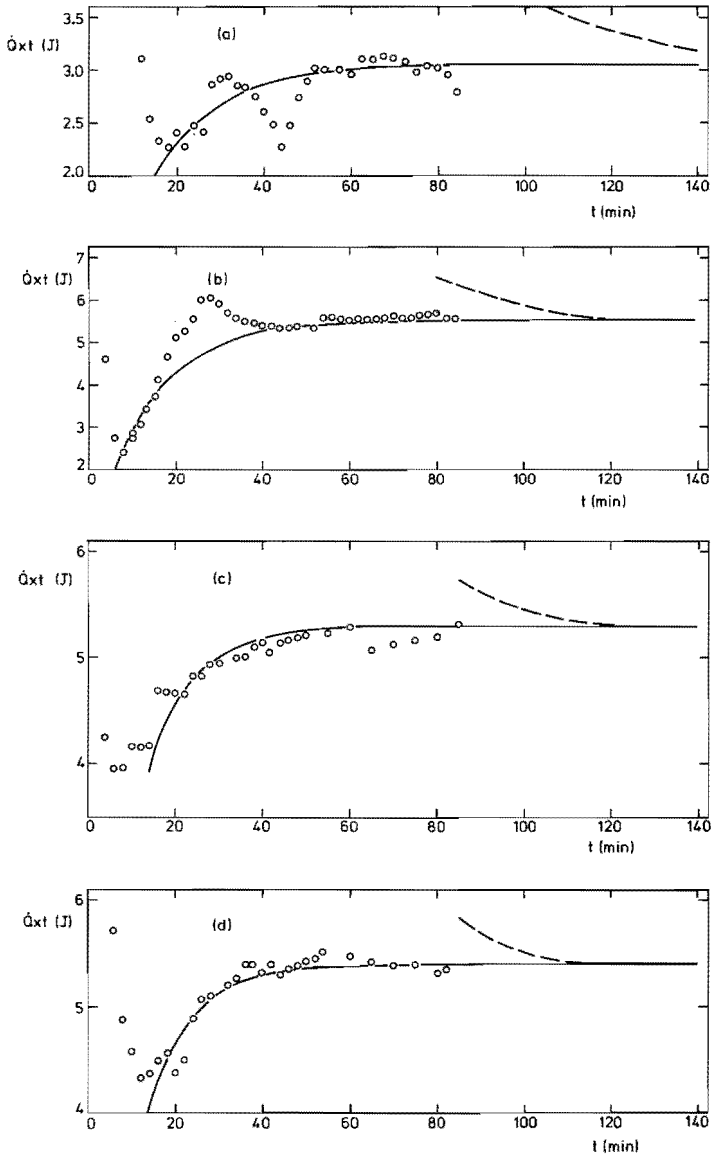

Fig. VI.5

Fitting functions of the form $A\{(1-\exp(-K_I t)\}$ for sarin decomposition on (K) alumina pretreated at 120°C;

(o) corrected, (--) uncorrected, (—) fitting curve.

Conditions: a. $T_r = 0^{\circ}C$, $W_a = 39.0$ mg
b. $T_r = 10^{\circ}C$, $W_a = 77.5$ mg
c. $T_r = 20^{\circ}C$, $W_a = 56.5$ mg
d. $T_r = 30^{\circ}C$, $W_a = 67.0$ mg

three experiments performed at 30°C a factor $A\{1-\exp(-K_1 t)\}$ was hardly recognisable; the assumed value of 0.2 is approximate; one of the other experiments is shown in Fig. VI.5d. The experiments at 40°C show no decrease in the $\dot{Q} \times t$ *versus* t plot. The values found for K_1 at different temperatures have been gathered in Table VI.1.

Table VI.1

Highest reaction rate constant of sarin decomposition on alumina pretreated at 120°C for various reaction temperatures.

T_r (°C)	0	10	20	30	40
K_1 (min^{-1})	0.07	0.075	0.09	0.15	$\rangle$ 0.2
			0.10	0.1	
			(HF) 0.09	0.2	

The temperature dependency of K_1 is illustrated in a semilogarithmic plot against reciprocal time (Fig. VI.6). The apparent activation energy may be calculated from this graph to be 4.3 kcal/mole.

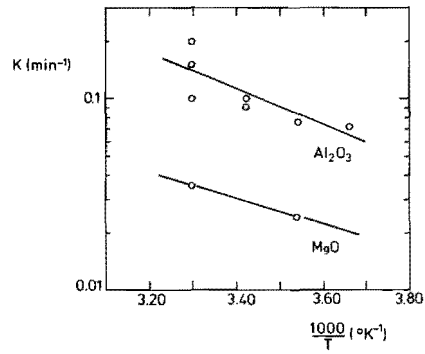

Fig. VI.6

Logarithmic plots of K_1 *versus* reciprocal temperature for (K) alumina pretreated at 120°C and magnesia pretreated at reaction temperature.

It may be concluded that the model explains the two most particular features of the observed kinetics; the proportional relation between temperature and rate as well as the hyperbolic relation between rate and time are fully understood within the model. It may be esteemed remarkable that

the rectangular distribution, expressed in the right time dependency in the first stage of the reaction, seems to answer to reality.

It appears that pretreatment of the sample with hydrogen fluoride does not affect the shape of the reaction rate curve but only diminishes the height with a constant factor (see Fig. VI.7).

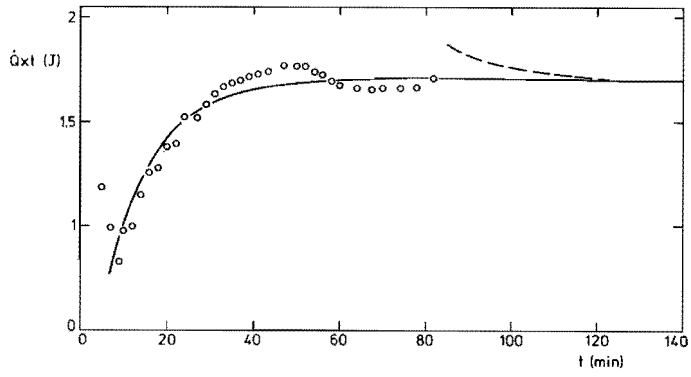

Fig. VI.7

Fitting function (—) of the form $A\{1-\exp(-K_1 t)\}$ for sarin decomposition on (K) alumina pretreated with hydrogen fluoride; reaction temperature 20°C; (o) corrected function, (--) uncorrected curve.

Using equation [13] it is possible to estimate the width of the total energy interval if the value for ΔH_r is known. From comparison with the extraction experiments carried out by Kuiper (1), the overall reaction enthalpy for sarin decomposition on alumina may be calibrated. His most accurate results are the ones obtained from experiments with radioactive sarin. These concern sarin decomposition at 25°C on a Ketjen alumina pretreated at 25°C. In Table VI.2 column 2, the fraction decomposed sarin in definite intervals, is listed as they are derived from Kuipers extraction experiments. The amount of heat liberated in the same period on a sample with a similar thermal history, is given in the third column. The overall reaction enthalpy (ΔH_r) is found from columns 2 and 3. The average of the three values amounts to 72 kcal/mole.

With this number of ΔH_r it is possible to calculate the span of activation energies involved in the model. The values are found from the equation

$$A = \frac{-\Delta H_r RT}{G_2 - G_1}$$

and are given in Table VI.3.

Table VI.2

Comparison of extraction experiments by Kuiper and calorimetric experiments in order to find the overall reaction enthalpy.

	Extraction experiment	Calorimetric experiment	
period (min.)	fraction decomposed (%)	heat developed (J/mmole)	$-\Delta H_r$ (kcal/mole)
60 - 1370	14	43.8	75
60 - 2970	17	54.6	77
60 - 3095	20	55.2	66

Table VI.3

Width of the distribution of activation free energy calculated with ΔH_r = -72 kcal/mole.

pretreatment (^{o}C)	$T_{reaction}$ (^{o}C)	A (J/mmole)	$G_2 - G_1$ (kcal/mole)
25	25	14.0	12.8
120	0	11.1	14.8
120	10	10.5	16.2
120	20	11.0	16.1
120	30	11.3	16.2
120	40	12.7	14.9

From this table it is seen that the energy distribution is very broad. It is about constant for similarly pretreated samples suggesting that the distribution is temperature independent. The average value for the samples pretreated at 120^{o}C is calculated to be 15.6 kcal/mole with a standard de-

viation of 0.7 kcal/mole. In paragraph 4.1 of this Chapter it will be seen that the physical meaning of G_2 is limited.

b. Other adsorbents

Too few sarin decomposition experiments have been performed on the other adsorbents to test the kinetic model as extensively as for alumina. However, the proportionality between reaction rate and reciprocal time, the most characteristic feature of the model, is observed for all oxidic surfaces.

Degussa alumina

Degussa alumina has the same values for A and ΔH_{a+r} as Ketjen alumina. The two types differ only in sensitivity for hydrogen fluoride poisoning. Essentially the same poisoning procedure inactivates (D) alumina completely, while (K) alumina retains part of its activity.

Magnesia

At one particular temperature the reaction rate on magnesia obeys the rate equation of the model. The temperature dependency of the factor A, however, is not in agreement with the rate equation. This anomaly probably must be related to the difference in temperature pretreatment, which leads to surfaces that are differently loaded with physically adsorbed water. As a consequence of this, a greater fraction sarin is involved in a preliminary and fast reaction, giving rise to a decrease in the amount of sarin taking part in the reaction following the Zeldovich kinetics. The occurrence of the fast reaction covering a considerable fraction, is sustained by two experimental data: (a) Kuiper found from his infrared study a very rapid defluoridation of sarin on magnesia during the first hour of the reaction; (b) the corrected thermograms for magnesia (see Fig. V.13a and b) revealed a high heat development during the first hour of the experiment compared to the heat effect of sarin on alumina in the same period.

The quantity K_1 could be derived from r x t against t plots for two temperatures (see Fig. VI.8a and b). It is, as in the case of alumina, only slightly temperature dependent. The activation energy, calculated from the ln K_1 against 1/T plot (Fig. VI.6) is 4.2 kcal/mole.

Calibration of ΔH_r was not possible because comparable extraction

experiments on magnesia were not practicable (1). Comparison of the quantities A for alumina and magnesia cannot be made, therefore.

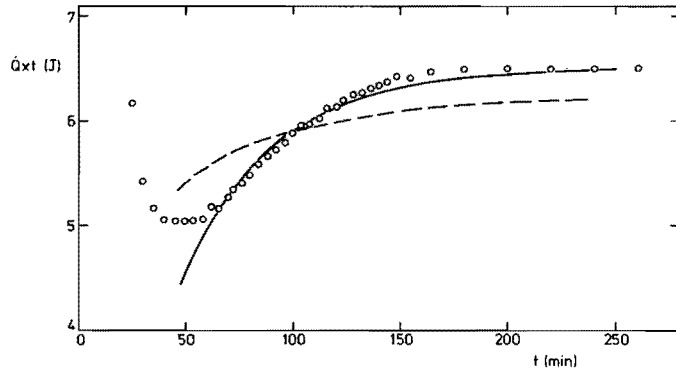

Fig. VI. 8a

The relation between $\dot{Q}xt$ and t for magnesia pretreated at reaction temperature; $T_r = 10^{\circ}C$; (o) corrected function, (—) best fitting curve of from $A\{(1-\exp(K_1 t)\}$, (--) best fitting curve of form $At/(t+B)$.

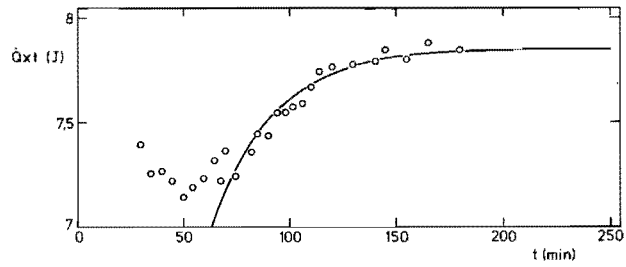

Fig. VI. 8b

The relation between $\dot{Q}xt$ and t for magnesia pretreated at reaction temperature; $T_r = 30^{\circ}C$; (o) corrected function, (—) best fitting curve of form $A\{(1-\exp(-K_1 t)\}$.

Impregnated carbon black

None of the experiments on carbon black impregnated with chromium oxide has been corrected. From the results given in Chapter V. 2. 2 no ex-

cessive conclusions may be derived for the model. However, the proportionality between rate and reciprocal time must be considered to sustain the existence of a distribution in activation energies.

Common for the three adsorbents (D) alumina, magnesia and impregnated carbon black is the hyperbolic relation between rate and time. The temperature dependency of rate on magnesia complicates the picture for this adsorbent, but the possibility to distinguish K_1 values is consistent with the model.

c. Conclusion

It appeared that the series of experiments performed on (K) alumina previously evacuated at 120°C may be fitted into the framework of the kinetic model as regards the inverse proportionality between reaction rate and time and with respect to the temperature dependence of the factor A. The results obtained with the three other adsorbents seem to justify the statement that the model for decomposition on alumina is equally valid for these adsorbents.

With regard to the nature of the active sites it seems probable that basicity is required. This conclusion is based upon two phenomena:

- adsorption of hydrogen fluoride acidifies alumina, and inhibits defluoridation of sarin
- a distinctly basic adsorbent as magnesia shows a considerable activity.

For partly different reasons Kuiper arrived also at this conclusion.

VI.4 DISCUSSION OF THE MODEL

The model described in section III.3.1 has been shown to be capable to explain the kinetics of the decomposition reaction of adsorbed sarin. Variation in activation free energy is the most essential feature of the model

The shape of the distribution function will now be discussed. Firstly, in an approach due to Roginskii (15), it will be shown that the distribution must have a constant value in a considerable interval. The assumption that the distribution is "continuous" is not essential. Discrete distributions with interval widths of RT give rise to similar reaction rates.

In the second paragraph it will be described how entropy and enthalpy contribute separately to the variation of activation free energy. Enthalpy ap-

pears to be the quantity that changes significantly.

The third paragraph discusses the implications of the established activation entropy. It deals also with the origin of the variation of activation energy.

VI.4.1 Shape of the distribution of activation free energy

The assumption concerning the block shaped distribution has been made for the sake of a simple mathematical treatment. Energy distributions of this shape are often proposed (13, 16), although they cannot be considered *a priori* to be the most likely ones. Energy distribution functions for several other phenomena have been derived on basis of physical description of the system under study. The first attempt was made by Constable (17) who tried to write the rate equation of a catalytic reaction as a function of the distribution in activation energy involved in the reaction. On basis of a statistical description of the strain energies between surface atoms, he arrived at an exponential distribution function. Unlike Constable, Halsey (18) took into account the possibility that the rate limiting step of the reaction is different for different sites. He concluded for catalytic reactions that the exact shape of the distribution is unimportant provided it is broad. For adsorption isotherms of the Freundlich-type Sips (19) derived an adsorption energy distribution neglecting adsorbate-adsorbate interaction; he arrived at a function, that closely resembles the Gaussian function.

The relative unimportance of the exact shape of the energy distribution function for catalytic reactions may be illustrated by an approach followed by Roginskii (15). He defines the activity B of a catalyst by

$$B = \int_{K_1}^{K_2} \rho(K)\ K dK \qquad [14]$$

in which $\rho(K)$ is the distribution in reaction rate constants resulting from a variation in activation energy. The pre-exponential factor is assumed not to vary with activation energy. Because of

$$K = K_o e^{-E/RT}$$

the relation

$$\rho(K)\,dK = \rho(E)\,dE$$

may be written as

$$\rho(K) = \rho(E)\,\frac{RT}{K}$$

in which the minus sign, originating from the antibatic relation between E and K, has been omitted.

By means of equation [14] the activity of some different distributions have been calculated. These are shown in Table VI.4.

Table VI.4

Catalyst activity (B) for some distribution functions of activation energy.

$\rho(E)$	$\rho(K)\,K$	B
H	HRT	$H\,RT(K_1-K_2)$
$\frac{H}{E}$	$\frac{H}{\ln(K_o/K)}$	$H\left\{RT\left(\frac{K_1}{E_1}-\frac{K_2}{E_2}\right)+K_1-K_2\right\}$
$H\exp(aE)$	$HRT\left(\frac{K_o}{K}\right)^{aRT}$	$HRT\,K_o^a\,\frac{1}{1-a}\,(K_1^{1-a}-K_2^{1-a})$

Except for steeply rising distribution functions the effective activity appears to be determined largely by the highest reaction rate constant (K_1), provided again that the distribution is broad.

The influence of activation energy distribution on the kinetics of the reaction system sarin-adsorbent, however, operates differently. Whereas in the case of a catalytic reaction the active sites are regenerated continually, the surface sites in the sarin decomposition react only once. In this respect the system resembles a chemisorption process in which also a finite amount of active sites is consumed gradually.

An alternative derivation may be given for the rate equation for a system of the type sarin-adsorbent. The method is essentially the one described by Roginskii (15); it differs from it by assuming a variation in free

energy instead of enthalpy. For the mathematical treatment this has no influence as may be seen from the expression for the reaction rate constant in terms of the transition state theory:

$$K = \frac{kT}{h} e^{-G/RT}$$

or $$K = \frac{kT}{h} e^{\Delta S/R} e^{-\Delta H/RT}$$

Roginskii considered the frequency factor to be constant, while in the derivation hereafter only kT/h is taken as a constant. The approach is approximative, as will be seen, but its great advantage is that it leads to an explicit expression for the distribution function; the variation in activation energy can be derived directly from the experimental results.

Let the distribution in activation free energy for the defluoridation of sarin be limited between the extreme values G_1 and G_2. The fraction sarin that is still intact at sites with energy G is called $\gamma(G)$. At time t this fraction is given by:

$$\gamma(G,t) = e^{-K(G)t}$$

Because of $K(G) = K_o \exp(-G/RT)$ it may be written:

$$\gamma(G,t) = \exp(-K_o t e^{-G/RT}) \qquad [15]$$

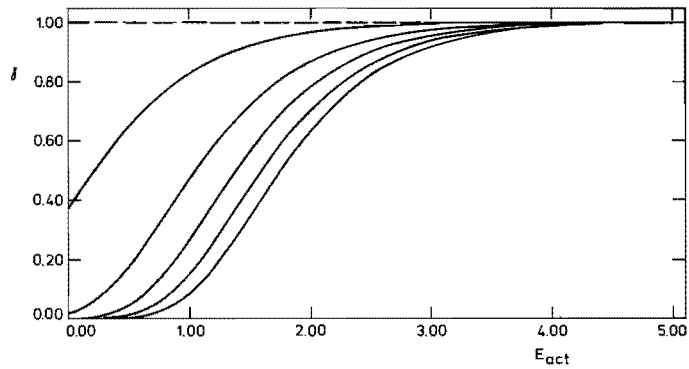

Fig. VI. 9

Illustration of equation [15] for $K_o = 1$; the time curves are presented for the following values of t respectively: 1, 4, 7, 10 and 13.

Figure VI. 9 shows the relation between γ and G for a number of equidistant times. The sigmoidal curve will be named time-curve. The shape of the time-curve remains exactly the same for increasing times, which may be seen from the following consideration. Every value of t may be written as $t = t_o \exp(-G_h/RT)$ in which t_o is a constant and $G_h = -RT \ln(t/t_o)$ by definition. γ May be written as:

$$\gamma = \exp(-K_o t_o e^{-\frac{G+G_h}{RT}})$$

This equation directly shows that in the course of time the time-curve shifts parallel to the energy axis.

To determine the rate of decomposition $d\gamma/dt$ at a given time, the curve may be approximated by the vertical in the inflexion point, because the width of the energy range covered by the curve can be shown to be relatively small.

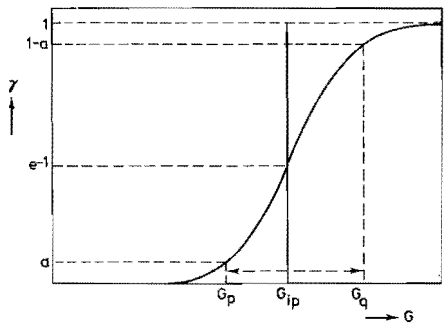

Fig. VI. 10

A relatively small activation energy interval comprises a large fraction of all reacting molecules. G_{ip} represents the average of the actually reacting sites at one moment.

If fractions of magnitude a are neglected (see Fig. VI. 10) the width of the actually reacting zone may be calculated. Let G_p and G_q be the activation energies corresponding to fractions a, respectively (1-a). The following equations may be written:

$$a = \exp(-K_o t e^{-G_p/RT})$$

$$1 - a = \exp(-K_o t\, e^{-G_q/RT})$$

If the logarithms are taken of both sides of these equations, they may be combined to:

$$\frac{\ln a}{\ln (1-a)} = e^{(G_q - G_p)/RT}$$

The energy interval $(G_q - G_p)$ is given in Table VI.5 for several values of a.

Table VI.5

Width of actually reactive energy zone in dependency of several neglections.

a(%)	$G_q - G_p$ (units of RT)	$G_q - G_p$ (kcal/mole; T = 25°C)
20	2.0	1.2
10	3.2	1.9
5	4.1	2.4
1	6.1	3.6

From this table it is seen that the approximation of the time-curve by a vertical leads to a "scrambling" of activation energies in an interval with a width of a few kcal/mole only.

For times between say t_1 and t_2 the contributions to the reaction rate of sites with energy G_1 and G_2 are negligibly small. The reaction rate may be represented by the shift of the vertical through the inflexion point parallel to the energy axis (see Fig. VI.10). The position of the inflexion point (G_{ip}) is found by differentiating expression [15] twice:

$$\frac{d\gamma}{dG} = \gamma \frac{K_o t}{RT} \exp(-G/RT)$$

$$\frac{d^2\gamma}{dG^2} = \left(\frac{d\gamma}{dG}\frac{K_o t}{RT} - \gamma \frac{K_o t}{(RT)^2}\right) \exp(-G/RT)$$

By setting the second derivative equal to zero it follows:

$$G_{ip} = RT \ln K_o t \qquad [16]$$

The distribution function $\rho(G)$ determines also the total reaction rate and must be taken into account. The amount decomposed $\Phi(G_{ip}(t))$ may be given by:

$$\Phi(G_{ip}(t)) = \int_{G_1}^{G_{ip}(t)} (1-\gamma)\ \rho(G)\ dG \qquad [17]$$

Because the real time-curve is approximated by a vertical, equation [17] transforms to

$$\Phi(G_{ip}(t)) = \int_{G_1}^{G_{ip}(t)} \rho(G)\ dG$$

Φ may be differentiated with regard to G_{ip}

$$\frac{d\Phi}{dG_{ip}} = \rho(G_{ip}) \qquad [18]$$

By means of equation [16] $d\Phi/dG_{ip}$ may be written as a function of time. It follows:

$$\frac{dG_{ip}}{dt} = \frac{RT}{t}$$

If this is inserted into equation [18] it is found for the total reaction rate:

$$\frac{d\Phi}{dt} = \frac{RT}{t}\,\rho(G) \qquad [19]$$

This expression is valid if the conditions $\gamma(G_1) = 0$ and $\gamma(G_2) = 1$ are fulfilled simultaneously. Equation [19] may be compared to the rate equation found by an exact derivation on the basis of a block shaped distribution (equation [8]).

$$r = \frac{RT}{G_2-G_1}\,\frac{1}{t}\,(e^{-K_2t} - e^{-K_1t}) \qquad [\ 8\ ]$$

It may be reminded that the factor $1/(G_2-G_1)$ stands for $\rho(G)$ (*cf* equation

[5]). The conditions under which equation [19] is valid are equivalent to the ones that allow equation [10] to be replaced by

$$r = \frac{RT}{G_2 - G_1} \frac{1}{t}$$

Apparently the derivations lead to the same result in the time interval where the extremes of the distributions furnish negligible contributions to the reaction rate.

The advantage of the approximative derivation is found in that $\rho(G)$ may be expressed explicitly as a function of t in intervals not too close to the limits of the distribution. From equation [19] it follows directly

$$\rho(G) = \frac{d\Phi}{dt} \frac{t}{RT} \qquad [20]$$

However, the values for $\rho(G)$ given by equation [20] must be considered to be mean values for the interval around G with a width of the order of magnitude given in Table VI.5. As was seen, this is the consequence of the fact that the reaction zone with a finite width has been replaced by an infinitely narrow front.

If equation [20] is applied to the experimental results it is seen that during a long period a constant distribution function is observed. The width of the actually observed energy interval with a constant $\rho(G)$ may be calculated from equation [16]. The time on which the relation $r = A/t$ starts to be valid varies with temperature; approximately it amounts to 70 minutes. Even in experiments lasting up to 3000 minutes the end of the period was not observed. The span of activation energy is calculated to be 2.8 kcal/mole at least.

This value is small if it is compared with the total span of activation free energy, *viz.* 15 kcal/mole (paragraph 3.2). It is clear that only a relatively small fraction of the molecules in the broad energy interval actually reacts. Molecules that experience an activation free energy above a definite value have not reacted, so no information on their kinetics is available. Extrapolation may be dangerous. The preposition "the distribution function is rectangular" must be interpreted with caution, because only a small fraction of the distribution has been traced experimentally. The physical meaning of G_2 is limited for this reason. It possibly is not more than

a virtual activation energy and serves as a quantity to establish the right height of the distribution function in the first stage. Thus it resembles a "dilution factor".

The assumption, made implicitly sofar, that the energy levels should vary continuously is not essential for the rate equation obtained, but such distribution may be shown to be feasible.

If the molecules of an amount of adsorbed sarin of 1 mmole are divided over the total energy interval at equidistant levels, the width of the separating intervals may be derived directly from the total span of about 15 kcal/mole, which may practically be interpreted as activation energy, as will be seen in paragraph 4.2:

$$\Delta E = \frac{14 \times 4.2 \times 10^{3}}{6 \times 10^{23}} = 10^{-19} \text{ J/molecule}$$

From the uncertainty principle of Heisenberg, $\Delta E \, \Delta t \quad h/2\pi$ or $\Delta E/\Delta\nu \quad h/2\pi$, it follows that the uncertainty in the frequency of the molecular vibration corresponding to the activated complex, should not exceed the order of 10^{15} sec^{-1} ($h = 6.63 \times 10^{-34}$ J sec). Compared to the actual value of the vibration, being 10^{12} to 10^{13} sec^{-1}, it is seen that, when 1 mmole is adsorbed, the energy intervals are a factor 10^{2} to 10^{3} larger than the limit put by the uncertainty principle. The limit for ΔE is about 10^{-21} J/molecule. At room temperature kT amounts to about 4.10^{-21} J/molecule. The lowest activation energy difference that may be discerned, is therefore about kT per molecule, which is not surprising.

It will be shown now that a distribution of equally occupied discrete activation energy levels gives rise to reaction rates that closely approximate the rate resulting from a continuous distribution. Several artificial distribution functions with equidistant energy levels of magnitude RT, were examined. The rate equation was given by the expression:

$$r = \sum_{i=o}^{n-1} C_o^i \, K_i \, e^{-K_i t} \qquad [21]$$

where the C_o^i were all taken unity and $K_i = K_o \exp\{-(E_o + iRT)/RT\}$ with $K_o = 150$ and $E_o = 4$ kcal/mole. Two of these functions are illustrated by the bar charts of Figures VI.11a and b. The same figures show the resulting rates in rxt against t plots. These plots are representations of the original

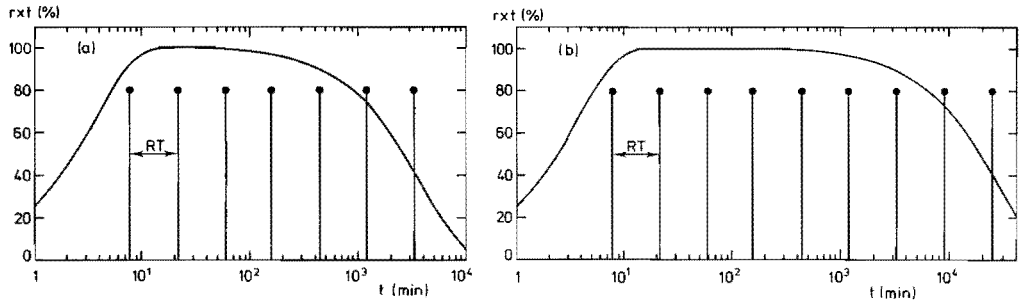

Fig. VI. 11a and b

(↑) Bar charts of activation energy distribution given by equation [21]
(a) n = 7; (b) n = 9; (—) product of rate and time as a fraction of the largest rxt value.

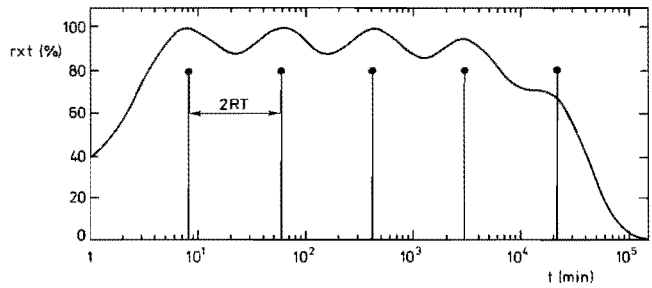

Fig. VI. 12

(↑) Bar chart of an activation energy distribution given by equation [21] with the exception of the width, which is 2RT, while n equals 5; (—) product of rate and time as a fraction of the largest rxt value.

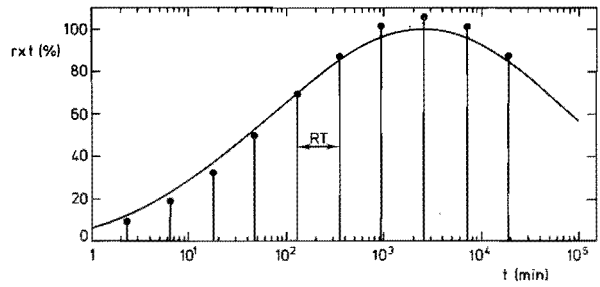

Fig. VI. 13

(↑) Bar chart of a part of a Gaussian distribution function of activation energy ($\mu = 8$, $\sigma = 3.26$); (—) product of rate and time as a fraction of the largest rxt value.

distribution functions, as follows directly from the Roginskii approximation which led to the equations

$$\rho(E) = \frac{r\,t}{RT}$$

and

$$E = RT \ln K_o t .$$

From the Figures VI. 11a and b it is concluded that a relatively small number of discrete energy levels gives rise to reaction rate patterns that are identical to patterns of continuous distributions. If it is realized that the continuous distribution function properly stands for an approximation of a distribution over discrete levels, it is allowed and sometimes advantageous to carry out calculations as if the distributions were continuous.

The same procedure was carried out on discrete distributions with equidistant energy levels of 2 x RT. One of these is illustrated by the bar chart of Fig. VI. 12. The result, also shown in Fig. VI. 12, indicates that a spacing of 2 RT is too large to explain the precise proportionality between r and 1/t of the sarin decomposition.

Following partly the method of Roginskii, the influence of the shape of the distribution may be illustrated by means of a Gaussian function.

Rates given by the equation

$$r = \sum_{i=1}^{15} C_o^i \, K_i \, e^{-K_i t}$$

were calculated for a set of C_o^i that represents a Gaussian distribution; the distribution is partly shown by the bar chart of Fig. VI. 13. The levels are equidistant with an interval width of RT. The product of rate and time is also shown as a function of log t in Fig. VI. 13.

Comparison of this representation with the original distribution reveals that the shape of $\rho(E)$ is largely preserved. The greatest difference appears to be a slight smoothing, that was expected *a priori*.

VI.4.2 The contributions of energy and entropy to the activation free energy distribution

A method resembling the procedure followed by Parravano (20) enables to find the separate contributions of activation energy and frequency factor to the activation free energy distribution. His reaction system was kinetically analogous to the system sarin-adsorbent.

Parravano studied the exchange reaction of adsorbed ^{14}C labelled benzene by gaseous benzene; the adsorbent was platinum black and the temperature range 40 to 100°C. The purpose of the study was to determine the distributions in K_o and E_{act}. The exchange reaction was assumed to be first order. When the distribution in reaction rate constants is called $\rho(K)$, the reaction rate may be written for each temperature as:

$$r(t) = \int_0^\infty \rho(K) \cdot K\, e^{-Kt}\, dK$$

This equation is interpreted as the expression for the Laplace transform of $\rho(K) \cdot K$. Therefore, it is concluded that $\rho(K) \cdot K$ may be uniquely derived from $r(t)$, which is experimentally measured:

$$\rho(K) = \frac{1}{K}\, \mathcal{L}^{-1} \{ r(t) \}$$

Parravano tacitly assumes that $K(E)$ decreases monotonously with E. Therefore, the cumulative distribution function $S(E)$, defined by

$$S(E) = \int_0^E \rho(E')\, dE'$$

may be given as

$$S(E) = \int_K^\infty \rho(K')\, dK'$$

To definite values of $S(E)$ the same sites correspond at all temperatures. By plotting the $\ln K$ related to one $S(E)$ value, against reciprocal

temperature a straight line is obtained with slope E/R. A similar plot of T ln K against T has a slope of $\ln K_o$. This procedure leads to formulations of S(E) and $\ln K_o$ as functions of E. The differential distribution function $\rho(E)$ is the derivative of S. The resulting relations for the exchange reaction of benzene on platinum black found by Parravano are given in Fig. 14a and b. The salient features of these results are the wide ranges of K_o and E and the occurrence of the flat levels in $\rho(E)$, which is named "uniform heterogeneity" by Parravano. Similar distribution functions have been found by Chornet and Coughlin for the kinetics of hydrogen desorption from iron (21).

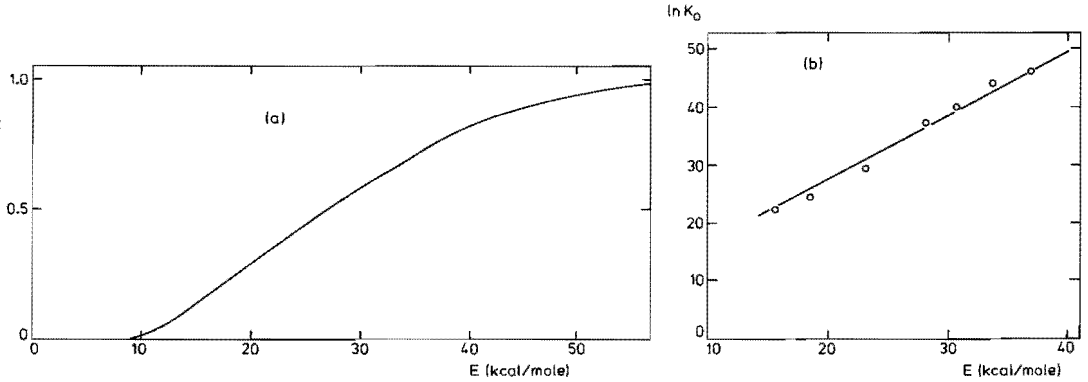

Fig. VI. 14

Results of a benzene exchange reaction described by Parravano;

(a) Cumulative distribution function of activation energy

(b) Relation between frequency factor and activation energy.

For the system sarin-alumina a somewhat different procedure was followed. Starting from the expression

$$K = \frac{kT}{h} e^{-\frac{G}{RT}}$$

where G represents the activation free energy, it was assumed, as Parravano did, that the functions $\rho(K_o)$ and $\rho(E)$ are temperature independent. This implies that $\rho(G)$ is also temperature independent. If the reaction has proceeded upto a definite fraction α, the same reaction centres have reacted at all temperatures, be it at different times. If α is known as a function of time at different temperatures, the K_o and ΔH related to each α may be

calculated.

In order to facilitate calculations, the K_1 values for the experiments at 0, 10, 20 and 30°C were taken from the best fitting straight line in Fig. VI.6.

Using the value $\Delta H_r = -72$ kcal/mole for the overall reaction enthalpy the fractions decomposed sarin (α) were calculated for the various temperatures by means of

$$\alpha = \int_0^t -\frac{dc}{dt}\,dt$$

$$\alpha = \frac{RTC^o}{G_2-G_1} \int_0^t \frac{1}{t}\,(1-\exp(-K_1 t))\,dt$$

For $RTC^o/(G_2-G_1)$ the values $A/(-\Delta H_r)$, that had been derived from the straight line in Fig. VI.4, were inserted. The resulting fractions decomposed sarin are plotted as a function of log t in Fig. VI.15.

Equation [16] may be written as:

$$\ln t = \frac{G}{RT} - \ln\frac{kT}{h}$$

or $$\ln t = \frac{\Delta H}{RT} - \frac{\Delta S}{R} - \ln\frac{kT}{h} \qquad [22]$$

Comparing this equation with

$$\ln K = -\frac{\Delta H}{RT} + \frac{\Delta S}{R} + \ln\frac{kT}{h}$$

it is seen that the time values on the ordinate axis of Fig. VI.15 represent 1/K.

From an intersection at one definite α of the four constant temperature curves of Fig. VI.15 four relations of the type of equation [22] may be set up. In a ln t against 1/T plot the activation enthalpy and the frequency factor may be found from the slope and the intersection with the ln t axis. For a number of α values these plots are shown in Fig. VI.16.

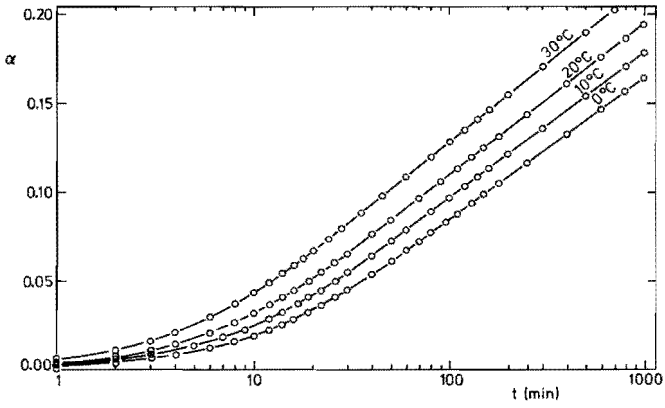

Fig. VI. 15

Sarin decomposition on (K) alumina pretreated at 120°C. Fraction decomposed sarin *versus* log t for different reaction temperatures.

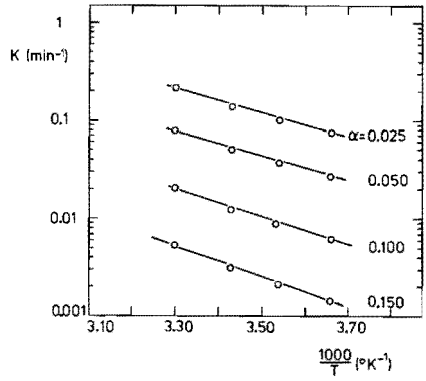

Fig. VI. 16

Reaction rate constant as a function of reciprocal temperature at various fractions decomposed sarin (α).

The values found for ΔH and $\ln K_o$ calculated from the relations between ln t and 1/T are presented as a function of α in Fig. VI. 17. Obviously the variation in G must be ascribed to variation in the activation energy; K_o is approximately 2 sec^{-1} and does not change substantially. The linear relation between ΔH_{act} and α expresses a "uniform heterogeneity", already recognised in the rectangular distribution of G.

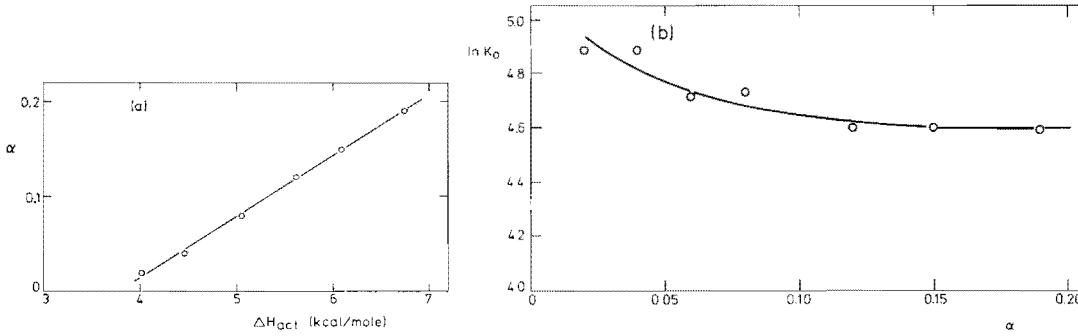

Fig. VI. 17

Variation of activation enthalpy and entropy in the defluoridation reaction of sarin adsorbed on alumina.

(a) Cumulative distribution function of activation enthalpy.

(b) K_o as a function of the fraction decomposed sarin.

The absolute value for K_o and the origin of the variation in activation energy will be discussed in the next section.

VI.4.3 Some considerations regarding the frequency factor and the origin of the variation in activation energy

A. Frequency factor

The rate limiting step in the defluoridation of adsorbed sarin implies the entrance of a hydroxyl into the coordination of the phosphorus (see section 1 of this Chapter). Therefore, the partition functions of a surface hydroxyl (Q_{OH}) and of adsorbed sarin (Q_s) must be inserted into the expression for the rate constant in the theory of absolute reaction rate (22):

$$K = \frac{kT}{h} \frac{Q^{\neq}}{Q_s Q_{OH}} e^{-\Delta H^{\neq}/RT}$$

In the preceeding section it appeared that the experimental frequency factor equals 2 sec^{-1}. By writing the factor as:

$$k_o = \frac{kT}{h} e^{\Delta S^{\neq}/R}$$

it is calculated from the rate constant and the experimental activation energy that $\Delta S^{\neq}$ amounts to -57 cal/mole ^{o}C (or e.u.). The reacting species are adsorbed in an immobilised state and cannot lose translational degrees of freedom. The entropy decrease has to be explained, therefore, from rotational and vibrational entropy losses.

The formation of the activated complex implies the loss of the rotations of hydroxyl and sarin. According to Kemball (23) the rotation entropy of a surface hydroxyl may be approximately set equal to 1.9 e.u. If an adsorbed sarin molecule is assumed to rotate freely about the Al-O-P axis, the moment of inertia for this axis (I) may be found from:

$$I = r_F^2 M_F + r_{ip}^2 M_{ip} + r_m^2 M_m \qquad [23]$$

where the r's represent the distances from the rotation axis to the mass centres of the phosphorus ligands. Actual values for these distances were estimated from an atomic model: $r_F = 1.5$, $r_{ip} = 2.0$ and $r_m = 1.7$ Å. If these values are inserted into equation [23] it follows:

$$I = 5.1 \times 10^{-38} \text{ g cm}^2.$$

The value for the moment of inertia may be inserted into the expression for rotational entropy calculated by Halford (24):

$$S_{rot} = R\left\{\frac{1}{2} + \ln \frac{1}{\pi\sigma}\left(\frac{8\pi^2 IkT}{h^2}\right)^{1/2}\right\}$$

$$S_{rot} = 8.1 \text{ e.u.}$$

where the symmetry number (σ) has been taken unity.
The other two rotational degrees of freedom are reduced to wagging vibrations of the Al-O(-P) bond.

The loss of the rotations of hydroxyl and sarin together accounts for 10.0 e.u. A large difference remains between this number and the experimentally established 57 e.u.; in terms of the frequency factor the difference amounts to a factor 10^{10}. An attempt to explain this discrepancy is based on the following considerations.

The theory of absolute reaction rates proceeds from the hypothesis that there is a complete thermodynamic equilibrium between reactants and

activated complex, except for one degree of freedom which is called the reaction mode. A displacement in the reaction mode leads to a transformation of a translational to a vibrational degree of freedom (or inversely) and constitutes the reaction. All other molecular vibrations are assumed not to influence the equilibrium between reactants and activated complex. Changes in rotational and translational modes, however, have to be taken into account.

In the reaction in study now certainly more than one vibrational mode is involved in the rate-determining step. Even when the uptake of a hydroxyl and the departure of the fluoride are not simultaneous, the reaction still is concerted, because all ligand bonds are subject to mutual changes in bond angles, and because bond distances change in the conversion from the tetrahedron to the trigonal bipyramid. Consequently all these bonds take part in the reaction mode and a substantial loss of vibrational entropy may derive. This has an important impact upon the equilibrium between reactants and activated complex.

Two examples of experimental evidence for the influence of bond vibrations of the entire molecule upon the activation entropy of displacement reactions may be cited from literature. Larsson (25) studied the hydrolysis of sarin and a number of its analogues in aqueous solution. He determined activation entropy and enthalpy in the temperature range of 20 to 35°C at a pH of 8.5. Some of his results are relevant here. The activation energy and enthalpy for the hydrolysis of two sets of phosphate esters are shown in Table VI.6; each set is characterised by a definite activation energy.

Table VI.6

Activation enthalpy and entropy for alkaline hydrolysis of some sarin analogues (25).

			E_{act} (kcal/mole)	$-\Delta S_{act}$ (e.u.)
1	methyl	methylphosphonofluoridate	10.5 ± 0.7	16 ± 2
	ethyl	"	11.2 ± 0.8	15 ± 3
	n-propyl	"	10.4 ± 0.7	18 ± 2
2	i-propyl	"	9.1 ± 0.3	24 ± 1
	i-propyl	i-propylphosphonofluoridate	9.2 ± 0.7	28 ± 2

It is seen that at equal activation energy the activation entropy is lower when the phosphorus possesses larger ligands. Because the reaction proceeds in solution, there is hardly any or no loss of rotational entropy in the formation of the activated complex. The differences in activation entropy must be attributed, therefore, to additional losses of vibrational entropy. The general trend in the results is in agreement with this explanation. This suggests that bonds in the molecule that are relatively far removed from the actually activated bond may exercise influence upon the activation entropy.

Taft (26) collected literature data on the alkaline Si-H cleavage of a homomorphic range of alkyl silanes. He recognised a parallel in the increase of activation entropy for larger ligands with the absolute entropy of the related hydrocarbons. This suggests that the entire molecule assumes a situation of low probability in the transition state (see Table VI.7). Again the additional losses are at least partly ascribed to losses in vibrational entropy. Taft mentions this effect a "freezing" of the vibration motions.

Table VI.7

Activation entropy of alkaline Si-H cleavage of some alkyl silanes and the relative entropy contents of the associated hydrocarbons (26).

Silane	ΔH_{act} (kcal/mole)	$-\Delta S_{act}$ (e.u.)	hydrocarbon	ΔS (e.u.)
$C_2H_5(CH_3)_2SiH$	0*	0*	2 methylbutane	0*
$iC_3H_7(CH_3)_2SiH$	-0.5	4	2,3 dimethylbutane	5.3
$n\text{-}C_3H_7(CH_3)_2SiH$	-1.5	5	2 methylpentane	8.9
$t\text{-}C_4H_9(CH_3)_2SiH$	-0.5	13	2,2,3 trimethylbutane	9.5
$(i\text{-}C_3H_7)_2(CH_3)SiH$	-1.0	12	2,3,4 trimethylpentane	20.2

)* by definition

The maximum attainable decrease in entropy of an adsorbed sarin molecule may be calculated if its bonds are assumed to be squeezed to an extent to lose virtually all their vibration entropy. The entropy contents of a vibration is coupled to its frequency by (23):

$$S_{vibr} = R\left\{\frac{h\nu}{kT}\left(e^{\frac{h\nu}{kT}} - 1\right)^{-1} - \ln\left(1-e^{-\frac{h\nu}{kT}}\right)\right\} \qquad [24]$$

The maximum amount of entropy to be lost can be estimated from the vibration frequencies that are known from the infrared and Raman spectra of sarin (1). Twenty frequencies below about 1000 cm^{-1}, recognised in the vibration spectrum of sarin, are listed in Table VI. 8. Higher frequencies hardly contribute to the entropy as may be seen from the graphical representation of equation [24] (Fig. VI. 18).

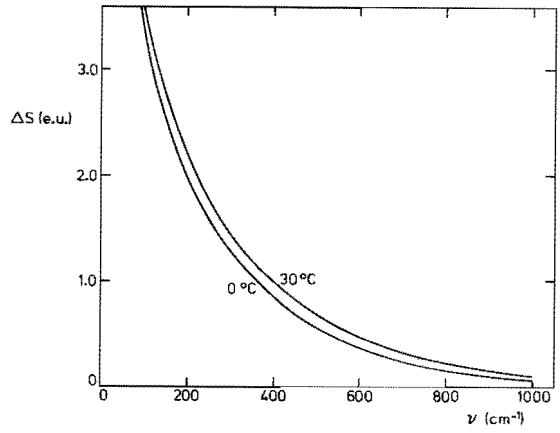

Fig. VI. 18

Equation [24] in graphical representation for two temperatures.

Besides the sarin vibrations, Table VI. 8 contains two wagging vibrations (ω) originating from the deformations of the Al-O(-P) bond, and two Al-O stretchings related to the aluminium ions that form bondings with the active hydroxyl ion and the sarin molecule. The frequencies of these vibrations are not known; the given values of 200 and 300 cm^{-1} are a reasonable estimate from what is known about deformation vibrations of surface groups (27). When all these vibrations are taken into consideration the total vibrational entropy of the adsorbed sarin molecule amounts to 24.2 e.u. at 273°K and 27.2. e.u. at 303°K. For entropies at intermediate temperatures a good measure is obtained by linear interpolation.

If the vibrational entropy is lost in the transition state the temperature dependency of the vibration entropy, visualised in Fig. VI. 18, has important impact upon the calculation of the activation enthalpy. So far the activation enthalpy was computed under the condition that the frequency

Table VI. 8

Entropy of bonding vibrations of adsorbed sarin according to equation [24].

	ν (cm^{-1})	S vibration (e.u.)	
		Temperature ^{o}K	
		273	303
Al-O-(P)	100	3.30	3.50
waggings	100	3.30	3.50
sarin bonding	150	2.52	2.72
vibrations	180	2.18	2.37
	248	1.60	1.78
	265	1.48	1.66
	295	1.30	1.48
	340	1.08	1.24
	367	.96	1.12
	420	.77	.92
	452	.68	.81
	496	.56	.69
	664	.28	.37
	755	.19	.26
	783	.17	.23
	840	.13	.19
	890	.10	.15
	913	.09	.14
	935	.08	.13
	1002	.06	.10
	1018	.06	.10
	1028	.05	.09
Al-O	300	1.28	1.45
stretchings	200	1.98	2.17
		24.20	27.20

factor does not change with temperature. This condition is not fulfilled if bond vibrations are assumed to contribute to the activation entropy. Correction is necessary; in the formula:

$$\ln K = \ln \frac{kT}{h} + \frac{\Delta S^{\neq}}{R} + \frac{d(\Delta S^{\neq})}{R} - \frac{\Delta H^{\neq}}{RT}$$

the variations in $\Delta S^{\neq}$ on account of the temperature are embodied in $d(\Delta S^{\neq})$. For one of the temperatures this correction may be set equal to zero, because only the relative change in $\Delta S^{\neq}$ with temperature is relevant. The temperature dependency of kT/h is still negligible. The corrections, determined from the summations in Table VI.8 are included in Table VI.9. The activation enthalpy is calculated from the slope of the $(\ln K - \frac{d(\Delta S^{\neq})}{R})$ plot against 1/T (see Fig. VI.19); it amounts to 12.0 kcal/mole.

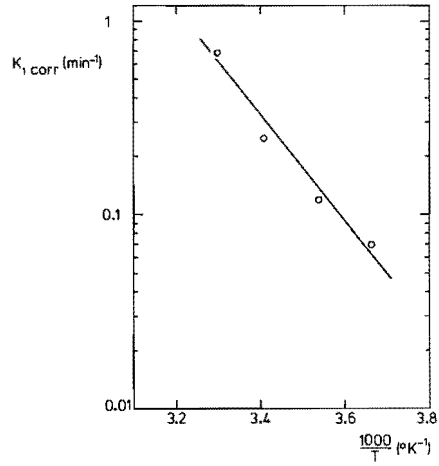

Fig. VI.19

The corrected value of K_1 *versus* reciprocal temperature (see Table VI.9).

If the values for $\Delta S^{\neq}$ and $\Delta H^{\neq}$ are inserted into the expression for the reaction rate constant, the experimental K_1 may be checked. If, for $T = 273^{o}K$, $-\Delta S^{\neq}$ is taken as 34 e.u. and $\Delta H^{\neq}$ as 12 kcal/mole, K_1 is calculated to be 7.0×10^{-5} sec^{-1}; the experimental value is 2.5×10^{-3} sec^{-1}; so the discrepancy would have decreased to a factor 35.

The hypothesis concerning the "freezing" of the vibration motions implies a departure of the theory of absolute reaction rate insofar the reac-

tion mode does not coincide with one vibrational degree of freedom of the activated complex. It is uncertain whether the factor kT/h still applies, when all vibrations are involved in the reaction mode. Therefore the hypothesis is to be considered as a possible indication to understand the origin of the discrepancy between experimental frequency factor and the one following from the theory of absolute reaction rate.

The hypothesis that the vibrational entropy is lost in the formation of the transition state has an important implication for the physical meaning of the activation enthalpy calculated in paragraph 4.2 of this Chapter. This quantity should be interpreted as a composition of the real activation energy and the temperature dependent part of the activation entropy.

Table VI.9

Correction term for the activation enthalpy $d(\Delta S^{\neq})$ accounting for the temperature dependency of the bond vibrations.

T (^{o}K)	K_1 (min^{-1})	$d(\Delta S^{\neq})$ (e.u.)	$\ln K_1 - \frac{d(\Delta S^{\neq})}{R}$	$K_{1\,corr}$ (min^{-1})
273	0.07	0*	-2.66	0.07
283	0.075	-1.0	-2.09	0.12
293	0.090	-2.0	-1.40	0.25
303	0.15	-3.0	-0.39	0.68

* By definition.

B. Origin of the distribution in activation energy

The origin of the distribution in activation energy may be found either in an intrinsic or in an induced heterogeneity. Alumina is known to possess surface acidity as well as basicity (28, 29). These properties possibly bear a relation to the variation in activation energy. Also the variation in distance between a sarin molecule and an active hydroxyl may be a determining factor. An induced heterogeneity may originate during the reaction from the adsorption of the fluoride ion as well as from the second P-O bonding with the surface. These two phenomena have similar consequences.

The induced heterogeneity can be understood from the acidifying effect that is caused by doping alumina with hydrogen fluoride (30). Lewis as well as Brønsted surface acids become stronger after adsorption of HF. Considering the rate limiting step of the reaction, *viz.* the entering of the hydroxyl into the phosphorus complex, two counteracting effects are expected:

- the phosphorus bonded by the Lewis acid becomes more positive; on account of this it is more susceptible to a nucleophilic attack by a hydroxyl and the rate constant increases;
- the character of the surface hydroxyls becomes less basic; consequently they are less active in starting an interaction with the phosphorus and the rate constant decreases.

If significant at all, the total inducing effect of HF, must operate through a weakening of the basicity, because the rate constant has been observed to decrease during the reaction. It was seen in paragraph 3.2 of this Chapter, that previously adsorbed HF did not affect the highest reaction rate constant (K_1), but decreased the rate uniformly during the reaction. This result cannot give a decisive answer to the question whether an induced effect exists, but may be considered to be indicative for the absence of it. The fact that K_1 is not changed by previous HF adsorption can be interpreted in two ways. (a) The HF adsorption is indifferent to the sites that are occupied, resulting in an even decrease in number of sites for all activities. If this is true, induced heterogeneity is inoperative. (b) The distribution of HF is macroscopically uneven like in the case of sarin adsorption; this implies that some parts are covered up to a monolayer while other fractions are still void. The sarin partly adsorbs on bare alumina and partly on the fluorinated part of the surface. In this case no decision can be made. However, the sarin that is primarily adsorbed on the fluorinated surface is bonded less strongly and may be expected to migrate to uncovered surface. This gives rise to an additional reaction rate, that is diffusion controlled. But no disturbance of the regular Zeldovich pattern has been observed. This is an argument for a random HF adsorption, which implies that the inductive effect would be insignificant.

So intrinsic inhomogeneity probably is the cause of the distribution in activation energy. It may be noted that the operation of inductive effects (described above) and of intrinsic variations in acidity and basicity operate essentially the same. The positive influence upon reaction rate of a stronger

intrinsic basicity has appeared from the work of Kuiper.

The influence of a variation in distance between sarin molecule and neighbouring hydroxyl is illustrated in Fig. VI.20. A smaller distance conveys a lower activation energy. The existence of a distribution in sarin hydroxyl distance may be understood from the exposure of different crystal planes.

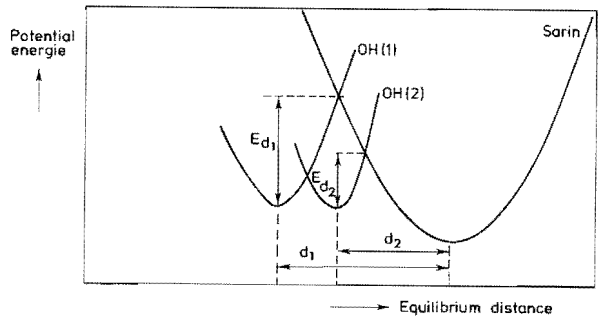

Fig. VI.20

Influence of equilibrium distance between the adsorbed sarin molecule and the hydroxyl ion upon the activation energy.

With the evidence available so far, it is impossible to decide unambiguously which property determines the variation in activation energy. The remarkable rectangular shape of the distribution function suggests that only one parameter determines the activation energy. If more factors were operative, the distribution should present more resemblance with a Gaussian distribution function.

VI.5 CONCLUSION

In this Chapter the observed Zeldovich kinetics for the defluoridation reaction of sarin adsorbed on an oxidic surface has been interpreted as a consequence of a distribution in activation free energy. The temperature and time dependencies are explained satisfactorily if a rectangular distribution in activation free energy is assumed. The constant part of this distribution can be verified directly on basis of the experimental results. This

variation appears to be seated in activation enthalpy, but its mechanistic origin is still uncertain. Variation in surface basicity or acidity as well as a distribution in distance between sarin and active hydroxyl may be determining. The uptake of a hydroxyl as a fifth ligand of the phosphorus is involved in the rate determining step. The value of the associated reaction rate constant shows a discrepancy with the rate constant following from the theory of absolute reaction rate. The origin of this discrepancy may be understood if it is assumed that the mechanism of the rate-determining step is completely concerted; this implies that the sarin molecule would lose the entropy of its bond vibrations in the transition state, which is contradictory to the basic assumption of the theory of absolute reaction rate.

REFERENCES

1. A.E.T. Kuiper, Thesis, Eindhoven (1974).
2. R.F. Hudson, "Structure and mechanism in organo-phosphorus chemistry", Academic Press, London (1965), Chapter 3.
3. I. Ugi, F. Ramirez, Chem. in Brit. 8 (1972) 198.
4. M.J.D. Low, Chem. Rev. 60 (1960) 267.
5. C. Aharoni, F.C. Tompkins, Adv. Catal. 21 (1970) 1.
6. A. Cimino, E. Molinari, E. Cipollini, Actes 2^{ième} Cong. Int. Catalyse, Paris (1960) p. 263.
7. H.A. Taylor, N. Thon, J. Am. Chem. Soc. 74 (1952) 4169.
8. F.F. Volkenshtein, Zhur. Fiz. Khim. 23 (1949) 917.
9. J. Halsey, J. Phys. Coll. Chem. 55 (1951) 21.
10. I.S. McLintock, J. Catal. 16 (1970) 126.
11. G. Parravano, M. Boudart, Adv. Catal. 8 (1955) 50.
12. A. Clark, "The Theory of Adsorption and Catalysis", Academic Press, London (1970) Chapter IX.
13. A.M. Peers, J. Catal. 4 (1965) 499.
14. M. Abramowitz and I.A. Stegun, "Handbook of Mathematical functions". Gen. Publ. Comp. Toronto (1965).
15. S.Z. Roginskii, "Adsorption und Katalyse an Inhomogenen Oberflachen", (Translated from Russian by H. Vogel) Akademie Verlag, Berlin (1958), Teil III.
16. Y. Kubakowa, Bull. Chem. Soc. Jap. 33 (1960) 734.
17. F.H. Constable, Proc. Roy. Soc. (London) Ser. A 108 (1925) 355.
18. G.D. Halsey, J. Chem. Phys. 17 (1949) 758.
19. R. Sips, J. Chem. Phys. 16 (1948) 490.

20. J.A. Brundege, G. Parravano, J. Catal. 2 (1963) 380.
21. E. Chornet and R. Coughlin, J. Catal. 27 (1972) 246.
22. H. Eyring, J. Chem. Phys. 3 (1935) 107.
23. C. Kemball, Adv. Catal. 2 (1950) 233.
24. J.D. Halford, J. Chem. Phys. 2 (1934) 694.
25. L. Larsson, Acta Chem. Scand. 11 (1957) 1131.
26. R.W. Taft, in "Steric effects in organic chemistry", Ed. M. Newman, J. Wiley & Sons Inc., New York (1956), p. 655.
27. J. Fripiat, H. Bosmans and P. Rouxhet, J. Phys. Chem. 71 (1967) 1097.
28. J. Medema, J.J.G.M. van Bokhoven and A.E.T. Kuiper, J. Catal. 25 (1972) 238.
29. A.E.T. Kuiper, J. Medema and J.J.G.M. van Bokhoven, J. Catal. 29 (1973) 40.
30. J.B. Peri, J. Phys. Chem. 72 (1968) 2917.

SAMENVATTING

Twee problemen van verschillende aard worden aan de orde gesteld. Het probleem dat centraal staat heeft betrekking op het vermogen van sommige adsorbentia om geadsorbeerde organische fosforverbindingen (zenuwgassen) te ontleden. De concrete combinatie van adsorbens en adsorbaat waaraan het meeste onderzoek werd verricht, is het systeem aluminiumoxide-isopropyl methylphosphonofluoridaat (sarin). Het molecule wordt via de phosphoryl zuurstof aan het oppervlak geadsorbeerd. De relevante ontledingsreactie is de hydrolyse van de P-F binding. Het onderzoek is gericht geweest op de fundamenteel kinetische parameters van het systeem. Het tweede probleem betreft de ontwikkeling van een experimentele techniek om de ontledingskinetiek van geadsorbeerd sarin vast te stellen. Calorimetrie werd als basis voor de meettechniek gekozen omdat de reactie *in situ* gevolgd kan worden en omdat de techniek algemeen toepasbaar is. Er bestaat een evenredige relatie tussen warmte-ontwikkeling en reactiesnelheid.

De oplossing van het experimentele probleem heeft twee fasen gekend, waarvan de eerste de constructie behelst van een microcalorimeter die volledig is aangepast aan het reactiesysteem. Het instrument is van het type dat algemeen als "heat-flow calorimeter" wordt aangeduid. Het wordt individueel gekenmerkt (a) door de aanwezigheid van een referentie-reactievat ter compensatie van temperatuursfluctuaties, en een vacuum-isolatieruimte tussen meetgedeelte en omgeving ter stabilisatie van temperatuursinvloeden; (b) door de mogelijkheid gassen te doseren aan het adsorbens in het reactievat en (c) door de isotherme werking. De gevoeligheid bedraagt 11 of 19 W/V, afhankelijk van het toegepaste type warmtestroommeter. Met de beschikbare electronische versterkingsmogelijkheden bedraagt de detectie-

grens ongeveer 1 microwatt. De instabiliteit over een periode van enkele dagen ligt in dezelfde orde van grootte.

De tweede fase betreft de ontwikkeling van een correctieprocedure voor de geregistreerde thermogrammen. Vanwege thermische traagheid vertonen calorimeters in het algemeen een betrekkelijk lage responsiesnelheid. Ofschoon door het gebruik van aangepaste reactievaatjes en warmtestroommeters de responsietijdconstante werd verlaagd van ongeveer 20 naar 8 minuten, kon de specifieke kinetiek van het reactiesysteem niet met voldoende zekerheid worden vastgesteld. De ontwikkelde correctieprocedure is gebaseerd op Fourier-analyse en vereist vóór elk thermokinetisch experiment de meting van een responsiecurve. De principiële bruikbaarheid van de procedure wordt aangetoond d.m.v. een serie aparte experimenten aan een thermisch goed gedefinieerd systeem. Hoewel de correctie voor de ontledingsexperimenten niet volledig is, komt er belangrijk meer informatie over de kinetiek van het reactiesysteem ter beschikking.

Met betrekking tot calorimetrie wordt ook enige aandacht besteed aan een classificatie van typen calorimeters; er bestaat geen rubricering die in de litteratuur algemeen gehanteerd wordt. Een voorstel wordt gedaan om een primair onderscheid te maken tussen "temperatuursverschil"-calorimeters en "energie"-calorimeters. Het grote voordeel van een dergelijk onderscheid is, dat het toegepaste meetprincipe als criterium voor de indeling geldt.

Op basis van spectroscopische gegevens en van vergelijkende calorimetrische experimenten kan worden vastgesteld dat de thermokinetiek van geadsorbeerd sarin betrekking heeft op de verbreking van de P-F band. De intrede van een hydroxyl-groep als vijfde ligand van het fosforatoom is de snelheidsbepalende stap. De defluorideringsreactie van geadsorbeerd sarin verloopt volgens Zeldovich-kinetiek. Dit geldt zowel voor aluminiumoxide als voor magnesiumoxide en kool dat geïmpregneerd is met chroomtrioxide. Er wordt een fysisch model geponeerd dat in staat is de experimentele relatie tussen reactiesnelheid (r) enerzijds en temperatuur (T) en tijd (t) anderzijds te verklaren: $r \div (1 - \exp(-Kt))\ T/t$. Het model gaat ervan uit dat de sarinmoleculen immobiel zijn geadsorbeerd. Deze immobiliteit wordt in een afzonderlijke meetopstelling experimenteel bevestigd; hierbij wordt gebruik gemaakt van sarin dat met radioactief fosfor gemerkt is. Het voornaamste kenmerk van het fysische model is de aanname van een spreiding in de activerings-vrije energie voor de defluorideringsreactie. De oor-

zaak van de spreiding in activeringsenergie is waarschijnlijk gelegen in inhomogeniteiten van het adsorbensoppervlak, ofschoon een inductief effect, voortkomend uit de gevormde reactieproducten, niet volledig kan worden uitgesloten.

De vorm van de distributiecurve kan gedeeltelijk berekend worden; een rechthoekige vorm blijkt de experimenten uitstekend te beschrijven. Omdat de temperatuursafhankelijkheid bekend is, kunnen de afzonderlijke bijdragen van enthalpie en entropie aan de vrije energie voor activering worden berekend. De spreiding blijkt voornamelijk in de enthalpie te liggen; deze heeft een laagste waarde van 4,0 kcal/mol en neemt lineair toe met de omzettingsgraad van de reactie. Deze lineariteit correspondeert met de rechthoekigheid van de energiedistributie. Hoewel deze vorm van energiedistributie vaker experimenteel is waargenomen, is elke verklaring vooralsnog hypothetisch. De absolute grootte van de frequentiefactor (~ 2 sec^{-1}) vertoont een verschil van een factor 10^{10} met die welke volgt uit de absolute reactiesnelheidstheorie. Een mogelijke verklaring van deze discrepantie wordt gezocht in de hypothese dat alle liganden van het centrale fosforatoom betrokken zijn bij de reactie. Dit wijkt af van de basis-aanname van de absolute reactiesnelheidstheorie die inhoudt, dat alleen de vrijheidsgraden van de binding die verbroken wordt (of tot stand komt) van belang zijn voor de evenwichtsinstelling tussen reactanten en geactiveerd complex.

STELLINGEN

I

Het ontbreken van een algemeen aanvaard systeem dat de verschillende typen calorimeters rubriceert, geeft aanleiding tot spraakverwarring.

II

Het criterium dat Rouquerol en Laffitte hanteren voor een classificatie van calorimeters, leidt tot een indeling die onvoldoende weerspiegelt welk meetprincipe wordt toegepast.

J. Rouquerol & M. Laffitte in "Thermochimie", Edition du C.N.R.S. Paris (1972) p. 181.

III

De inrichting van de stemlokalen in Nederland biedt de kiezer niet altijd voldoende garantie, dat hij zijn stem in het geheim kan uitbrengen.

IV

In de scheikundige vaklitteratuur wordt aan referenties soms ten onrechte de status van een bewijs verleend.

V

Professioneel voetbal vertoont een bedrieglijke gelijkenis met sport.

VI

Parravano en Brundege berekenen uit een distributie in reactiesnelheidsconstanten een verdeling in activeringsenergieën; zij nemen daarbij stilzwijgend aan, dat de snelheidsconstante monotoon daalt met toenemende activeringsenergie.

J.A. Brundege, G. Parravano, J. Catal. 2 (1963) 380

VII

Adsorptie en meting van de vrijkomende adsorptiewarmte vormen in principe een geschikte methode voor een gevoelige quantitatieve detectie in gaschromatografische analyses.

VIII

Breysse e.a. spreken van variaties in het gedrag van ceriumoxidemonsters ten aanzien van kooldioxideadsorptie; de betreffende variaties zijn evenwel onherkenbaar in de experimentele gegevens die zij presenteren.

M. Breysse e.a., J. Catal. 28 (1973) 54

IX

Op grond van zijn grote waarde als voedingsmiddel heeft brood gedurende eeuwen belangrijke functies vervuld op het gebied van politiek, kunst en religie.

J.J.G.M. van Bokhoven Eindhoven, 21 mei 1974